5-2013

Delayed Thrombus Resolution and Fibroproliferative Vascular Wound Healing From Deficiency of Type III Collagen: a Paradoxical Mechanism for Tissue Fragility

Amy J. Reid

DELAYED THROMBUS RESOLUTION AND FIBROPROLIFERATIVE

VASCULAR WOUND HEALING FROM DEFICIENCY OF TYPE III COLLAGEN:

A PARADOXICAL MECHANISM FOR TISSUE FRAGILITY

by

Amy Jean Reid, A.B.

APPROVED:

_____

Dianna Milewicz, M.D., Ph.D.
Supervisory Professor

_____

Michael Blackburn, Ph.D.

_____

Robert Bryan, Jr., Ph.D.

_____

Magnus Höök, Ph.D.

_____

Joseph McCarty, Ph.D.

APPROVED:

_____

Dean, The University of Texas Graduate School of Biomedical Sciences

DELAYED THROMBUS RESOLUTION AND FIBROPROLIFERATIVE VASCULAR WOUND HEALING FROM DEFICIENCY OF TYPE III COLLAGEN: A PARADOXICAL MECHANISM FOR TISSUE FRAGILITY

A DISSERTATION

Presented to the Faculty of The University of Texas Health Science Center at Houston

and The University of Texas M. D. Anderson Cancer Center

Graduate School of Biomedical Sciences

in Partial Fulfillment

of the Requirements

for the Degree of

DOCTOR OF PHILOSOPHY

by

Amy Jean Reid, A.B.

Houston, Texas

May, 2013

Acknowledgments

First, I would like to thank the MD/PhD Program and all the current and former students who have traveled on this wacky journey that seems to have no destination until you suddenly find yourself arriving. Wisdom rolls downhill, and I have been both the recipient and the dispensary at various points over the climb. Unending thanks to the Program Coordinators, Doris Thornton and Jo Cheatwood, for the stewardship that not coincidentally looks like and probably feels a lot like parenting. I can say that the students look to you for nonjudgmental love and care in times of doubt or frustration, and that this role may be the most necessary out of any to helping us find our own way out of the dark woods.

Many thanks to Lorenzo Perez and Julie Cheng for earning completely all the trust I placed in them to handle my precious data when I often couldn't handle it on my own. I now know what a godsend is. Effusive thanks to Limin Gong, Bindu Pappu, Jiumei Cao, Deborah Vela, Tommy Reese, and Callie Kwartler for teaching me the right and wrong ways around the assays in the first place, so that I could begin to know which data to trust. And thanks to Dianna Milewicz for handing down this mysterious and thorny project. I couldn't have predicted how gratifying it would be to untangle all of the preconceptions and put the pieces back together into a more intellectually satisfying picture. I really hope with all my heart that my numerous "aha!" moments can make a difference in the lives of your patients some day. Special thanks to Maximilian Buja for cracking the case, so to speak, by doing what he does every day and reading what the slides have to tell us.

Thanks to my friends for making the time in Houston unforgettable and worthwhile: Audrey, Chirag, Angela, Callie, Alex, Daniel, Ray, and Harry. I laughed a lot because so much was funny. Thanks to the Rice Loop, Montrose Boulevard, the Buffalo Bayou trail, and the asphalt track at Memorial Park for many hours and buckets of sweat. I wouldn't be the person I am today without you. Thanks to the sangha at the Shambhala Meditation Center for teaching me what really matters, which is no small feat. Such personal insight into life's fortunes does not come easily, as they only manifests themselves when you're forced by misfortune to stop and look for them. Thanks to my parents and family, by and for whom this project was originally inspired. I love you, and I hope this effort helps us out a little bit.

DELAYED THROMBUS RESOLUTION AND FIBROPROLIFERATIVE VASCULAR WOUND HEALING FROM DEFICIENCY OF TYPE III COLLAGEN: A PARADOXICAL MECHANISM FOR TISSUE FRAGILITY

Publication No. _____
Amy Jean Reid, A.B.

Supervisory Professor: Dianna M. Milewicz, M.D., Ph.D.

Vascular Ehlers-Danlos syndrome is a heritable disease of connective tissue caused by mutations in *COL3A1*, conferring a tissue deficiency of type III collagen. Cutaneous wounds heal poorly in these patients, and they are susceptible to spontaneous and catastrophic rupture of expansible hollow organs like the gut, uterus, and medium-sized to large arteries, which leads to premature death. Although the predisposition for organ rupture is often attributed to inherent tissue fragility, investigation of arteries from a haploinsufficient *Col3a1* mouse model ($Col3a1^{+/-}$) demonstrates that mutant arteries withstand even supraphysiologic pressures comparably to wild-type vessels. We hypothesize that injury that elicits occlusive thrombi instead unmasks defective thrombus resolution resulting from impaired production of type III collagen, which causes deranged remodeling of matrix, persistent inflammation, and dysregulated behavior by resident myofibroblasts, culminating in the development of penetrating neovascular channels that disrupt the mechanical integrity of the arterial wall.

Vascular injury and thrombus formation following ligation of the carotid artery reveals an abnormal persistence and elevated burden of occlusive thrombi at 21 post-

operative days in vessels from *Col3a1*$^{+/-}$ mice, as opposed to near complete resolution and formation of a patent and mature neointima in wild-type mice. At only 14 days, both groups harbor comparable burdens of resolving thrombi, but wild-type mice increase production of type III collagen in actively resolving tissues, while mutant mice do not. Rather, thrombi in mutant mice contain higher burdens of macrophages and proliferative myofibroblasts, which persist through 21 days while wild-type thrombi, inflammatory cells, and proliferation all regress. At the same time that increased macrophage burdens were observed at 14 and 21 days post ligation, the medial layer of mutant arterial walls concurrently harbored a significantly higher incidence of penetrating neovessels compared with those in wild-type mice.

To assess whether limited type III collagen production alters myofibroblast behavior, fibroblasts from vEDS patients with *COL3A1* missense mutations were seeded into three-dimensional fibrin gel constructs and stimulated with transforming growth factor-β1 to initiate myofibroblast differentiation. Although early signaling events occur similarly in all cell lines, late extracellular matrix- and mechanically-regulated events like transcriptional upregulation of type I and type III collagen secretion are delayed in mutant cultures, while transcription of genes encoding intracellular contractile machinery is increased. Sophisticated imaging of collagen synthesized *de novo* by resident myofibroblasts visualizes complex matrix reorganization by control cells but only meager remodeling by *COL3A1* mutant cells, concordant with their compensatory contraction to maintain tension in the matrix.

Finally, administration of immunosuppressive rapamycin to mice following carotid ligation sufficiently halts the initial inflammatory phase of thrombus resolution

and fully prevents both myofibroblast migration into the thrombus and the differential development of neovessels between mutant and wild-type mice, suggesting that pathological defects in mutant arteries develop secondarily to myofibroblast dysfunction and chronic inflammatory stimulation, rather than as a manifestation of tissue fragility. Together these data establish evidence that pathological defects in the vessel wall architecture develop in mutant arteries as sequelae to abnormal healing and remodeling responses activated by arterial injury. Thus, these data support the hypothesis that events threatening the integrity of type III collagen-deficient vessels develop not as a result of inherent tissue weakness and fragility at baseline but instead as an episodic byproduct of abnormally persistent granulation tissue and fibroproliferative intravascular remodeling.

Table of Contents

List of Illustrations

List of Tables

List of Abbreviations

2D/3D	two-dimensional/three-dimensional
α-SMA	smooth muscle α-actin
ACTA2/*Acta2*	smooth muscle α-actin gene (human/mouse)
COL1A1/*Col1a1*	type I collagen, α1 subunit gene (human/mouse)
COL1A2/*Col1a2*	type I collagen, α2 subunit gene (human/mouse)
COL3A1/*Col3a1*	type III collagen, α1 subunit gene (human/mouse)
DAB	3,3'-diaminobenzidine
E_{inc}	incremental elastic modulus
FOV	field of view
GAPDH/*Gapdh*	glyceraldehyde-3-phosphate dehydrogenase gene (human/mouse)
H&E	hematoxylin and eosin stain
HIER	heat-induced epitope retrieval
ITGA1/*A2*/*B1*	integrin α1/α2/β1 subunit genes
LAD	left anterior descending coronary artery
LCA/RCA	left/right common carotid artery
MMP1/*2*/*9*	matrix metalloproteinase-1/2/9 genes
NLOM	nonlinear optical microscopy
NSAIDs	nonsteroidal anti-inflammatory drugs
PCNA	proliferating cell nuclear antigen
pH3	phosphorylated histone H3
pN/Ccollagen	partially-cleaved procollagen

POD	post-operative day
pRb	phosphorylated retinoblastoma protein
ROI	region of interest
sCAD	spontaneous cervical artery dissection
SHG	second harmonic generation
SMCs	smooth muscle cells
TGF-β1	transforming growth factor-β1
TGFB1	TGF-β1 gene
TGFBR1/2	TGF-β1 receptors 1 and 2 genes
TPF	two-photon excited fluorescence
vEDS	vascular Ehlers-Danlos syndrome

Chapter 1: Introduction

Vascular Ehlers-Danlos Syndrome and Type III Collagen

Ehlers-Danlos syndrome describes a group of heritable multiorgan diseases that share features of abnormal skin and loose joints, and often the causative genetic mutations severely impinge on the structural integrity of collagen in the extracellular matrix. The symptoms and signs associated with type IV, otherwise known as vascular type Ehlers-Danlos syndrome (vEDS) and the most malignant of all types, occur as a result of autosomal dominant mutations in *COL3A1* that alter the biosynthesis of type III collagen[2-5]. Type III collagen forms as a super-helix of three α1(III) polypeptides each encoded by *COL3A1* and containing large regions of ~330 -Gly-X-Y- repeats. Such glycine residues are essential to super-helical structure as a function of their minimal side chains, which occupy the spatially-limited central channel of the assembled trimers[2]. However, heterozygous missense mutations associated with vEDS (the most common alterations, followed by exon skip mutations) instead encode amino acid substitutions for an essential glycine residue in half of the α1(III) monomers produced[6].

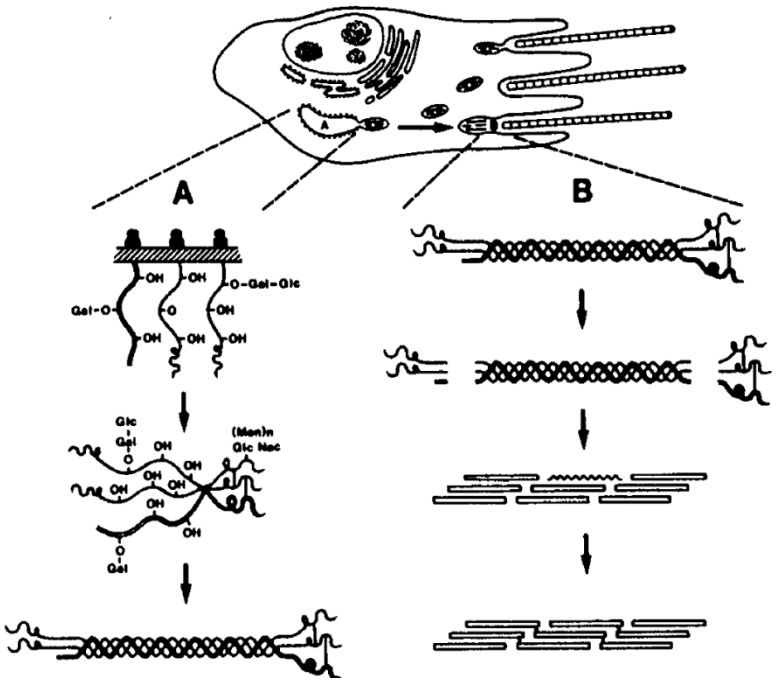

Figure 1.1. Fibroblast assembly of collagen fibrils. Panel A shows intracellular post-translational modifications of proα chains, association of C-propeptide domains, and folding into triple-helical conformation. Gal denotes galactose, Glc glucose, GlcNac N-acetylglucosamine, and $(Man)_n$ mannose residues. Panel B shows enzymatic cleavage of procollagen to collagen, self-assembly of collagen monomers into fibrils, and cross-linking of fibrils. Reprinted with permission from Massachusetts Medical Society [Heritable diseases of collagen. Prockop DJ, Kivirikko K. *New England Journal of Medicine*. 1984].

Once the synthesized α1(III) monomers mature via post-transcriptional modification in the endoplasmic reticulum, a nidus spontaneously associates the C-termini of three chains and propagates association toward the N-terminus like a zipper to manufacture the triple helix. After secretion of soluble procollagen, proteinases cleave propeptides at both termini, allowing the highly ordered helical domain to self-polymerize into cross-striated fibrils of insoluble molecules regularly staggered along the fibrillar axis[7] (Figure 1.1). Type III collagen shares this ability with type I, II, V, and XI collagens, which together comprise the family of fibrillar collagens[2].

Under the influence of *COL3A1* missense or exon skip mutations, on the other hand, structurally altered monomers lead to retention of partially-assembled type III

procollagen trimers within the endoplasmic reticulum and inhibit the extracellular accumulation of mature type III collagen as a dominant negative effect[8,9]. Presumably, assembly of homotrimers from a pool of monomers in which one-half is defective would produce altered structures in seven-eighths of resulting polymers, while only the normal one-eighth would proceed to secretion[9]. However, the severity of type III procollagen retention in fibroblasts from vEDS patients varies more extensively than this would predict and corresponds to the proximity of glycine substitutions or skipped exons to the C-terminus, where trimerization initiates[9]. Interestingly, the location of mutations also produces a measurable effect on the size and heterogeneity in diameter of extracellular collagen fibrils formed mostly by type I collagen, as C-terminal mutations lead to smaller fibrils overall while N-terminal mutations lead to wider variability and sometimes *higher* average diameter[9] (Figure 1.2). This effect occurs despite the theoretical concept that any extracellular type III collagen secreted would be structurally normal in all genetic scenarios, perhaps implicating the specific genotype's effect on the *rate* of type III collagen secretion, in addition to a generalized effect depressing steady-state levels, in the development of pathologically heterogeneous matrix with either abnormally small or large collagen fibrils. At the same time, this particular correlation between genotype and phenotype at the level of cellular production of collagen does *not* extend to the level of an individual patient's risk for severe clinical complication[10,11].

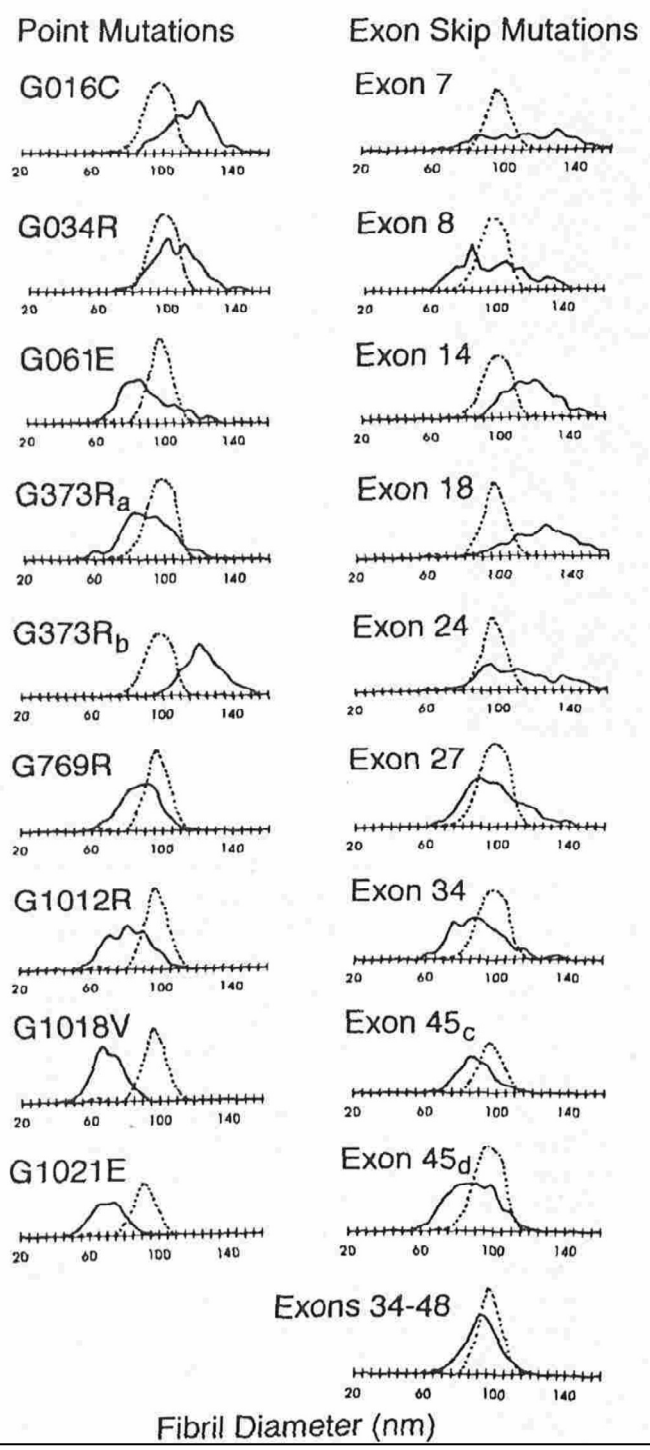

Figure 1.2. In EDS type IV with glycine substitution and exon skip mutations, the change in size and distribution of collagen fibril diameters compared to controls depends on the mutation. Collagen fibril diameters in the reticular dermis of individuals with EDS type IV (—) are plotted with similar measurements for sex-matched controls (····). The range of fibril diameters is slightly greater in EDS type IV compared to the control. Reprinted with permission from Nature Publishing Group [Mutations in the *COL3A1* gene result in the Ehlers-Danlos syndrome type IV and alterations in the size and distribution of the major collagen fibrils of the dermis. Smith LT, Schwarze U, Goldstein J, Byers PH. *Journal of Investigative Dermatology*. 1997].

Clinical Effects of Vascular Ehlers-Danlos Syndrome

The rigidity of the collagen triple helix contributes to the resistance against compression or extension, defined as stiffness, in collagenous tissues[2,12]. This notion likely contributes to the interpretation that tissues deficient in type III and type I collagen are inherently fragile[4,13,14]. Clinical complications of vascular Ehlers-Danlos syndrome, namely catastrophic rupture of hollow organs, would seem to support the idea that abnormal collagen fibrils would directly lead to mechanical failure[15]. Nevertheless, a closer examination of clinical features of vEDS reveals a more complicated and perplexing picture of the disease. As stated above, the location or type of the most common mutations, despite predicting the nature of baseline collagen derangement in tissues[9], does not predict clinical risk for type or frequency of major complication[10].

The distribution of type III collagen among tissues is highest in *distensible* organs, often hollow viscera, including the skin, arterial tree, bowel, and uterus[2,10,16], rather than in stiffer collagenous tissue like tendons, although type III collagen is transiently abundant during the collagen fibrillogenesis of early tendon development[17,18]. Life-threatening clinical complications of vEDS predictably occur in the organs normally maintaining high levels of type III collagen into adulthood, including dissection and rupture of large or medium-sized arteries (the most common cause of premature death), bowel rupture and sepsis, and rupture of the gravid uterus during labor. Although rare before puberty, as many as 25% of human patients with vEDS have suffered a non-lethal but emergent complication by age 20, while 80% suffer at least one complication by the age of 40 years. Overall, despite emergent intervention, median

lifespan for these patients is 48 years, representing a dire prognosis and exceptionally high risk of premature death[4,10].

The most striking clinical characteristic of vEDS, however, is the relatively silent attack of such catastrophic events, occurring with little or no premonitory signs or symptoms, such that patients often remain undiagnosed (or incorrectly diagnosed for more minor complications like easy bruising) until such major catastrophic episodes spontaneously present themselves[6,10,16]. This particular feature of the disease defies the simplicity of the hypothesis that less collagen in the tissues directly causes tissue fragility, as low levels of type III collagen would presumably exist all of the time and the vast majority of the time without major incident. Thus, it is much more likely that additional covert events, i.e., multiple hits accumulating over a lifetime, converge to overwhelm the structural integrity of type III collagen-deficient organs.

A relevant example of covert events involving the hollow, distensible organs in question is the matrix remodeling these tissues undergo episodically throughout adult life to repair intraluminal injuries. These include thrombus formation and organization in arteries[19], mucosal ulceration in the gut[20], and menstruation in the uterus[21,22]. Remodeling also serves to mechanically adapt the walls of these organs in response to dynamic intraluminal forces, such as blood pressure and pulsatile flow[12,23,24], obstruction of peristalsis[25,26], and gestation, parturition, and involution of the uterus[21,27].

Cutaneous wound healing supplies the ultimate, prototypical example of episodic matrix remodeling following tissue injury, thanks to the vast literature of studies describing its features (summarized by Singer and Clark[28]), so it should not be surprising that vEDS patients also present to medical attention for skin findings and dystrophic

wound healing. The most recent expert-recommended diagnostic criteria depend on readily observable skin features and less severe cutaneous complications, designed for their usefulness to generalist physicians in hopes of identifying patients with these rare syndromes well before major complications occur. The most specific criteria include, of course, organ rupture, as well as thin, translucent skin with easily visible veins over the chest and abdomen, the characteristic facies of vEDS (thin, pinched nose, thin lips, hollow cheeks, lobeless ears, and prominent staring eyes), and extensive bruising[4].

Abnormal cutaneous scars in vEDS patients have been described as distended and atrophic or papyraceous, but hypertrophic and fibrotic keloids also occur[16,29]. Paradoxically, organ rupture always necessitates emergent surgery, but as a result it has been well-documented that these patients often fare poorly in response to invasive intervention, such that invasive diagnostics are contraindicated, pregnancy advised with extreme caution, and surgery largely recommended *only* under imminent or frank threat of life. Although surgeons note that internal tissues are friable with handling and difficult to repair, the frequent and severe propensity for dehiscence of surgical wounds and evisceration, fistulas, or adhesions threatens the post-operative course of even successful procedures[4,10,30].

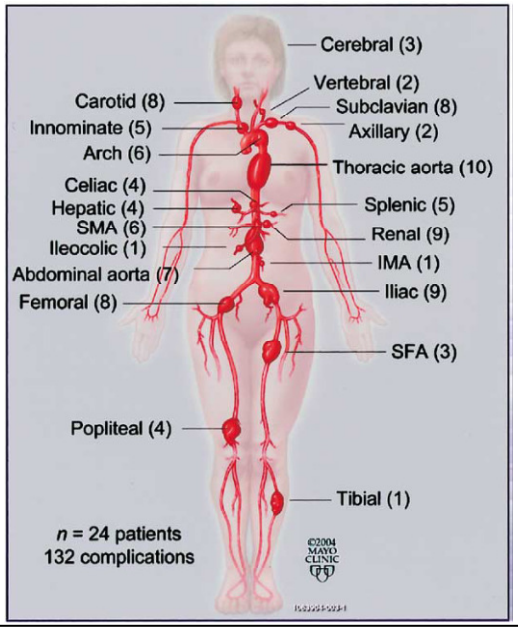

Figure 1.3. Distribution of 132 vascular complications in 24 patients with a clinical diagnosis of Ehlers-Danlos syndrome type IV. Reprinted with permission from Elsevier [The spectrum, management and clinical outcome of Ehlers-Danlos syndrome type IV: a 30-year experience. Oderich GS, Panneton JM, Bower TC, et al. *Journal of Vascular Surgery*. 2005].

Biomechanics of Large and Medium-Sized Arteries

As the most deadly complication in vEDS patients, the pathogenesis of the dissection and/or rupture of large or medium-sized arteries merits the most urgent attention by biomedical science. A retrospective survey of a cohort of vEDS patients presenting to vascular surgeons revealed the incidence of vascular complications in these arteries and their distribution throughout the body[30] (Figure 1.3). Since dissection and/or rupture of arteries represents biomechanical failure of the walls of these organs, an understanding of normal properties of arterial wall architecture would illuminate more fruitful avenues of further investigation. The functions of elastic and muscular arteries and how these correlate with their different histological structures has been introduced by Reid and Milewicz:

"**Structures of Arteries: Elastic Versus Muscular**

The arterial system is an extensive and dynamic network of vessels transporting blood under high pressure to deliver necessary nutrients and oxygen throughout the body. Although blood vessels vary not only in size but also in function, they share many basic structural elements. All arteries are composed of three concentric layers, relative to the central lumen: the tunica intima, tunica media, and tunica adventitia. The medial (middle) layer is composed largely of highly specialized vascular smooth muscle cells (SMCs), which serve under various circumstances both as the agents of contraction and as the manufacturers of extracellular matrix, functions that provide structure and mechanical strength to arteries to withstand the forces of fluid flow. The innermost intima consists of a single layer of endothelial cells that abuts the lumen and is continuous with the endocardium of the heart. The outer adventitial layer contains fibroblasts and the collagenous connective tissues they produce, lymphatics, nerves, mast cells, and—in the largest and thickest arteries—the vasa vasorum (the "vessels of the vessels," i.e., the smaller arteries supplying nutrients to the vessel wall itself). The adventitia blends with the surrounding connective tissue and anchors the artery to adjacent structures.

The structures of medial layers differ between types of arteries based on location of an artery in the arterial tree and on the functional role of that artery in controlling blood flow and pressure at that site. Large elastic arteries like the aorta act as conduits of high-energy flow from the heart, accommodating the volume pulse of systole through their high compliance. During diastole, these arteries are then able to deliver the volume through their recoil, resulting in the *windkessel* effect of dampened pulse pressures and more continuous flow downstream. Thus bearing lower (but still relatively high) pressures, the muscular distributing arteries form medium-sized branches that more precisely direct flow toward end-organs yet still offer little resistance. Only within smaller arterial branches and arterioles forming the final vascular beds of end-organs, effectively forming parallel paths in the vascular circuit, does the contraction of medial SMCs substantially decrease diameter enough to generate the resistance to favor flow to some regions over others.

Large elastic arteries—such as the thoracic and abdominal aorta, common carotids, pulmonary, and iliac arteries—are characterized by a medial layer arranged into concentric lamellae (alternating layers of different materials) formed by zigzagging elastic fibers interspersed with layer-spanning, helically-oriented SMCs (Figure 1.4). This architecture allows the distending stress of blood pressure to be distributed evenly throughout the vessel wall, and the number of lamellar units in a vascular segment (as many as 56 in the ascending aorta) varies linearly with tensional forces generated in the wall[23]. The contractile units in SMCs are linked to the matrix scaffold in a manner similar to how skeletal muscles are linked to bone. Sliding protein filaments extending across the cytoplasms of SMCs are first linked to multiprotein transmembrane clusters on the cell surface called focal adhesions, or dense plaques under microscopy, which are in turn attached to bundles of microfibrils that extend from the cell surface to the elastic fibers, thus forming a "contractile-elastin

unit[31]." These ordered units may help explain the properties of contracted arteries (isometric contraction and stress relaxation) that allow these arteries to withstand excessive distention, suggesting that even though the largest arteries do not constrict against the high pressures they endure, their SMCs are still actively regulating vessel caliber.

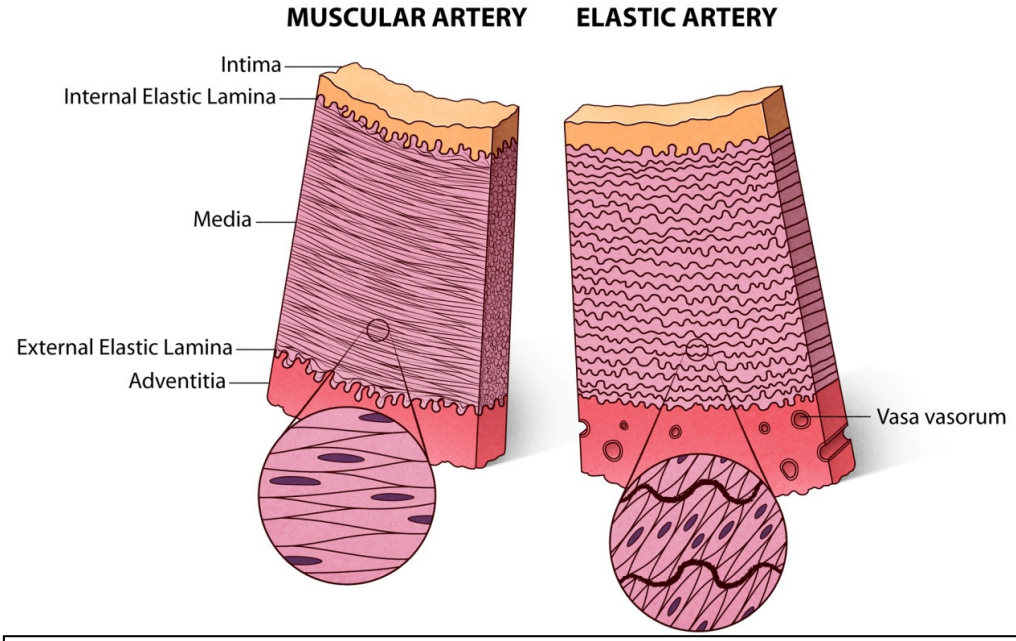

Figure 1.4. Schematic comparison of medial architecture in a muscular artery (left) and an elastic artery (right). The media of a muscular artery is bordered by the internal and external elastic laminae and contains overlapping and concentrically-oriented smooth muscle cells. The media of an elastic artery instead contains many elastic laminae alternating with muscular layers of smooth muscle cells that each span the full thickness. The adventitia in a larger elastic artery also contains small blood vessels (vasa vasorum) that nourish the outer layers of the wall. [Arteries, Smooth Muscle Cells, and Genetic Causes of Thoracic Aortic Aneurysms. Chapter 12: Inflammatory Diseases of the Blood Vessels, 2nd ed. Reid AJ and Milewicz DM[1]].

In contrast, the medial layers of muscular distributing arteries—such as the coronary, cerebral, renal, and mesenteric arteries—are composed of end-to-end, concentrically overlapping SMCs and only two elastic fibers that delineate the medial boundaries: the internal elastic lamina (between media and intima) and the external elastic lamina (between media and adventitia). Bearing less force, elastic fibers are not as essential to the function of muscular arteries[32]. However, the medial layer continues to be the thickest layer, ranging from 40 SMCs in width down to as few as 6, suggesting that the SMCs must contribute largely to the integrity of the vessel (Figure 1.4)."
Quoted text and figure reprinted with minimal modification and permission from John Wiley and Sons [Arteries, Smooth Muscle Cells, and Genetic Causes of

Thoracic Aortic Aneurysms. Chapter 12: Inflammatory Diseases of the Blood Vessels, 2nd ed. Reid AJ and Milewicz DM[1]].

The major components of the arterial matrix in both types of arteries are elastin and collagen, largely type I, but in differing ratios. Further discussion will be limited to the matrix-derived properties of elastic arteries, since these arteries withstand higher forces, conduct higher flow, and pose higher risk for fatal hemorrhage when ruptured, but the biomechanical principles outlined here likely apply to the lower-pressure muscular arteries as well, albeit to a lesser extent. Elastic arteries allowed the evolutionary development of closed circulatory systems by providing the elastic reservoir of the *windkessel* effect to distribute high energy input from the heart continuously throughout the entire loop, as described above, and evolutionary trends demonstrate the addition of elastin to less-sophisticated vessel matrices of collagen and microfibrils with this increased complexity[23].

The relative compositions of elastin and collagen in elastic vessels consequently determine vessel distensibility, as described by mechanical relationships between stress and strain. Circumferential strain (related to deformation) is defined as $\epsilon_\theta = \frac{\Delta r}{r_0}$, and circumferential stress in a thin-walled cylinder is defined as $\sigma_\theta = \frac{P * r}{h}$, where r is radius, P is pressure, and h is wall thickness. Stress is often discussed in hemodynamics in the form of the Law of Laplace, where tension is $T = \frac{P*r}{h}$, as tension provides a more specific description of the strength of the wall material in opposing distending forces acting to pull apart its component particles. Indeed, elastin fibers behave mechanically like a polymer of long chains acting almost independently, as if unraveling and sliding past each other with distention. Collagen fibers, on the other hand, are highly stabilized

by interchain bonds in helices and regular cross-chain striations in polymers (Figure 1.1) that heavily resist sliding with distention[12].

Thus, the composite material properties of elastic arteries like the aorta have been characterized as a "two-phase" model, where the elasticity or stiffness of the vessel approximates that of one or the other component in different mechanical scenarios. Overall, the vessel is less stiff than the stiffest component and more stiff than the lesser, and absolute stiffness is a function of the cross-sectional area occupied by each[33]. The elastic modulus quantifies the stiffness of a material by relating stress to strain, $E = \frac{\sigma}{\epsilon}$, and a plot of stress or tension in elastic arteries as a function of strain or deformation is nonlinear (Figure 1.5A), i.e., not a constant ratio. A calculation of incremental elastic

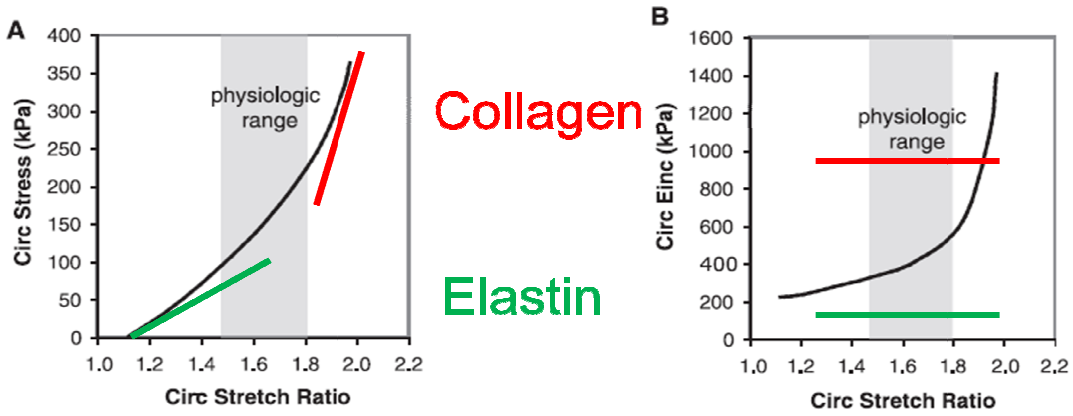

Figure 1.5. Nonlinear mechanical behavior of the adult mouse aorta. *A*: average circumferential stress versus stretch ratio. *B*: circumferential incremental elastic modulus (E_{inc}) versus stretch ratio. E_{inc} was calculated by determining the local slope of the stress-stretch ratio relationship in *A*. The physiological region is highlighted in gray for each graph. Note the decreased incremental elastic modulus at low stretch ratios where elastin dominates the vessel mechanical behavior and the increased modulus at high stretch ratios where collagen dominates. The physiological range is just at the intersection of these two regions. The sharp increase in modulus just beyond the physiological range prevents distention of, and damage to, the vessel with increased pressure. Modified and reprinted with permission from The American Physiological Society [Vascular extracellular matrix and arterial mechanics. Wagenseil JE, Mecham RP. *Physiological Reviews*. 2009].

modulus,$E_{inc} = \frac{\Delta\sigma}{\Delta\epsilon}$, represents the local slope, which at low strain is similar to the slope of the modulus of elastin but is more similar to slope of the modulus of collagen at high strain (Figure 1.5B). Thus, elastic arteries are highly extensible at low pressures (as elastic fibers predominantly redistribute to bear increasing loads, going from wavy and crumpled to straight) and appropriately compliant in response to pulse pressures in the physiologic range (as less than 10% of rigid collagen fibers are engaged from inconsistent arrangements at rest into circumferential orientation). At supraphysiologic pressures, however, collagen fibers are quickly recruited into parallel order to achieve rapid increases in tension and stiffness, limiting further distention[12,23,33].

Fortunately, the two-phase material of elastic arteries provides a substantial further benefit to wall integrity: two-phase materials may actually achieve higher tensile strengths than the ultimate strength of the stronger component alone (Figure 1.5B). The reality of structural defects and abnormally focused stresses often undermine the ideal theoretical strength of a single material's intermolecular binding forces and cause premature yield, much like a knot in a plank of wood represents the most likely place for the plank to break. The two-phase material, on the other hand, takes advantage of the more extensible component to distribute stresses more evenly, transferring focal stresses by recruiting more remote fibers of the stiffer component. This serves to normally prevent wall failure despite increasing incidence and size of irregularities in matrix composition and structure with age[33].

TABLE 3. Carotid Artery Parameters

Parameters	vEDS (n=16)	Control Subjects (n=16)	*P*
Internal diastolic diameter, mm	5.25±0.45 (4.70–6.11)	5.09±0.48 (4.41–6.22)	NS
Stroke change in diameter, mm×10^{-3}	578±205 (177–929)	543±194 (230–726)	NS
IMT, mm×10^{-3}	408±56 (257–513)	598±171 (417–968)	<0.001
WCSA, mm^2	7.3±1.2 (4.0–9.0)	10.7±3.6 (7.0–19.0)	<0.001
Wall-to-lumen ratio	0.16±0.03 (0.11–0.20)	0.24±0.07 (0.13–0.37)	<0.001
DC, kPa^{-1}×10^{-3}	61±30 (16–122)	48±20 (15–92)	<0.05
Young's elastic modulus, kPa×10^3	0.27±0.22 (0.08–1.02)	0.23±0.11 (0.08–0.43)	NS
Steady standard circumferential wall stress, kPa	68.9±14.3 (53.6–110.7)	48.2±12.1 (29.5–78.4)	<0.001
Steady midwall circumferential wall stress, kPa	74.4±14.5 (58.9–116.8)	53.5±12.2 (33.8–83.7)	<0.001
Pulsatile wall stress, kPa	28.2±7.7 (13.6–45.2)	23.1±5.7 (14.1–33.0)	<0.05

DC indicates cross-sectional distensibility. Values are mean±SD (minimum–maximum).

Figure 1.6. Carotid artery parameters of vEDS and control subjects as measured by vascular echography. IMT indicates intima-media thickness, WCSA indicates wall cross-sectional area. Reprinted with permission from Wolters Kluwer Health [Increased carotid wall stress in vascular Ehlers-Danlos syndrome. Boutouyrie P, Germain DP, Fiessinger J-N, et al. *Circulation*. 2004].

In the case of vEDS, such irregularities likely exist at baseline, or occur more frequently and earlier in life, because of the presumably deranged levels of collagen in elastic arteries. In fact, a group of investigators noninvasively identified decreased intima-media thickness in the common carotid arteries of a cohort of clearly dysmorphic vEDS patients, although half had not suffered any vascular complications and more than 25% had not suffered any complications at all before the study. They concluded that decreased wall thickness imposed a pulsatile circumferential stress on the carotids 22% higher than that borne by arteries in control subjects, and that the carotids of vEDS patients distended significantly more with systole, despite finding no differences in blood pressure between the two groups. However, because of increases in strain accompanying increases in stress, carotid arteries in the two groups also did not differ in elastic modulus, or stiffness, and a wider variance for the vEDS patients suggests that the arteries for some patients were actually *more* stiff (Figure 1.6). The investigators

interpreted their findings to mean that decreased thickness and increased wall stress contribute to "tissue fragility" associated with vEDS[13].

However, comparative vascular mechanics have elucidated the existence of a universal elastic modulus in elastic arteries across species with different matrix compositions, such that evolutionary pressure seems to favor a physiologic modulus in a defined range of 0.3-1.0 MPa. Observers of this phenomenon speculate that this target range, which both vEDS patients and control subjects from the study above occupy, serves as an optimum for providing the recoil appropriate for large arteries in a closed circulatory system and possibly guides the physiologic regulation of matrix remodeling by cells native to these arteries[23]. Thus, decreased baseline collagen levels in vEDS patients plausibly contribute to the thinning of the media in carotids, but further thinning to re-equilibrate distensibility to a target modulus may actually represent a *beneficial* adaptation to promote continuous blood flow. The clinical investigators above indeed note that the extent of medial thinning in vEDS patients exceeds that expected from estimated loss of collagen as a result of mutations and suggests that altered regulation of vascular smooth muscle cell signaling contributes further to thinning[13].

Nonetheless, considering the two-phase model of elastic arteries, decreased cross-sectional area occupied by collagen could lower the ceiling of achievable tensile strength[33]. Since elastic arteries in vEDS patients bear higher stress and must generate higher tension at baseline, they are likely more vulnerable to episodes of excessive stress. Additionally, and perhaps critically, they are also likely more vulnerable to the influence of structural defects in the walls of their arteries, if fewer collagen fibers are available for the redistribution of excessive *focal* stresses by elastin.

Trial of Celiprolol Decreases Incidence But Not Severity of Vascular Complications

Such a vulnerability to defects might help explain the again perplexing results of a clinical trial aiming to reduce circumferential wall stress in the arteries of vEDS patients. The same group measuring carotid artery wall thickness above suggested first and then conducted a trial using vasodilating β-blockers to prevent vascular complications of vEDS[13,14]. They chose celiprolol, a β_1-adrenoceptor antagonist and additional β_2-adrenoceptor agonist with vasodilatory action, under the rationale that its vasodilation of large conducting arteries in addition to resistance-generating arterioles would reduce local pulse pressure in the elastic arteries proximal to the heart[13]. In theory, the reduction in local pulse pressure would counteract the decrease in local wall thickness and outweigh the increase in radius to restore normal circumferential wall stresses ($\sigma_\theta = \frac{\downarrow\downarrow P * \uparrow r}{\downarrow h}$).

Surprisingly, celiprolol elicited the *opposite* mechanical effects in patients, *increasing* systolic and pulse pressure in the carotids, *decreasing* intima-media thickness, and *increasing* circumferential wall stress even further ($\sigma_\theta = \frac{\uparrow P * r}{\downarrow\downarrow h}$). However, the only statistically significant change in measured physiological parameters was an increase in stiffness/elastic modulus, corresponding with a nearly significant decrease in distensibility. Despite conflicts between hypothesis and result, prospective and randomized administration of celiprolol still successfully and significantly reduced the incidence of arterial rupture and/or dissection in treated vEDS patients in comparison with untreated vEDS patients[14].

The authors suggest that the effects of β_2-adrenoceptor agonism depend on the sympathetic milieu already present in recipients, which would lead to vasodilation in

already hypertensive subjects but to sympathomimetic effects in normotensive subjects, like the vEDS patients treated here. At the same time, celiprolol, like all β-blockers, would prevent excessive blood pressure and heart rate spikes, as during exercise[34] (or anxiety), so the authors speculate that celiprolol, rather than reducing global wall stress, may instead have *stabilized* hemodynamics[14]. This is a subtle but crucial distinction, as, in the context of a two-phase model for elastic arteries, it implies that the treatment prevented episodic fluctuations of *especially* high stress. So vEDS may not pose so much a risk of "fragility" due to baseline weakness but instead confer a vulnerability in the safety mechanisms designed to deflect the threat of episodic injury.

The clinical endpoints of vEDS patients in the trial validate this distinction–not only do the untreated patients suffer the episodic and catastrophic vascular complications already well-characterized for vEDS, some of the *treated* vEDS patients suffer the same episodic and catastrophic complications as well. The conclusions of the trial declare that significantly fewer patients suffer complications under the treatment, but the severe and mostly unheralded nature of the arterial dissections and ruptures remain the same, even deadly. Notably, some connection to a precipitating event is mentioned for the one patient who died under celiprolol treatment, who suffered sudden death with acute chest pain radiating to the right arm one day after practicing shot put. Otherwise, blinded experts on a committee reviewing clinical endpoints were unable to discern a patient's assignment to the treatment or control arm based on the severity of outcome[14]. One explanation consistent with these results is the possibility that celiprolol decreased the risk for discrete injury to arteries in vEDS patients by decreasing the likelihood of episodes of excessive wall stress, but that celiprolol is ineffective at preventing the

sequelae of injury once breakthrough injuries occur. The role of sequelae deserves attention here in lieu of the moderate delay between the minor trauma of shot put practice and the onset of deadly dissection or rupture, rather than the activity of shot put itself eliciting sudden death.

Together, the findings from this trial seed skepticism in the assumption that tissue fragility in vEDS patients results directly from deranged collagen levels at baseline. Although effects of deranged matrix on biomechanics clearly contribute to vascular complications, the link is not direct, and manipulating baseline circumferential wall stress does not cure the disease. Separate proximal events are likely necessary for the rapid development of arterial pathology and the precipitous failure of biomechanical strength. Further insight and improvements in therapy may come from exploring the events *between* injury and mechanical failure, which likely include aberrant remodeling of the vasculature and the dysregulation of *new* collagen synthesis. We predict that episodic arterial injury unmasks the vulnerability to arterial dissection and/or rupture in vEDS patients, and that this vulnerability involves the evolution of structural defects in the media of arteries. We further predict that genetic mutations inhibiting the production of type III collagen disrupt the normal regulation of vascular remodeling to promote the occurrence of such structural defects.

In the following chapters, we introduce the concepts of thrombus resolution as a form of vascular wound healing and the organization of thrombi by resident myofibroblasts as akin to the formation and remodeling of new matrix within vascularized granulation tissue. **Thus, we hypothesize that injury eliciting the formation of occlusive thrombi within genetically-vulnerable arteries unmasks**

defective thrombus resolution resulting from impaired production of type III collagen. This causes deranged remodeling of matrix, persistent inflammation, and dysregulated behavior by resident myofibroblasts, culminating in persistent granulation tissue and the development of penetrating neovascular channels that disrupt the mechanical integrity of the arterial wall. The following research project will, first, confirm delayed thrombus resolution and persistent neovascularization following arterial injury in type III collagen-deficient mammals; second, confirm dysregulated myofibroblast synthesis and organization of a collagenous matrix in the absence of sufficient type III collagen during remodeling of a fibrin lattice, and finally, confirm the necessity of dysregulated matrix production and organization by resident myofibroblasts for the generation of wall defects by impeding myofibroblast involvement in thrombus resolution and preventing the differential incidence of neoangiogenesis. **In short, we are presenting a novel and paradoxical model of pathogenesis wherein deficiency of type III collagen leads to a fibroproliferative vascular wound healing program that episodically leads to an increased burden of vascular wall defects, rather than the baseline "tissue fragility" in the tension generated by organ wall matrix more commonly assumed to be the etiology of complications in vEDS patients.**

Chapter 2: Injury to Carotid Arteries in Type III Collagen-Deficient Mice Unmasks Delayed Thrombus Resolution and Persistent Neoangiogenesis

Introduction

Correlation of the Clinical and Cellular Phenotypes in Patients and Mice with COL3A1/Col3a1 Mutations

Most vEDS patients harbor missense or exon skip mutations in *COL3A1*, leading to a dominant negative effect on the cellular secretion of type III collagen that inhibits its accumulation and consequently alters the otherwise uniform diameters of type I collagen fibrils[9]. With the creation of a type III collagen knockout mouse by targeted deletion of the promoter and first exon of the *Col3a1* gene[15], other researchers confirmed similarly

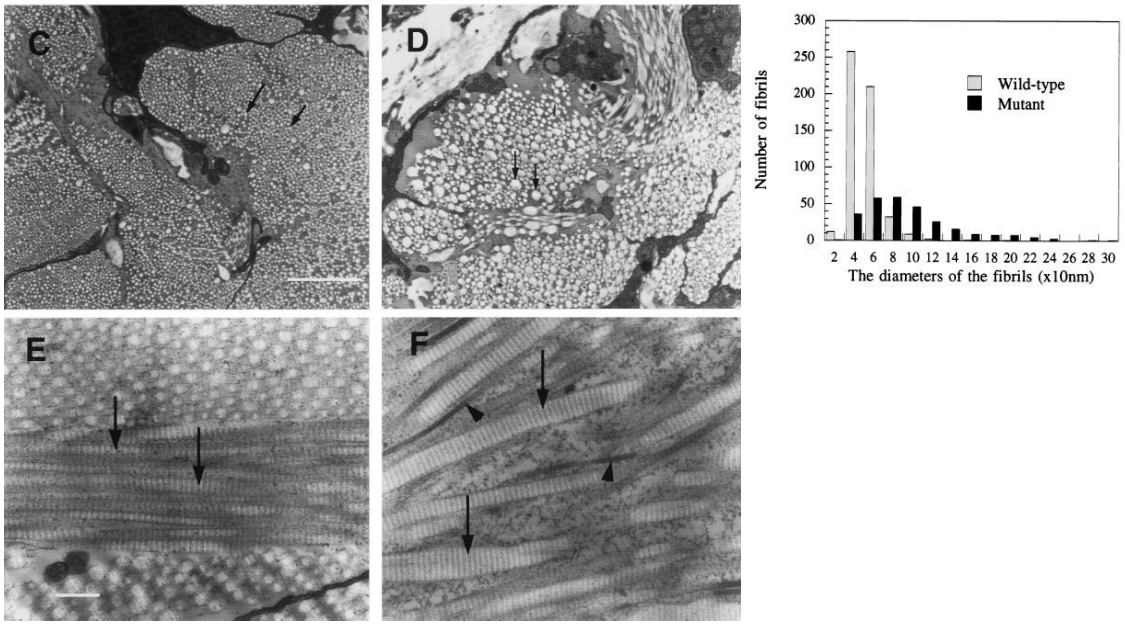

Figure 2.1. Transmission electron microscopic analyses of aorta and skin from wild-type and mutant mice. (*C*) Cross section of the collagen fibrils in the adventitia of wild-type aorta. Arrows point to individual fibrils. The diameter of the collagen fibrils is smaller and relatively uniform compared with the fibrils (arrows) of mutant aorta in *D*. (*E*) Skin section of wild-type mouse. The collagen fibrils (arrows) are uniform in diameter. (*F*) Skin section of mutant mouse. The collagen fibrils are often thicker (arrows) or thinner (arrowheads) than control fibrils and are not uniform in diameter. *Right*, Comparison of the diameters of collagen fibrils in the adventitia. A 2µm x 2µm area in the adventitia was randomly chosen, and all the fibrils were measured for their diameters and counted. Reprinted with permission from the National Academy of Sciences of the United States of America [Type III collagen is crucial for collagen I fibrillogenesis and for normal cardiovascular development. Liu X, Wu H, Byrne M, et al. *Proceedings of the National Academy of Sciences*. 1997].

variable diameters and a higher mean diameter in collagen fibers from the tissues of *Col3a1*$^{-/-}$ mice. In fact, the number of fibrils in cross-sections of the adventitia was around one-third the number in normal mice, but the average diameter was twice that of controls, roughly computing a 33% *greater* cross-sectional area occupied by collagen fibrils in *Col3a1*$^{-/-}$ tissues (Figure 2.1). Adult *Col3a1*$^{-/-}$ mice appeared grossly indistinguishable from littermates, except for a 15% decrease in body size, but they also developed spontaneous skin lesions and organ rupture, most often dissection and rupture of large elastic arteries, limiting their life-span to 20% of that in their wild-type littermates. Interestingly, no obvious sentinel characteristics of collagen deficiency were observable by histochemical analysis (Masson's trichrome stain) of non-dissected *Col3a1*$^{-/-}$ arteries compared with controls, but electron microscopy identified a subtle deficiency of collagen fibrils in the small spaces between smooth muscle cells and elastin fibers in the media[15].

However, the creators reported only a rare 5% survival rate of null mice to weaning age, with the majority of deaths occurring perinatally within 2 days of birth[15]. Only one similar young vEDS patient who possessed two null alleles has been reported, and she succumbed very prematurely to the catastrophic complications of vEDS at 11 years of age[35]. Thus, the *Col3a1*$^{-/-}$ mouse does not provide a tractable or entirely translatable model for the study of type III collagen deficiency in adult mammalian tissues. In fact, a group of collaborators maintaining a colony of these knockout mice at the National Institutes of Health Institute of Aging, Wilfried Briest and Mark Talan, claimed to have never observed *Col3a1*$^{-/-}$ offspring despite appropriate breeding schemes.

Unfortunately, the creators of the type III collagen-deficient mouse model neglected to report very extensively on the haploinsufficient *Col3a1*$^{+/-}$ mouse, only mentioning that collagen extracts from the skin of heterozygous mice contain ~50% of normal type III collagen (α1(III)) levels. Of note, they also report electrophoresis evidence that type I collagen levels in skin from mutant mice (as separated into α1(I) and α2(I) monomers on the gel) may *exceed* those in wild-type littermates (Figure 2.2), although they explain this as underloading of the gel. Otherwise, the manuscript concludes that *Col3a1*$^{+/-}$ mice are "phenotypically normal[15]," and this presumably includes their life span.

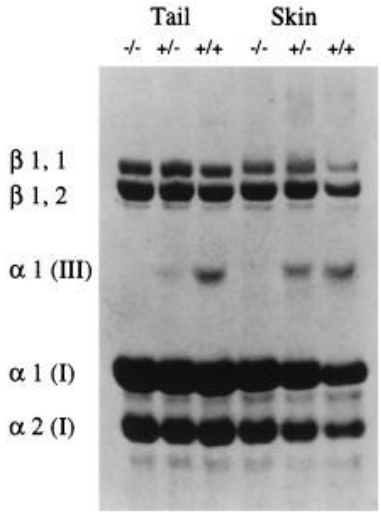

Figure 2.2. Collagens from tails and skin of wild-type mice and type III collagen mutants. Collagens were resolved by SDS/PAGE and stained with Coomassie blue. The type III collagen molecule consists of three α1(III) chains. The β1,1 and β1,2 dimers and the α1(I) and α2(I) chains are all from type I collagen and serve as internal controls for the loading. Reprinted with permission from the National Academy of Sciences of the United States of America [Type III collagen is crucial for collagen I fibrillogenesis and for normal cardiovascular development. Liu X, Wu H, Byrne M, et al. *Proceedings of the National Academy of Sciences*. 1997].

Ironically, these *Col3a1*$^{+/-}$ mice may actually pose a more attractive model for precisely investigating the role of injury in precipitating pathology, since the animals do not spontaneously die in the absence of manipulation. Furthermore, experiments

investigating vascular mechanics in *Col3a1*$^{+/-}$ arteries determined that those explanted in middle age (14 months) withstand rupture even under extreme supraphysiologic pressures (>800mgHg) comparably to explanted wild-type arteries and that significant differences in mechanical strength as a function of *Col3a1* gene dose only emerge in old age (21 months) and again only under extreme pressures (>700mmHg), providing strong evidence against the idea that type III collagen-deficient tissues are inherently weak or fragile at baseline[36] (Figure 2.3). This normal phenotype (and apparently normal

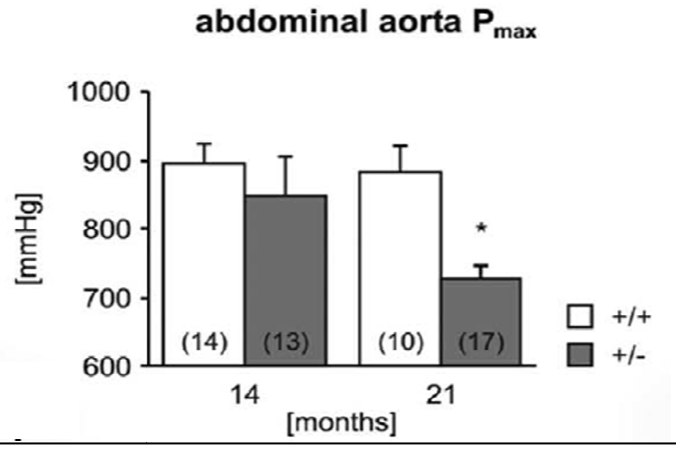

Figure 2.3. The maximum pressure in the abdominal aorta was measured in 14- and 21-month old wild-type (+/+) and heterozygous (+/-) mice. Number of experiments show in parentheses. Reprinted with permission from SAGE Publications [The haploinsufficient *Col3a1* mouse as a model for vascular Ehlers-Danlos syndrome. Cooper TK, Zhong Q, Krawczyk, et al. *Veterinary Pathology*. 2010].

mechanical strength) is a stark contrast to reports of human vEDS patients with haploinsufficiency of type III collagen due to heterozygous frameshift mutations causing premature termination codons and nonsense-mediated decay of the message. These haploinsufficient vEDS patients suffer arterial aneurysms, dissections, and/or rupture, with precipitous clinical courses at premature ages virtually identical in severity to those described for patients with dominant negative missense mutations. Strikingly, cell culture experiments testing the secretion of type III procollagen by explanted patient

fibroblasts failed in three of four cases to demonstrate any diminished production[37] (Figure 2.4).

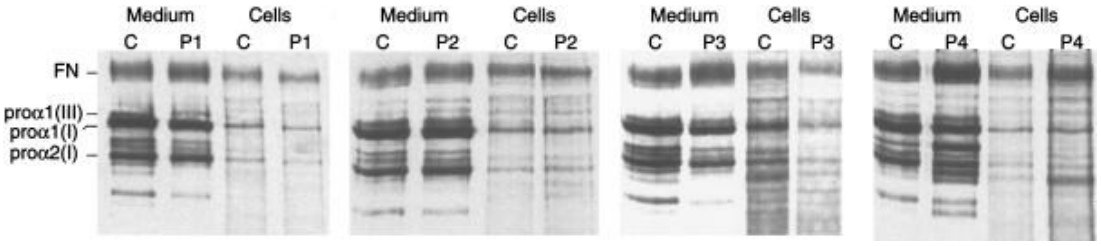

Figure 2.4. SDS/PAGE of radiolabeled procollagens from medium and fibroblast cell layer, analyzed under reducing conditions, from a control cell line (lanes C) and cell strains from four individuals with EDS type IV (P1-P4). In cells from P1 the dimunition in the amount of pro- α1(III) is evident, but it is not clear in the other three individuals. FN = fibronectin. Reprinted with permission from Elsevier [Haploinsufficiency for one *COL3A1* allele of type III procollagen results in a phenotype similar to the vascular form of Ehlers-Danlos syndrome, Ehlers-Danlos syndrome type IV. Schwarze U, Schievink WI, Petty E, et al. *American Journal of Human Genetics*. 2001].

However, the researchers identifying these patients later widened their investigation to include family members and discovered that many relatives carrying identical mutations had survived beyond 50 years of age with no life-threatening complications. From this larger cohort of type III collagen haploinsufficient patients, they determined that these genotypes conferred a milder phenotype characterized by extended life spans, delayed age of first complication, and a complete predominance of lethal complications in the vascular system over the gastrointestinal or female reproductive systems[38]. Thus, the severity of complications affecting the index patients from the first report likely involved exposure to additional risk factors, possibly vascular injuries, that did not occur in their less affected family members, since their identical genotypes alone cannot explain the susceptibility to mechanical failure. At the same time, the ability of cells from these index patients to produce normal levels of

extracelluar type III collagen *at baseline* was intact. It is plausible that such patients would be more vulnerable to pathological events in which the *rate* of type III collagen production, rather than absolute production, was more crucial to outcome.

Stroke, Spontaneous Cervical Artery Dissection, and Precipitating Injury

Despite suggestive episodic and catastrophic clinical courses in vEDS patients, injurious events within the vasculature remain elusive and likely subtle. Fortunately, the development of complications in another cohort of patients bearing significant clinical overlap with vEDS are *very* strongly associated with vascular injury. Between 10 and 25% of strokes in patients younger than 45 years of age result from "spontaneous" dissection in one of the major cervical arteries (the carotid or vertebral arteries)[39]. Multiple observations suggest the presence of constitutive arteriopathies in many of these patients: increased risk for recurrence with youth at first occurrence; increased risk for dissection of other arteries; familial cases of cervical artery dissection; association of dissection with familial intracranial aneurysms; and 15% co-occurrence of fibromuscular dysplasia, arterial redundancies, or abnormal distensibility on angiography[40]. However, identifiable single-gene mutations occur only rarely. Despite the fact that spontaneous cervical artery dissection (sCAD) is a common presentation for arterial complication in vEDS[30,41], vEDS patients only constitute 2% of sCAD patients. Patients with Marfan syndrome, caused by mutations in *FBN1* affecting the integrity of microfibrils connecting smooth muscle cells to elastic laminae in the arterial matrix, are responsible for only 0.6-0.9% of sCAD cases. Patients with Loeys-Dietz syndrome (a syndrome caused by mutations in *TGFBR1* or *TGFBR2* with two distinct clinical subtypes

overlapping with both Marfan syndrome and vEDS) are responsible for only rare cases of sCAD[42].

Nonetheless, in the non-syndromic population, the risk for dissection of arteries in the neck greatly exceeds the risk in arteries of similar size elsewhere in the body, such as the coronary or renal arteries, and clinician scientists have suggested an explanation arising from greatly increased mobility of cervical arteries and particular vulnerability to trauma[39]. Although severe and direct trauma to the neck can precipitate dissection, as following motor vehicle accidents or sports injuries[39,43], patients suffering "spontaneous" dissections may report histories of minor or trivial trauma involving extension or torsion of the neck, such as coughing, vomiting, sneezing, painting a ceiling, or lying the head back for a dental exam or over a sink at a salon[39,44]. From our own clinical experience, the most colorful incidences of similar trauma preceding dissections involved scuba diving, lifting a chair overhead at a Jewish wedding, and performing the "extreme" yoga poses of the P90X exercise regimen (Table 2.1).

Table 1. "Trivial" Causes of Carotid Dissection.

Eating[3]	Brushing teeth[2]
Coughing[2]	Childbirth[5]
Nose blowing[2]	Turning the head while leading a parade[2]
Basketball[4]	Old whiplash injury[2]
Tennis[2]	Car sliding on ice without collision[4]
Skiing[2]	Neck flexing with child scolding[6]
Volleyball[2]	Straightening up after bending[3]
Polo[4]	"Head banging" during punk-rock dancing[7]
Hockey[3]	Trampoline exercises[8]
Football[2]	Tree falling on back without apparent neck injury[6]
Bowling[2]	Diving into water[3]
Shaving[3]	Heavy lifting[9]

Table 2.1. Trivial causes of carotid dissection. Reprinted with permission from the Massachusetts Medical Society [Bottoms-up dissection. Trosch RM, Hasbani M, Brass LM. *New England Journal of Medicine*. 1989].

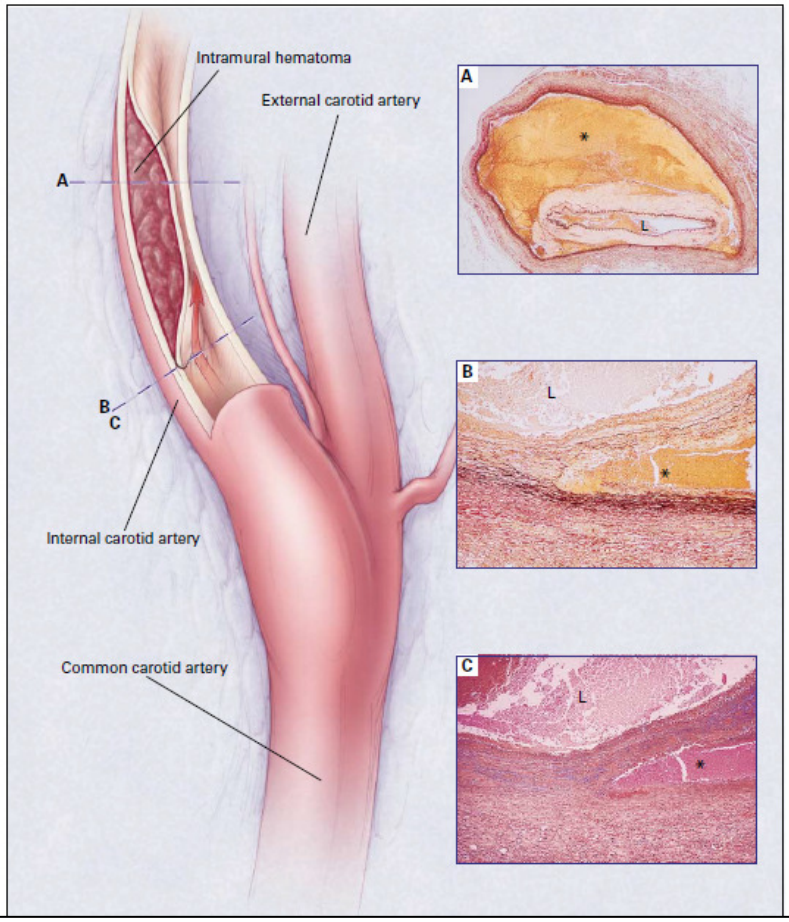

Figure 2.5. Pathological findings in a 37-year old woman with a dissection of the internal carotid artery. Photomicrographs of the right extracranial internal carotid artery (Panels A, B, and C) show a dissection within the outer layers of the tunica media, resulting in stenosis of the arterial lumen (L). The rectangles outlined in blue on the left indicate the sites of the photomicrographs. The intramural hemorrhage (asterisk) extends almost entirely around the artery (Panel A, van Gieson's stain, x4). Higher-power views of the internal carotid at the point of dissection show fragmentation of elastic tissue (Panel B, van Gieson's stain, x25), with the accumulation of pale ground-glass substance in the tunica media, indicated by the blue-staining mucopolysaccharides (Panel C, Alcian blue, x25). These changes are consistent with the diagnosis of cystic medial necrosis. Reprinted with permission from the Massachusetts Medical Society [Spontaneous dissection of the carotid and vertebral arteries. Schievink WI. *New England Journal of Medicine*. 2001].

Dissections originate from a breach of the arterial wall integrity and are less severe than–though increasing the risk for–a complete rupture of all three layers. Instead of frank hemorrhage, dissection involves the entry of pressurized blood into a false lumen within one of the layers of the artery, most often the media, or between layers, like between the media and adventitia (Figure 2.5). Many speculate that blood enters through an intimal tear, which makes sense with the stretching nature of neck injuries.

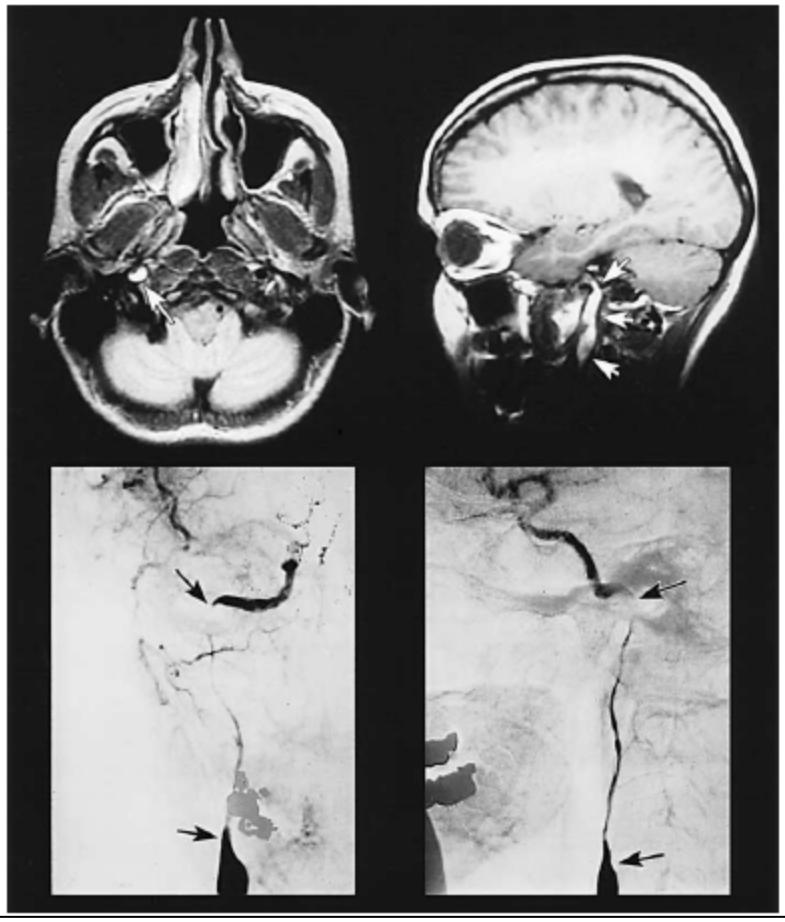

Figure 2.6. Findings on magnetic resonance imaging and angiography in a in a 37-year old woman with a dissection of the internal carotid artery. On T1-weighted magnetic resonance imaging, an axial view (upper left) and a sagittal view (upper right) show a subacute intramural hematoma in the wall of the right internal carotid artery (arrows). On carotid angiography, a frontal view (lower left) and a lateral view (lower right) show a corresponding long segment of high-grade stenosis extending from about 2cm distal to the carotid bulb to the base of the skull (arrows). Reprinted with permission from the Massachusetts Medical Society [Spontaneous dissection of the carotid and vertebral arteries. Schievink WI. *New England Journal*

However, these tears or any other communication between false and true lumina are notoriously difficult to locate on close inspection of postmortem or surgical specimens, providing evidence of *primary* intramural hematomas in at least some cases.

Displacement of the wall impinges on flow in the true lumen, which can cause widely distributed ischemia downstream of the occlusion and ~10% of the time create a "candle flame" or "string sign" on angiography[39] (Figure 2.6), but more often promotes arterial

thrombosis through altered flow dynamics and the discharge of emboli that induce ischemic strokes located remotely from the dissection[45].

The onset of dissection can present as one-sided neck pain with or without ipsilateral headache, but the onset of neurological deficits and stroke occurs after a delay of hours to days following internal carotid dissection and two weeks following vertebral artery dissection[39]. At the same time, the onset of pain may itself follow a delay of hours, days, and weeks after minor or blunt traumas[46,47] or even after respiratory tract or varicella infection[48,49], obscuring a precise cause-to-effect link. The classic but contentious association between chiropractic manipulation and stroke, with 1 in 20,000 manipulations preceding stroke and one-quarter of those affected harboring a generalized connective tissue disorder, is consistent with a role for injury, although it belies the confusing temporal relationship between injury and symptoms. Patients with neck pain (of note, the posterolateral pain of vertebral artery dissection mimics musculoskeletal pain) often seek chiropractic relief[39], but in our experience in a medical genetics clinic, patients with generalized connective tissue disorders often suffer chronic pain and may seek chiropractic manipulation on multiple occasions. Regardless, it is possible that covert events pathologically altering arterial structure in response to *repeated* subacute injury could lower the threshold for acute dissection in response to any one particular episode of injury.

Carotid Ligation: A Surgical Model for Vascular Injury

Ligation of the carotid artery in mice was developed as a reproducible model for vascular injury and the robust development of neointimal lesions, which resemble

pathological intraluminal lesions such as fibromuscular caps in atherosclerosis or restenotic scarring following endovascular interventions. Though smaller than pigs or rats used in similar studies, mice allow investigators to assess genetic influences on vascular remodeling[50]. Neointimal lesions are a generic response to a wide variety of arterial insults, analogous to cutaneous scars in the skin or gliosis in the brain. They are characterized by the new and abnormal appearance of hyperplastic vascular smooth muscle cells and/or myofibroblasts (fibromuscular cells, more generally) and the new fibrotic matrix they synthesize within the intima, i.e., between the endothelial cells lining the lumen and the internal elastic lamina[51]. The apparent inward expansion of these lesions occludes the lumen of ligated vessels [52,53]. Formation of neointima is of interest to this project as a scenario of vascular remodeling occurring exclusively in response to local injury, and it involves substantial production and organization of *new* extracellular matrix.

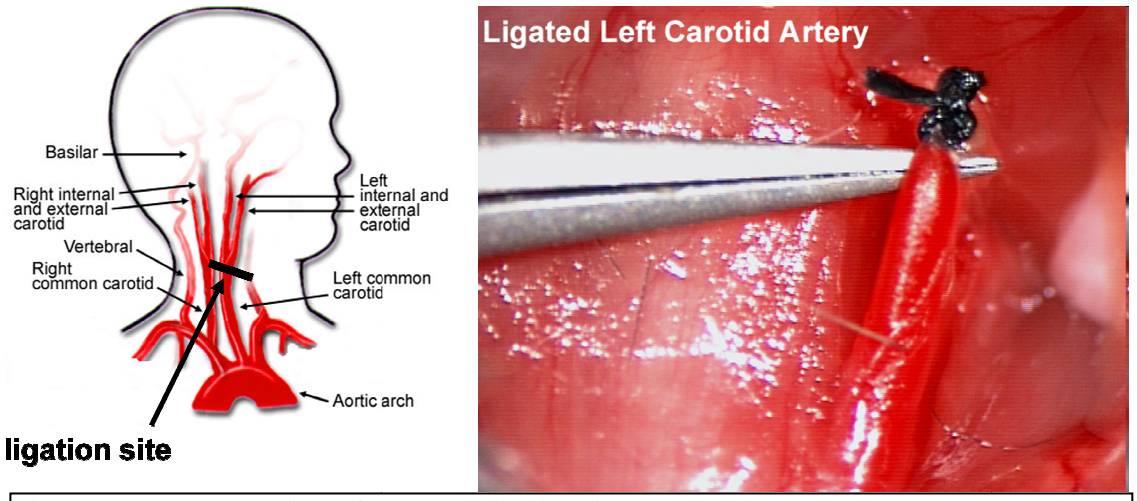

Figure 2.7. Illustration of the carotid ligation procedure. The left common carotid artery is dissected away from fascial layers in the neck, just lateral to the trachea, and silk suture is used to tie off the artery just proximal to the bifurcation between the internal and external carotid arteries. This interrupts net forward flow from the heart, although the vessel remains pressurized proximally at physiologic blood pressures.

The procedure involves dissection of the left common carotid artery away from the carotid sheath and vagus nerve in the neck and permanent ligation with silk suture just proximal to the bifurcation forming the left internal and external carotid arteries (Figure 2.7). The result is the abolition of net forward flow through a section of elastic artery that arises as a branch off the aorta but contains no other branches of its own, while pulsatile pressures remain intact and active until sacrifice[50]. Most animals survive the procedure without symptoms of stroke, due to relatively robust collateral cerebral circulation in rodents[54,55], and continue normal behavior. In our experience, a brief period of weight loss and recovery occurs in the first 3-7 post-operative days related to neck pain and decreased motivation for eating and drinking. Animals are supported through this period with analgesics and limited subcutaneous administration of fluids.

Alterations in blood flow and shear stress on the walls of arteries can independently induce adaptive vascular remodeling. A classic example is the "Glagov phenomenon," where increased flow velocity and shear stress, in Glagov's case due to narrowing of a coronary artery lumen by atherosclerotic plaque buildup but also through exogenous narrowing by partial ligation of the carotid, appears to direct enlargement of the arterial media diameter[56,57]. On the other hand, decreases in flow velocity and shear stress promote narrower vessels, either by restriction of medial enlargement[58] or by driving orientation and hyperplasia of occlusive fibromuscular cells in the neointima[59]. The stereotyped development of atherosclerotic lesions at certain anatomical locations, namely bifurcations, branch ostia (openings), and curvatures, has long been associated with vascular geometries susceptible to decreased flow and shear stress[60].

However, decreased flow, as in the carotid ligation injury model, also promotes formation of thrombus through the accumulation of platelets and coagulation factors, expediting the kinetics of platelet activation and fibrin polymerization[61]. Investigations of early events in arteries following carotid ligation (e.g., one week post-operatively) reveal extensive platelet-rich and fibrin-rich thrombi in the lumen[62]. Thus, an intense interaction between thrombus formation/resolution and neointimal hyperplasia in the carotid ligation model of injury captures this element of the pathophysiology of diseases like atherosclerosis[63] or restenosis following endovascular intervention[64,65], which involve localized wall injury, flow disruption, and thrombogenesis. In vEDS and sCAD patients, risk factors for thrombosis could include decreased flow but may also include minor tears in the wall, as from stretch or from hypertensive episodes that expose the "hemostatic envelope" of tissue factor protein embedded in the media and adventitia, which quickly activates the coagulation cascade[66].

The initial descriptions of neointimal formation in arteries following ligation indeed mention the histological appearance of organizing thrombus in injured vessels but neglect to link the phenomenon with intimal hyperplasia, since most arteries contain no evidence of thrombus at the later time points of investigation[53]. Other researchers ligating veins in order to study thrombus organization noted occasional continuity between resolving thrombi and "invading" intimal hyperplasia[67]. However, the strongest evidence of thrombus resolution necessarily preceding neointima formation emerges from studies exploiting carotid injury in animals genetically deficient in fibrinolytic enzymes. These studies found that inhibiting resolution of thrombus prevents the development of neointima by late time points (e.g., three weeks post-operatively)[68].

Although these studies exogenously applied ferric chloride to arteries to injure them, other researchers performing carotid ligation discovered that depleting animals of fibrin or platelets also prevents development of neointima by late time points[62].

Thrombus Resolution, Wound Healing, and New Matrix Production

Thrombus organization and resolution remarkably resembles wound healing, where polymerized fibrin at the site of injury forms a nidus for recruitment of inflammatory cells, followed by a wave of migrating fibromuscular cells to remodel and contract the provisional fibrin matrix into a collagenous scar[62,69,70]. We suspect that defective wound healing in vEDS patients, which necessitates the new synthesis of both type III and type I collagen, may comprise not only dysfunctional responses to cutaneous injury but also dysfunctional responses to arterial injury. Familiarity with the orchestrated processes of wound healing and scar formation would guide a more purposeful investigation of processes driving thrombus resolution and neointima formation.

Wound healing progresses through three overlapping phases: the inflammatory phase extending through post-injury days 3 to 7, the tissue formation/proliferative phase extending through day 14, and the more indefinite tissue remodeling/contraction phase[19,28]. The early inflammatory phase entails the recruitment, activation, and infiltration of circulating inflammatory cells into fibrin clots via chemoattractants released by platelet degranulation and/or coagulation/complement activation. In this phase, initial sources of the pro-fibrotic cytokine transforming growth factor-β1 (TGF-β1) include both platelets and activated macrophages, although depletion of platelets

permits normal wound healing while depletion of macrophages does not, suggesting that the sustained, amplified signaling by macrophages critically drives downstream repair activity by resident cells[19,28,71]. Although not acknowledging thrombus resolution as such, vascular biologists also describe very early platelet and inflammatory production of TGF-β1, as well as enzymatic release of its active form from the local matrix, that is necessary for later neointimal thickening following vascular injury[72].

The tissue formation or proliferative phase begins with the activation, proliferation, and migration of previously sedentary cells into the wound margin or thrombus. TGF-β1 acts both as chemotactic agent and mitogen for skin fibroblasts[71], initiating their transformation into myofibroblasts with a comparatively striking capacity for matrix synthesis and cellular contractility[73]. The effect of TGF-β1 on vascular smooth muscle cells is less clear from the cell culture literature, where TGF-β1 can stimulate or inhibit proliferation based on cell density or dose[72]. Following *in vivo* injury by balloon angioplasty, however, infusion of recombinant TGF-β1 stimulated proliferation of cells in the neointima but *not* cells in the media, suggesting that the cells residing in the neointima behave more like myofibroblasts than smooth muscle cells[74].

Rapid synthesis of new matrix and angiogenesis necessary to supply nutrients for high metabolic activity in this middle phase earn the name of "granulation tissue" for the emerging stroma, as gross inspection reveals a red granularity from dense capillaries[28]. One of the first associations of TGF-β1with wound healing arose from its subcutaneous injection into neonatal mice, which was sufficient to induce new granulation tissue including neovascularization and fibrosis[75]. Formation of granulation tissue could prove to be a critical juncture of events in wound healing for type III collagen-deficient vEDS

patients and mice, as *de novo* conversion of provisional fibrin matrix into collagenous matrix in the skin heavily involves the new secretion of both type I *and* type III collagen[73,76], while a similar burst of gene expression for type I and type III collagen synthesis, as measured by transcription of *Col1a2* and *Col3a1*, coincides with neointimal formation following intraluminal injury in rats[74].

The extent of neovascularization positively correlates with the rate of thrombus resolution in experimental models of deep vein thrombosis[69,70], suggesting that neovascularization is essential for recanalizing the lumen of occluded vessels. In thrombus resolution, neovascularization appears both as endothelial cell-lined vascular channels continuous with lumen that extend axially through the body of the thrombus and as endothelial cell lining at the circumferential thrombus surface that invaginates into perforating clefts, sometimes observed in continuity with inward extensions of the adventitial vasa vasorum[70] (Figure 2.8). In diseases involving arterial thrombosis, however, neovascularization is often regarded as a problem. Fragile neovessels limited to sites of injury extend from the vasa vasorum through the media and into intimal plaque, where they are thought to increase the risk for intramural hemorrhage and plaque instability in atherosclerosis[77]. Following intravascular stenting, the incidence of neovessels corresponds with neointimal thickness, and investigators predicted later strategies of reducing stenotic neointimal growth by the use of agents to prevent neovascularization[78].

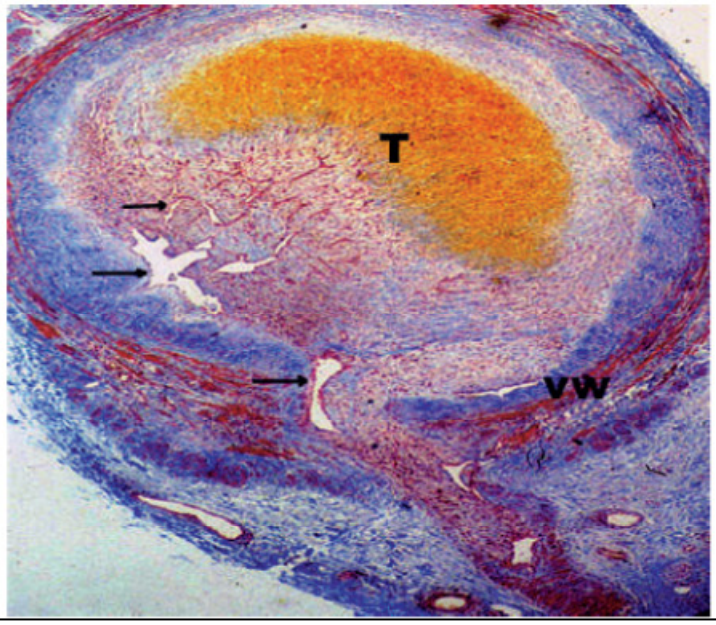

Figure 2.8. Transverse section through a human vein containing organizing thrombus stained by MSB. Erythrocytes yellow, fibrin and smooth muscle cells red, and collagen blue. Note areas of neovascularization (arrows) appearing at the thrombus wall interface and within the body of the thormbus. Reprinted with permission from Schattauer GmbH [The role of neovascularisation in the resolution of venous thrombus. Modarai B, Burnand KG, Humphries J, et al. *Thrombosis and Haemostasis*. 2005].

The final stage of wound healing, the remodeling and contraction phase, involves the contraction of volume of granulation tissue through a compaction and reorganization of the newly synthesized matrix, as well as a drop in the cellularity and vascularity of the resulting scar[28,79]. This phase will be discussed in much more depth in Chapter 3.

For the first aim of this project, we sought to confirm defective vascular wound healing in type III collagen-deficient mice. We induced vascular injury in type III collagen-deficient mice through carotid ligation and followed the development and subsequent resolution of thrombus alongside the development of neointimal hyperplasia at various post-operative timepoints. From this we discovered delayed thrombus resolution in *Col3a1*$^{+/-}$ mice in association with a significantly higher incidence of neovascularization penetrating into media. Overexuberant neovascularization began in the proliferative and tissue formation phase of vascular wound healing, which was also

associated with excessive burdens of tissue macrophages and proliferating fibromuscular cells in resolving thrombi. Neovessels persisted over time in type III collagen-deficient animals, in contrast to wild-type littermates, abnormally appearing even in arterial segments containing mature neointimal lesions. We suggest that the abnormal persistence of these neovessels and dysfunctional vascular wound healing contributes to the risk for dissection and/or rupture of arteries in patients with vEDS and sCAD.

Methods

Mouse Husbandry, Breeding, and Genotyping

Cryopreserved embryos derived from the *Col3a1* knockout on BALB/c background mouse line developed by Liu, et al.[15] were purchased and transferred into surrogate BALB/c mothers for the recovery of two litters of $Col3a1^{+/+}$ and $Col3a1^{+/-}$ adult mice by Jackson Laboratories (Bar Harbor, ME). Adults were subsequently mated in-house in $Col3a1^{+/+}$ x $Col3a1^{+/-}$ (wild-type crossed with heterozygote) pairs for a breeding scheme to produce litters with Mendelian ratios of ~50% $Col3a1l^{+/+}$ and ~50% $Col3a1^{+/-}$ offspring. No differences in size, genotype ratios, or number of litters were obvious in regards to the genotype of mated females, nor were any differences noted in the ability of mothers to nurse pups to weaning age. All animals were housed and maintained in the Center for Laboratory Animal Medicine and Care at the University of Texas Medical School at Houston according to standards set by the NIH Guide for the Care and Use of Laboratory Animals and the institutional Animal Welfare Committee. Genotyping of weanlings was performed on DNA extracted from ear pieces and

amplified by a modified PCR protocol using primers for *Col3a1* exon/intron 1 and the *Neo* cassette knockout allele designed by Stevenson, et al.[80].

Carotid Ligation Injury

Ligation of the left common carotid artery was surgically performed on animals weighing between 27 and 33g and aged between 22 and 24 weeks (unless otherwise stated), corresponding to the tail end of the mature adulthood phase in mice (age 3 to 6 months) through which animals have completed development but are not yet influenced by senescence, according to estimation from the gerontology laboratory of David Harrison, PhD at Jackson Laboratories. This phase approximates the span of 20 to 30 years of age in humans (http://research.jax.org/faculty/harrison/ger1vLifespan1.html), in which the risk of fatal complications in vEDS patients rapidly increases[10]. However, this phase in the *Col3a1* knockout mouse model is not associated with any differences between $Col3a1^{+/+}$ and $Col3a1^{+/-}$ mice in risk for complication or survival[15].

Anesthesia was induced with 4% isoflurane inhaled in an induction chamber and maintained by 2-2.5% isoflurane inhaled through a nosecone. The surgical procedure involved preemptive analgesia with subcutaneous ketoprofen (5 mg/kg), a midline incision in the neck, dissection of the left common carotid artery away from the carotid sheath and vagus nerve, and ligation of the artery with 5-0 silk suture just proximal to the bifurcation of the internal and external carotid arteries[50]. Wounds were irrigated with sterile saline and closed by 2-3 interrupted stitches with absorbable 5-0 suture.

Approximately 20% of animals either recovered from the procedure with symptoms of stroke, developed symptoms of stroke over the first 7 post-operative days,

or failed to maintain less than 20% loss in body weight and were sacrificed. Risk of stroke following carotid ligation in mice from a BALB/c background corresponds to strain-specific relative insufficiency in collateral cerebral flow[55]. Nonetheless, neurologically intact animals were supported post-operatively for 2 days with subcutaneous ketoprofen (2-5 mg/kg) twice a day for analgesia and for 7 days following daily weighing with subcutaneous 0.5-1 ml injections of lactated Ringer's solution as needed for >10% drops in body weight. No unexpected deaths occurred after post-operative day 7 (POD7), and animals were sacrificed on POD7, POD14, and POD21 for the various experiments described below.

qPCR Analysis of Col3a1 *Expression in Injured Arteries*

For extraction of cellular RNA from whole tissues, thoracotomy at sacrifice was followed by immediate dissection and harvest of fresh carotid arteries. To measure baseline expression of *Col3a1* in normal tissues, we harvested the lengths of normal left and right common carotid arteries (LCAs and RCAs) from 7-month-old mice, both $Col3a1^{+/+}$ and $Col3a1^{+/-}$, which had not undergone carotid ligation ($N = 3$ $Col3a1^{+/+}$, 3 $Col3a1^{+/-}$). Each harvested LCA extended from the ligature proximally to the branchpoint from the aorta, and each RCA extended from just proximal to its bifurcation down to the branchpoint from the brachiocephalic artery. To then measure the normal effects on *Col3a1* expression elicited by injury, we also harvested the injured LCAs and uninjured RCAs from 7-month-old $Col3a1^{+/+}$ mice ($N = 5$) on POD7 following carotid ligation.

Fresh arteries were quickly dipped in sterile RNase-free water to wash away excess blood and each immediately immersed in 1ml TRI reagent (Sigma, Saint Louis, MO) and frozen at -80°C. After confirmation of genotypes, separate artery samples were quickly thawed and tissues and TRI solvent pooled among experimental groups (normal left and right *Col3a1*$^{+/+}$ carotids together, normal left and right *Col3a1*$^{+/-}$ carotids together, injured post-operative *Col3a1*$^{+/+}$ LCAs together, and uninjured post-operative *Col3a1*$^{+/+}$ RCAs together) for homogenization within the same round-bottom tube using an electric Polytron homogenizer (Thomas Scientific) for at least one minute to disrupt connective tissue and lyse resident cells. Further RNA extraction was performed according to manufacturer's instructions, resulting in the dissolution of extracted RNA in sterile RNase-free water.

Resulting RNA concentration was measured by absorbance at 260nm using a NanoDrop ND-1000 spectrophotometer, and only samples with RNA purity determined by $A_{260}/A_{280} \geq 1.8$ were used. Reverse transcription of cDNA was performed according to instructions from a High-Capacity cDNA Reverse Transcription Kit (Applied Biosystems). Quantitative PCR was performed using pre-designed TaqMan assays for mouse *Col3a1* (the target gene) and *Gapdh* (the internal control gene) on an ABI Prism 7000 Sequence Detection System (Applied Biosystems). Quantification of normalized gene expression related *Col3a1* message levels from various post-injury samples to normalized baseline levels in an equivalent mass of RNA derived from uninjured carotid arteries according to the Comparative C_T method[81]. As we suspected that separate biological samples would be insufficient in size to yield RNA concentrations necessary for qPCR, we pooled similar samples during homogenization to generate only one

cDNA sample per experimental condition. Thus, we did not perform PCR on one cDNA sample per tissue within each experimental condition, and statistical analysis accounting for standard deviation between biological replicates by Student's *t* test was not possible. However, reported results still represent *Col3a1* message levels "averaged" among biological replicates by means of chemical diffusion rather than by statistical means. Error bars represent assay precision, i.e., standard deviation between fold-changes derived from triplicate PCR reactions performed on each cDNA sample.

Histological Analysis: Morphology

For histological analysis of arteries at POD7 (N = 5 *Col3a1*$^{+/+}$, 4 *Col3a1*$^{+/-}$), POD14 (N = 7 *Col3a1*$^{+/+}$, 4 *Col3a1*$^{+/-}$), and POD21 (N = 8 *Col3a1*$^{+/+}$, 9 *Col3a1*$^{+/-}$), thoracotomy at sacrifice was followed by puncture of left ventricles with a 22-guage needle. Right atria were incised to allow outflow of perfusate, and animals were perfused at <20 ml/min with phosphate-buffered saline until exsanguination was confirmed by blanching of the liver. We then perfused the mice with 10 ml of 4% paraformaldehyde or 10% buffered formalin at the same rate to initially fix arteries in their native geometry. We harvested the lengths of injured left common carotids and uninjured right common carotids as above.

Harvested arteries were further fixed by submersion in 4% paraformaldehyde or 10% buffered formalin overnight and routinely processed by automated machine. After processing, the arteries were chilled and cut twice with a scalpel: first just proximal to the ligature to remove the suture and preserve as much of the distal length as possible and secondly to bisect the artery into two pieces. With careful attention to maintaining

orientation, the pieces were each embedded into paraffin vertically in the same block with the distal tips downwards to allow for axial cross-section. Serial sectioning was performed through the entire block, collecting three 4 µm-thick sections per slide, with almost all sections each containing samples from both halves of tissue, until all of the original length of the artery had been collected in sequence. Every tenth slide from this sequence was then subjected to routine automated hematoxylin and eosin (H&E) staining and a representative section microscopically photographed at 20x and 40x power. This set of systematically sampled images allowed us to reconstruct an index of arterial histology as it varied along the full axial length of the injured tissues. Left common carotid arteries from each mouse supplied approximately 90 to 120 slides, corresponding to 18 to 24 index images per artery. All images are presented at 40x, unless otherwise stated, and scale bars represent 200µm. For 100x images, scale bars represent 50 µm.

Statistical Analysis: Incidence of Unresolved Thrombus and Neovessels

The cell-dependent resolution of intraluminal thrombi progresses like a migrating wave in the direction of blood flow[69], so that the maturity of wound healing represented by any given tissue section varies extensively as a function of non-uniform, especially localized phenomena related to the longitudinal location of the segment within the artery. Thus, arterial segments photographed in cross-section at a systematic distance from each other, even those from the same artery, each present highly unique information. The aggregated information resembles discrete, independent biological

events occurring at certain frequencies much more than it resembles dependent, clustered technical estimations of a continuous parameter.

As such, we treated each index H&E-stained slide as an independent sample and judged whether the individual arterial segment contained unresolved, occlusive thrombus or not and whether the individual segment contained circumscribed neovessels penetrating the arterial media or not. Multiple observers were blinded to the genotype of the arterial segments, and positive and negative ratings for all arterial segments under an experimental condition were decided independently by the same observers and agreed upon consistently, recorded, and pooled by genotype, $Col3a1^{+/+}$ or $Col3a1^{+/-}$. Results were entered into a 2x2 contingency table, and the actual frequencies of events were compared with expected frequencies predicted by the hypergeometric distribution by determining an exact probability using the Fisher's exact test. Significantly low *p*-values ($p < .05$) were interpreted to reject the null hypothesis that frequency of occlusive thrombus or of neovessels occurred independently of the genotype of the arterial segment.

Histological and Statistical Analysis: Immunohistochemistry, Macrophage Burden, and Prevalence of Proliferating Myofibroblasts in Unresolved Thrombi

Records of indexed H&E- stained arterial segments as obtained above provided the relative locations of segments containing occlusive thrombi. Unstained slides neighboring each of the thrombus-positive slides were subjected to immunohistochemical probes to determine the local burden of macrophages and the local prevalence of actively proliferating myofibroblasts within the resident thrombi.

Thus, each original thrombus-positive slide corresponded to a local slide measuring the number of Mac2-positive cells present and a second local slide measuring the number of phosphorylated histone H3 (pH3)-positive nuclei present. Unstained slides neighboring neovessel-positive index slides were similarly subjected to probes for the presence of CD31, a marker for immature endothelial cells and/or circulating endothelial cell precursors[82].

Unstained sections were deparaffinized and rehydrated by immersion in xylenes followed by immersion in a graded alcohol series. Most tissues were then subjected to heat-induced epitope retrieval (HIER citrate pH 6.0) and were blocked for 1h at room temperature with diluent. For imaging of resident macrophages, tissues were incubated for 1h at room temperature with rat anti-mouse Mac2 primary antibodies (Cedarlane, Burlington, NC). For imaging of mitotic nuclei, tissues were incubated overnight at 4˚C with rabbit anti-mouse pH3 primary antibodies (Millipore, Billerica, MA). To visualize neovessels, antigens were first retrieved with EDTA digestion (pH 8.0) instead of HIER, blocked, and incubated overnight at 4˚C with rat anti-mouse CD31 primary antibodies for formalin-fixed paraffin-embedded tissues (Dianova, Hamburg, Germany).

Tissues were then washed with phosphate-buffered saline, incubated for 1h with the appropriate biotinylated secondary antibodes, and primed with peroxidase-conjugated avidin/biotin complexes (Vectastain ABC-AP Kit, Vector Laboratories, Burlingame, CA). Peroxidase activity was imaged by the developing brown precipitate following immersion of the tissues in a solution of 3,3'-diaminobenzidine (DAB) chromogen (Dako, Glostrup, Denmark). Slides were counterstained with hematoxylin, methyl green, or a combination of methyl green and alcian blue.

As only slides with occlusive thrombi were sampled for prevalence of macrophages or proliferative cells, and as slides reflect local phenomena, it was appropriate to count the number of positive cells or nuclei from each of the relatively independent slides and determine a mean±SD from the pooled thrombus-positive slides corresponding to each genotype, *Col3a1*$^{+/+}$ or *Col3a1*$^{+/-}$. Significant differences between the means ($p < .05$) were determined by Student's *t*-test.

Results

Injury by carotid ligation induces substantial upregulation of Col3a1 *expression.*

The common carotid arteries from uninjured *Col3a1*$^{+/+}$ and *Col3a1*$^{+/-}$ mice at 7 months of age were pooled and RNA harvested to assess baseline *Col3a1* expression in adult arteries. Transcript levels in *Col3a1*$^{+/-}$ arteries were lower than in *Col3a1*$^{+/+}$ arteries, at 68.6±0.12% of those in normal arteries (Figure 2.9A). To determine whether *Col3a1* expression increases following acute arterial injury, we harvested both left and right common carotid arteries 7 days after ligation of the left common carotid in 7 months-old wild-type mice. In comparison to baseline levels in normal adult carotids, ligation of the left common carotid arteries directly induces a 34.5-fold upregulation (34.5±10.6) in *Col3a1* expression (Figure 2.9B). Interestingly, ligation of the left common carotids also induced a 6.74-fold upregulation (6.74±1.22) of *Col3a1* message levels in the unligated *right* common carotids (Figure 2.9B), presumably as a result of increased, redirected cerebral blood flow through these arteries.

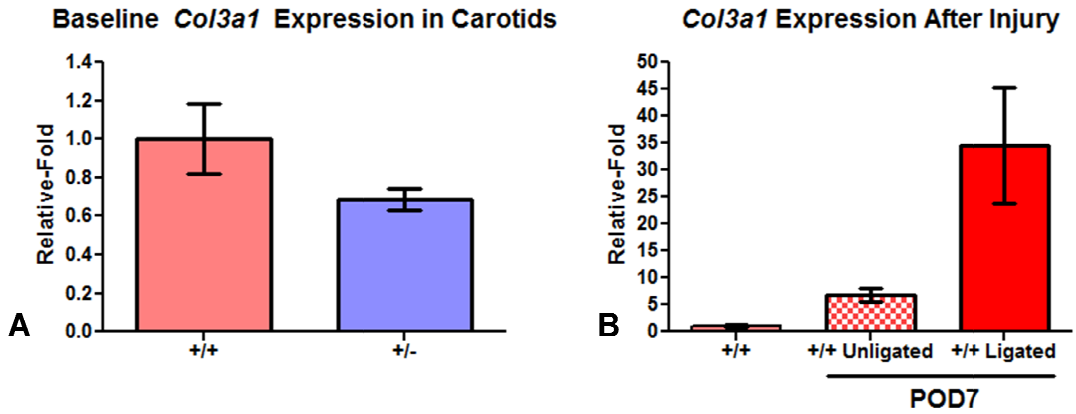

Figure 2.9. Expression of *Col3a1* at baseline and following arterial injury by carotid ligation. (*A*) *Col3a1* expression in heterozygous carotid arteries is 68.6±0.12% of that detected in wild-type carotids. (*B*) Relative to the baseline *Col3a1* expression in uninjured arteries as determined in *A*, expression following ligation injury to left common carotids increases 34.5±10.6-fold. At the same time, injury to the left common carotid also increases expression in the uninjured right common carotid by 6.74±1.22-fold.

Injury by carotid ligation reveals significantly higher burden of unresolved thrombi in Col3a1$^{+/-}$ *vs.* Col3a1$^{+/+}$ *arteries after 21 days.*

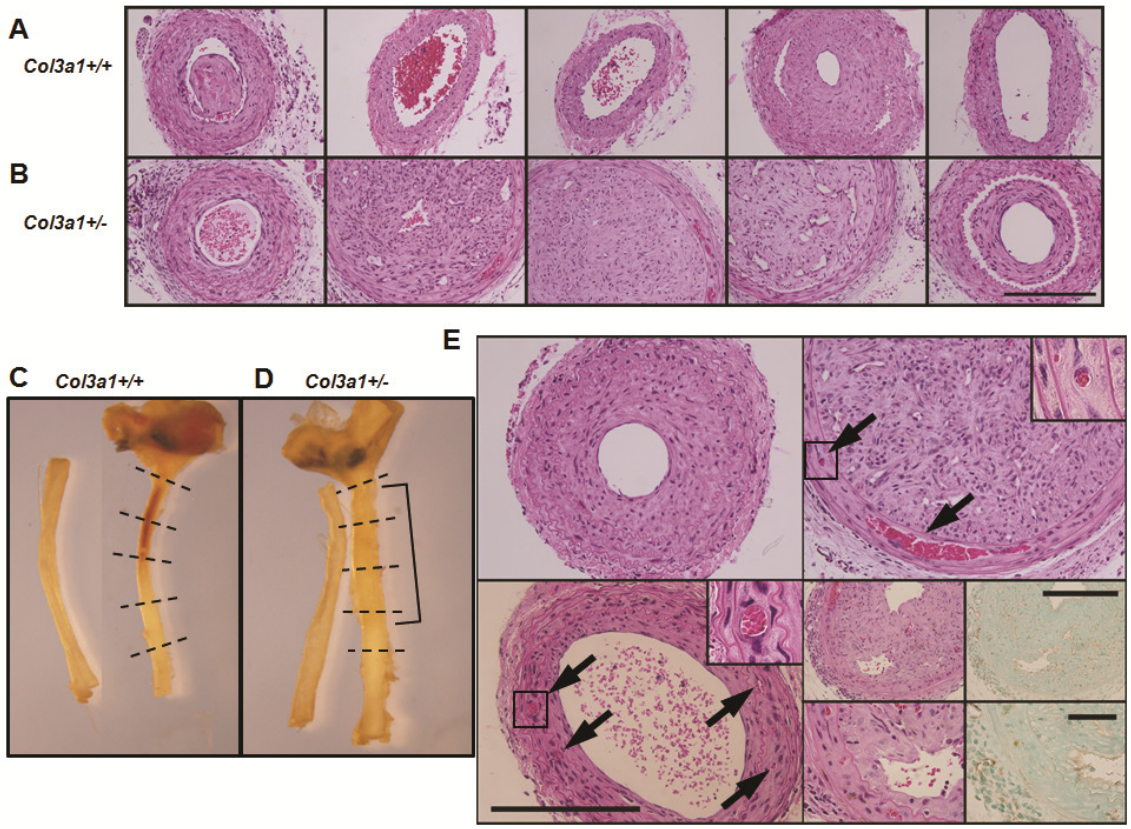

Figure 2.10. Morphology of arterial responses to carotid ligation by 21 post-operative days. (*A* and *B*) Representative sections (40x) showing variation of morphology along the arterial axis from the distal segments (left) down to proximal segments (right). Wild-type arteries display limited fibronoid thrombus with mostly patent arteries except for areas of neointimal thickening located remotely from the site of ligature. Mutant arteries contain significantly higher incidence of occlusive thrombi that are densely populated by myofibroblasts. Note penetrating endothelial cell-lined vascular channels extending upward and downward into the thrombus body from the poles. (*C* and *D*) Whole mounts (7x) of injured left common carotid arteries and uninjured right common carotid arteries, as positioned in the animal during surgery. Hatched lines indicate on injured arteries where representative sections were sampled. Brace on mutant artery denotes length of opacity correlating to occlusive thrombi in images. (*E*) Appearance of neovascular channels (arrows) penetrating the arterial media in mutant arteries both in areas with occlusive thrombus (upper right) and in areas with mature neointima (lower left), as compared with near total absence in wild-type arteries (upper left). Insets (100x) show endothelial cell lining. Positive CD31 stains of cells occupying these vascular channels (40x and 100x) confirm the presence of immature endothelial cells and/or circulating endothelial cell precursors (lower right).

To determine if *Col3a1* haploinsufficiency alters vascular wound healing after injury by carotid ligation, we ligated left common carotid arteries from 5.5-month old mice ($N = 8$ *Col3a1*$^{+/+}$, 9 *Col3a1*$^{+/-}$) and harvested the arteries at post-operative day 21 (POD21). We serially sectioned the entire length of the vessels from the distal blind pouch formed by the ligature down to the proximal branchpoint from the ascending aorta, subjecting every tenth slide to H&E stain to create a series of index slides. Thus, a representative map was constructed of the complete histological response as it varied along artery length. Normal wild-type arteries show limited residual fibrinoid thrombus near to the ligature, medial thickening along the entire length, and a more proximally located mature neointimal lesion, i.e., distant from the ligature (Figure 2.10A). A complete depiction of index slides derived from the entire length of a representative *Col3a1*$^{+/+}$artery is contained in Figure 2.11.

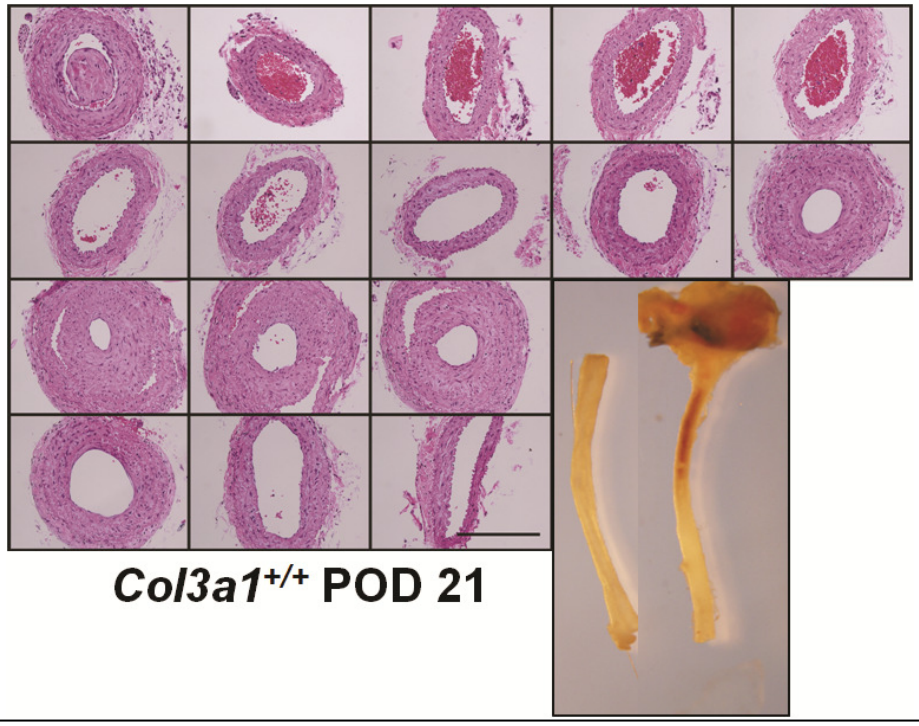

Figure 2.11. Representative map of varying morphology along the length of injured *Col3a1*$^{+/+}$ arteries at 21 days post-injury. Index images photographed from every tenth slide systematically collected during serial section. Organized here from right-to-left and top-to-bottom along the distal-to-proximal orientation, picturing the pole near the ligature at top left and the pole near the branchpoint from the aorta at bottom right. Whole mounts included for correlation with histology.

In contrast, many *Col3a1*$^{+/-}$ arterial segments resemble their *Col3a1*$^{+/+}$ counterparts in terms of medial thickening and isolated lengths of neointimal scarring, but we noted a significantly higher number that contain thrombi (Table 2.2, $p = .0289$). These segments displayed features of active thrombus organization, including matrix-rich luminal contents containing floridly dense myofibroblasts, macrophages (as determined below), and endothelialized vascular channels penetrating the thrombus (Figure 2.10B). A complete depiction of index slides derived from the entire length of a representative *Col3a1*$^{+/-}$ artery is contained in Figure 2.12, which demonstrates the linear continuity between areas notable for classic neointimal hyperplasia and those notable for recanalizing thrombus via axial neovascularization.

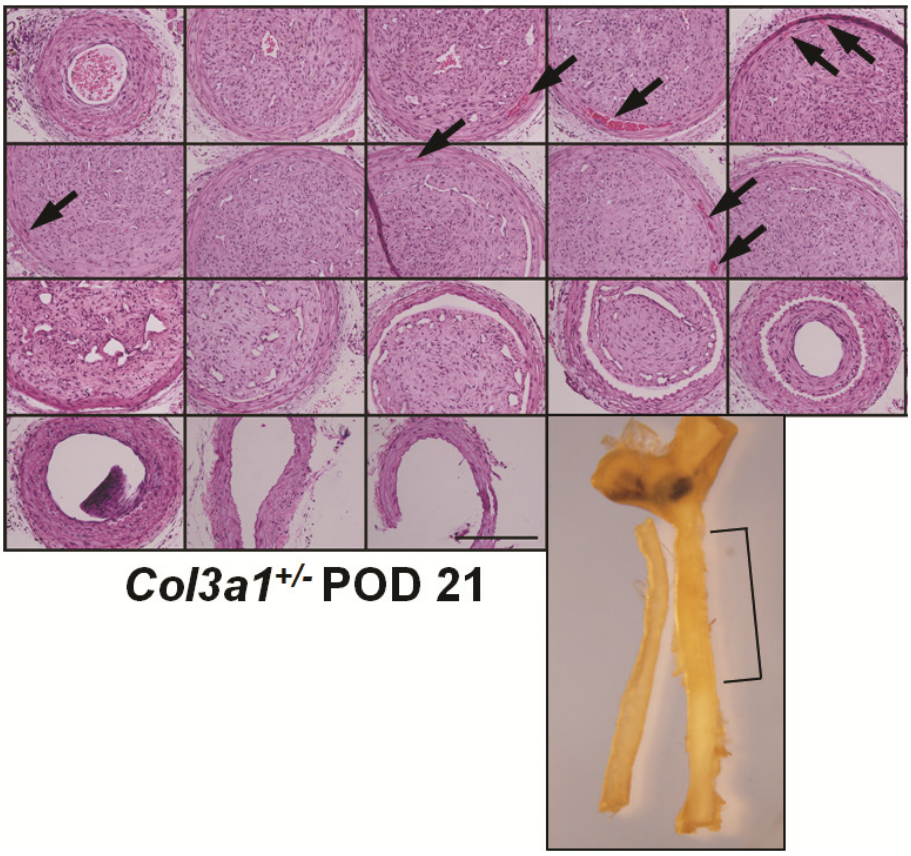

Figure 2.12. Representative map of varying morphology along the length of injured *Col3a1*$^{+/-}$ arteries at 21 days post-injury. Index images photographed from every tenth slide systematically collected during serial section. Organized here from right-to-left and top-to-bottom along the distal-to-proximal orientation, picturing the pole near the ligature at top left and the pole near the branchpoint from the aorta at bottom right. Whole mounts included for correlation with histology. Note the continuity between segments depicting classic neointimal hyperlasia with segments containing resolving thrombus and recanalization by neovascularization. Arrows indicate medial vascular channels.

It was also notable that uninjured right common carotid arteries do not differ in gross histological appearance or size between *Col3a1*$^{+/-}$ and *Col3a1*$^{+/+}$ mice, as apparent both on whole mount (Figure 2.10C and D) and in cross section (data not shown), consistent with findings from Liu, et al.[15]. Thus, differential morphology is locally limited to areas of arterial injury.

Persistent neovascularization occupies media of injured Col3a1$^{+/-}$ *arteries at 21 days.*

In addition to the increased thrombus burden of ligated carotids from *Col3a1*$^{+/-}$ versus wild-type mice, blood-filled vascular channels are present within the medial layer of mutant arteries (arrows, Figures 2.10B and E and 2.12) and absent in wild-type carotids (Figures 2.10A and E and 2.11). Immunostaining for immature endothelial cells using an antibody directed against the CD31 marker not only confirmed endothelial lining of intrathrombotic vascular channels but also identified CD31-positive cells within the vascular channels of the media. Often these channels appeared near to CD31-positive vaso vasorum in the adventitia or to CD31-positive intrathrombotic clefts in resolving thrombi, and sometimes they appeared in between both (Figure 2.10E). This evidence suggesting neovascularization in *Col3a1*$^{+/-}$ arteries occurred not only in segments of still-active thrombus resolution but also in remote sections containing mature neointimal scars (Figure 2.10E), even occurring in *Col3a1*$^{+/-}$ arteries in which no residual thrombi were detected at all. Arterial segments containing vascular channels, although rare within any individual artery, were present at least once in almost all arteries from *Col3a1*$^{+/-}$ mice, in comparison to a near complete absence in those from *Col3a1*$^{+/+}$ mice (Table 2.2, $p = .0016$).

Timepoint	Measure	+/+ Pos	+/+ Neg	+/- Pos	+/- Neg	*p*-value
POD7	Thrombus	8	62	7	48	1.000
N=5,4	Medial Bleed	21	49	18	37	0.8462
POD14	Thrombus	44	98	24	55	1.000
N=7,4	Neovessels	15	127	20	59	**0.0065**
POD21	Thrombus	7	70	25	91	**0.0289**
N=8,9	Neovessels	1	76	17	99	**0.0016**

Table 2.2. Incidence of occlusive thrombi within the lumen and blood-filled channels within the media of arteries at 7, 14, and 21 days after carotid ligation. Although *N* denotes number of mice receiving carotid ligation from wild-type and mutant groups, respectively, we compared the number of slides positive or negative for thrombi or blood-filled channels in each of the groups to the expected hypergeometric distribution for statistical analysis using the Fisher's exact test. Results showed no difference in incidence of thrombi or channels at POD 7, no significant difference in incidence of thrombi at POD14 but a very significant increased incidence of neovessels in mutant arteries, and significantly increased incidence of thrombi and very significant increased incidence of neovessels in mutant arteries at POD 21. POD = post-operative day.

Delayed thrombus resolution and increased incidence of medial neovessels are a late consequence of carotid ligation.

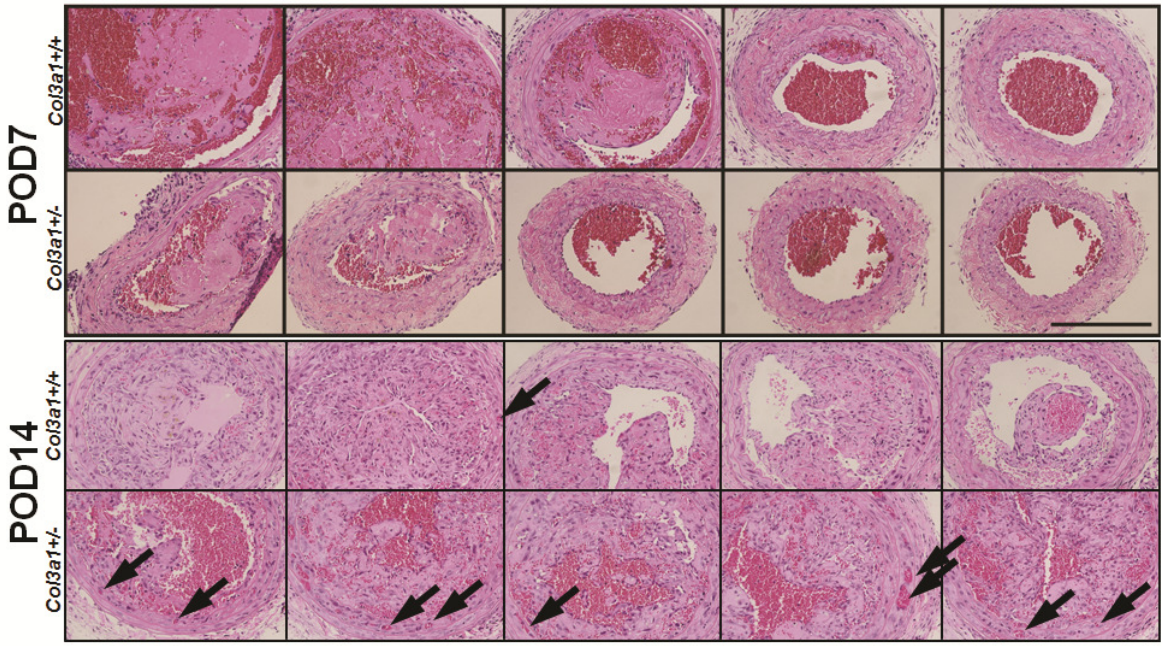

Figure 2.13. Morphology of thrombus and neovessels in wild-type and mutant arteries at 7 and 14 days after carotid ligation. *Top*, At POD 7, wild-type and mutant arteries harbored minimal fibrin-rich thrombi (pink acellular material) in the lumina, as depicted in the five most distal arterial segments collected as index slides. *Bottom*, In stark contrast, both wild-type and mutant vessels at POD 14 often contained thrombi floridly dense with myofibroblasts and invaginating clefts that were lined by endothelial cells. Although arteries from both genotypes contained medial neovessels (arrows), the overabundance in mutant arteries diverged significantly by 14 days.

We sought to determine if the increased thrombus burden observed 3 weeks after carotid ligation in mutant mice resulted from differences in early thrombogenesis. To address this question, carotid arteries were harvested 7 days ($N = 4$ Col3a1$^{+/-}$ arteries, 4 Col3a1$^{+/+}$ arteries) and 14 days ($N = 4$ Col3a1$^{+/-}$ arteries, 7 Col3a1$^{+/+}$ arteries) after ligation for systematic histological analysis performed as described above. At post-operative day 7 (POD7), minimal acellular fibrinoid thrombi, if observed at all, were located just proximal to the ligature and occupied a relatively low proportion of arterial

segments (Figures 2.13, 2.14, and 2.15). Between the two genotypes, there were no differences in the frequency of early thrombogenesis (Table 2.2; $p = 1.000$).

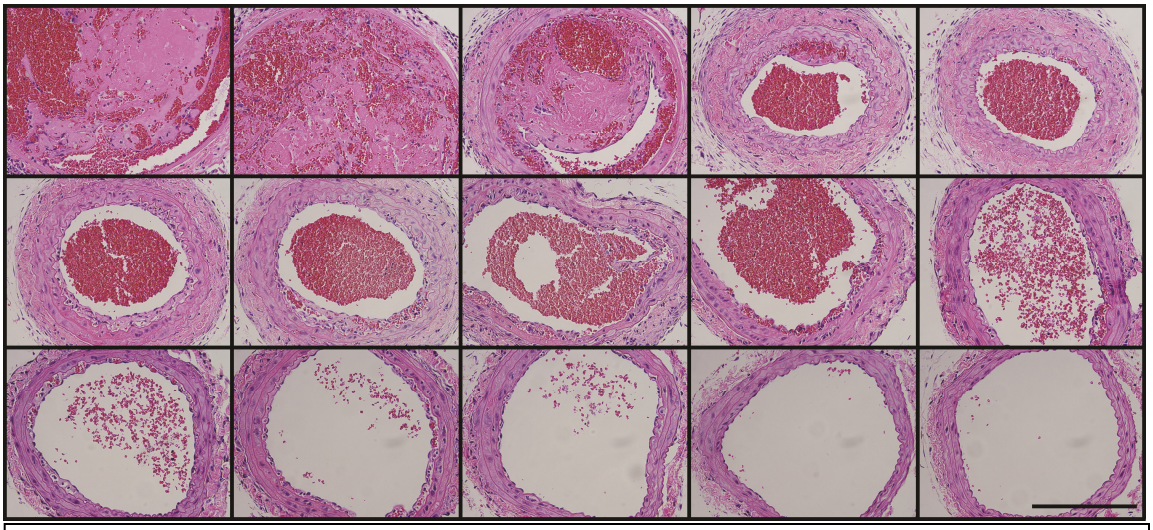

Figure 2.14. Representative map of varying morphology along the length of injured *Col3a1*$^{+/+}$ arteries at 7 days post-injury. Note the paucity of occlusive thrombogenesis at the distal pole of the artery. A slight fibrinous layer encircles the lumen in more proximal segments.

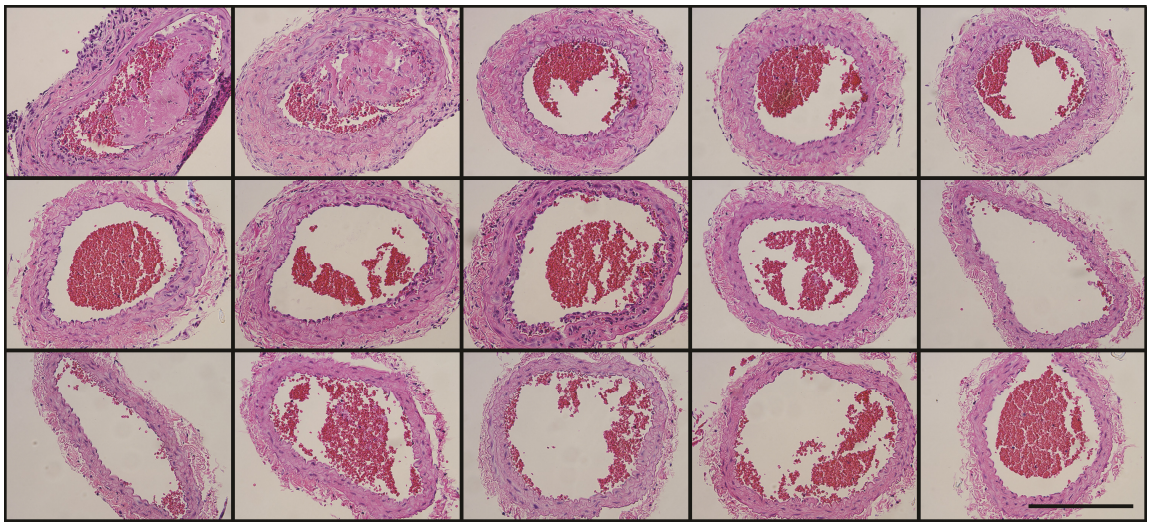

Figure 2.15. Representative map of varying morphology along the length of injured *Col3a1*$^{+/-}$ arteries at 7 days post-injury. As in 2.13, note the paucity of occlusive thrombogenesis at the distal pole of the artery. Also, a similar fibrinous layer lines the lumen in some more proximal segments.

In arterial segments from both genotypes in this early phase of vascular wound healing, we also note blood-filled spaces within the medial layer, although histologic characteristics suggest a process apart from neoangiogenesis. These spaces lack the circumscribed appearance of neovessels from Figure 2.10E and instead occupy thin bands or gaping tracts within the media, often in areas lacking nuclei of resident smooth muscle cells. We speculate that red blood cells within acellular areas of fibrinoid necrosis in the wall may have arrived by means less purposeful than neoangiogenesis and possibly arrived secondary to local weakening of injured arteries during early hemostasis. In any circumstance, the appearance of blood-filled spaces occurs at similar frequencies in arteries from both groups (Table 2.2; $p = 0.8462$).

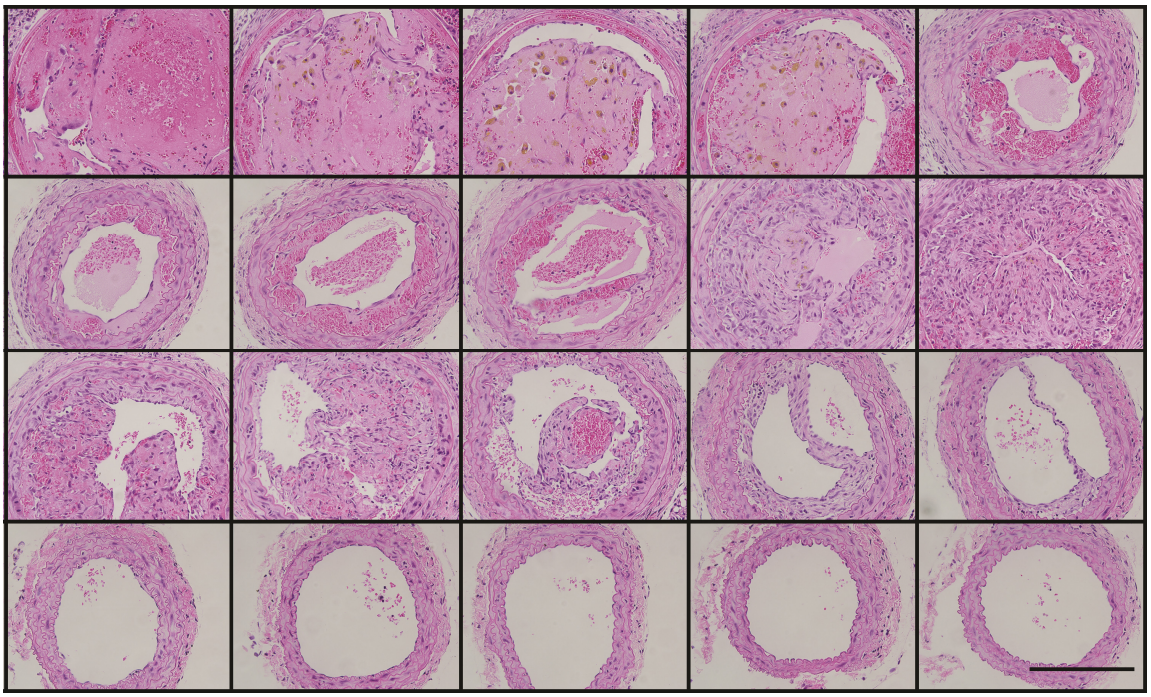

Figure 2.16. Representative map of varying morphology along the length of injured *Col3a1*$^{+/+}$ arteries at 14 days post-injury. Note hemosiderin-laden macrophages migrating into the acellular fibrin-rich thrombus at the distal pole, followed by invaginating clefts. In more proximal segments, fibrinous collar lined by endothelial cells. Central occlusive thrombi are densely cellular and contain newly synthesized matrix, showing progressive resolution with decreasing distance from the more proximal pole.

To examine the intermediate steps in the progression of thrombus organization we examined injured left common carotid arteries after 2 weeks (POD14). These arteries show the greatest morphological variation along the length of organizing thrombi, with the most advanced stages of resolution and nearly complete recanalization seen near the proximal pole and primitive fibrin-rich thrombi containing hemosiderin-laden macrophages and initial recruitment of fibroblasts at the peripheries in segments nearest to the ligature at the distal pole (Figures 2.16 and 2.17). The thrombus burden in both mutant and wild-type arteries increases dramatically between POD7 and POD14, and the total burden at POD14 was statistically equal in both genotypes (Table 2.2; p =

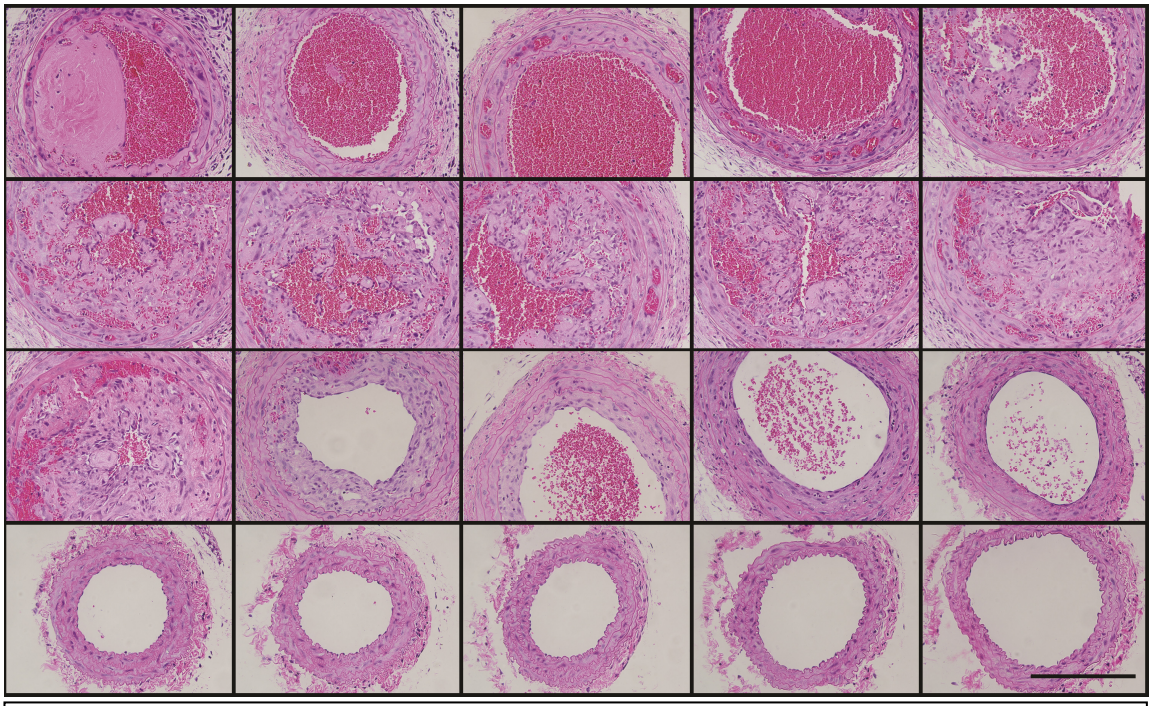

Figure 2.17. Representative map of varying morphology along the length of injured *Col3a1*$^{+-+}$ arteries at 14 days post-injury. Note macrophages migrating into the acellular fibrin-rich thrombus at the distal pole and endothelial lining continuous with fibrinous collar. In more proximal segments, occlusive thrombi are densely cellular and contain newly synthesized matrix, showing progressive resolution with decreasing distance from the more proximal pole and even resolving into areas with the appearance of classic neointimal formation. Abundant neovessels are apparent in segments surrounding actively resolving thrombi.

1.000). However, *Col3a1+/-* contain a very significant higher number of segments containing medial neovessels, similar to the findings at POD21 (Table 2.2; $p = .0065$).

Unresolved thrombi in Col3a1$^{+/-}$ *arteries at 14 and 21 days post-injury retain higher burdens of inflammatory macrophages.*

The increase in medial neovessels in *Col3a1*$^{+/-}$ segments at POD14 suggests increased pro-neoangiogenic signaling in association with a deficiency in new synthesis of type III collagen in the resolving thrombus. Infiltration of thrombi with inflammatory cells, including first-wave neutrophils and second-wave macrophages, is normally necessary for effective wound healing in the skin. This inflammatory phase of wound healing then initiates the recruitment of fibroblasts and sustains their subsequent orchestration of the proliferative phase[28]. Within the parallel scenario of thrombus resolution, we sought to determine whether any differences between *Col3a1*$^{+/-}$ and *Col3a1*$^{+/+}$ arteries in the numbers of macrophages residing in the thrombi could possibly contribute to differential regulation of thrombus resolution.

Arterial segments from POD7, POD14, and POD21 slide sets were immunoprobed for the mouse macrophage marker, Mac2. Mac2-postive cells were counted in all sections representing occlusive thrombi, revealing no significant differences at POD7 (Figure 2.18; $N = 8$ *Col3a1*$^{+/+}$, 7 *Col3a1*$^{+/-}$ segments; $p = .5698$) but an extremely significant higher mean number of macrophages per segment of occlusive thrombus in *Col3a1*$^{+/-}$ arteries at POD14 (Figure 2.18; $N = 44$ *Col3a1*$^{+/+}$, 24 *Col3a1*$^{+/-}$ segments; $p < .0001$).

By POD21, the number of *Col3a1*$^{+/+}$ segments containing occlusive thrombus decreases dramatically (Table 2.2) with a low number of macrophages identifiable in the residual thrombi. Macrophages residing in *Col3a1*$^{+/-}$ segments, on the other hand, maintain very significant higher numbers on average through POD21 (Figure 2.18; $N = 7$ *Col3a1*$^{+/+}$, 19 *Col3a1*$^{+/-}$ segments; $p = .0036$). Notably, many of these segments retain the high-density, high-activity appearance described at POD14, and some segments even contain numbers of inflammatory cells in excess of those identified at the earlier timepoint.

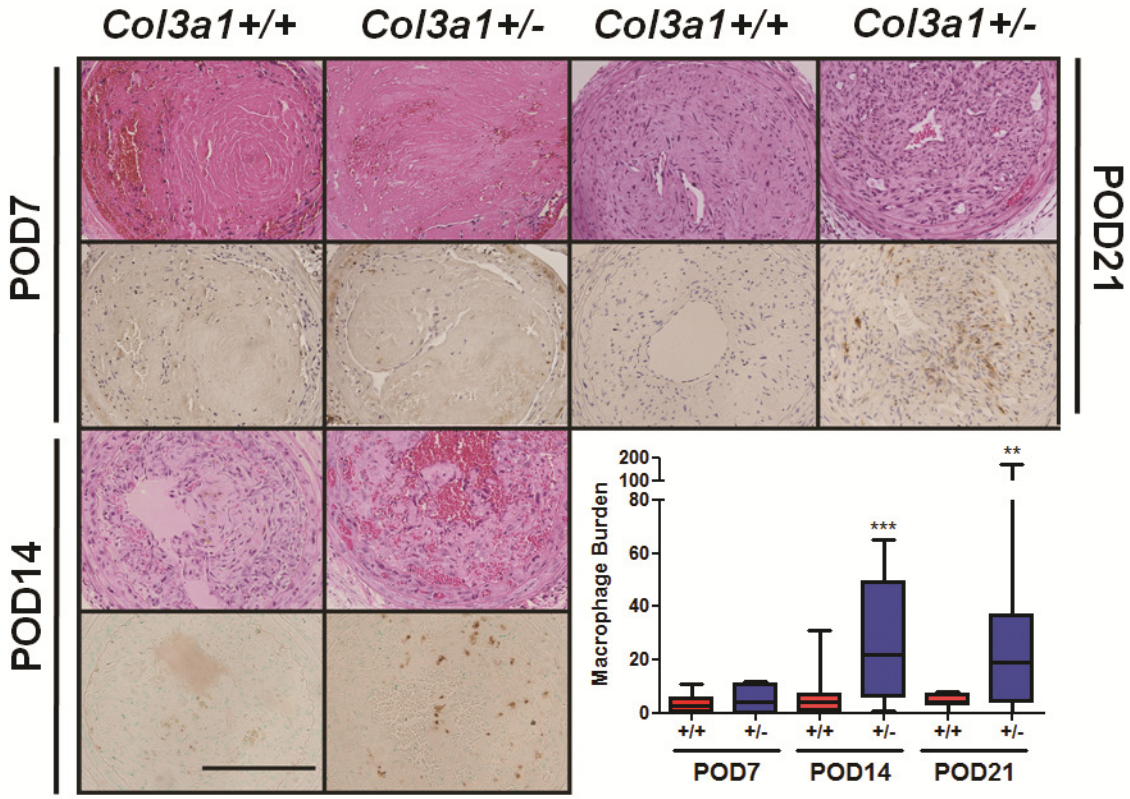

Figure 2.18. Macrophage burden in occlusive thrombi at 7, 14, and 21 days after carotid ligation. Thrombi were immunoprobed with an antibody directed against the mouse macrophage marker, Mac2. Counts revealed significantly higher numbers in mutant arteries at POD14 and POD21 but not in POD7. Note that the mean numbers increase at POD14 and are maintained at POD21 in mutant thrombi but slightly increase and peak at POD14 but regress by POD21 in wild-type thrombi.

Unresolved thrombi in Col3a1$^{+/-}$ *arteries at 14 and 21 days post-injury contain higher numbers of proliferative myofibroblasts.*

As thrombus burden increases with time from POD7 to POD14 (Table 2.2), apparently through the synthesis of new matrix by resident myofibroblasts (Figures 2.16 and 2.17) , we attempted to determine if the proliferative behavior of myofibroblasts could potentiate thrombus burden and contribute to a scenario akin to unresolved granulation tissue and fibrocontracture[73], perhaps helping explain the persistence of macrophages and neovessels at POD14 and persistence of thrombus at POD21. Arterial segments again from POD7, POD14, and POD21 were stained with antibodies directed against the nuclear phospho-histone H3 (pH3) marker of mitotic cells.

Quantitation of pH3-positve nuclei demonstrate a very significant higher mean number of mitotic cells per segment of occlusive thrombus in *Col3a1*$^{+/-}$ arteries at POD14 (Figure 2.19; $N = 42$ *Col3a1*$^{+/+}$, 24 *Col3a1*$^{+/-}$ segments; $p = .0059$) and at POD21 ($N = 6$ *Col3a1*$^{+/+}$, 22 *Col3a1*$^{+/-}$ segments; $p = .0038$) but not as early as POD7 ($N = 7$ *Col3a1*$^{+/+}$, 7 *Col3a1*$^{+/-}$ segments; $p = .5523$). Although many segments from *Col3a1*$^{+/+}$ arteries also contain a large number of mitotic cells in areas of fulminant proliferative phase wound healing at POD14, we observed yet higher numbers of proliferative myofibroblasts in *Col3a1*$^{+/-}$ thrombi. Similar to the assessment of macrophage burden, a dramatic drop occurs in the number of mitotic cells present in the few residual *Col3a1*$^{+/+}$ thrombi at POD21, while the average number of mitotic cells in *Col3a1*$^{+/-}$ thrombi continues to increase (Figure 2.19).

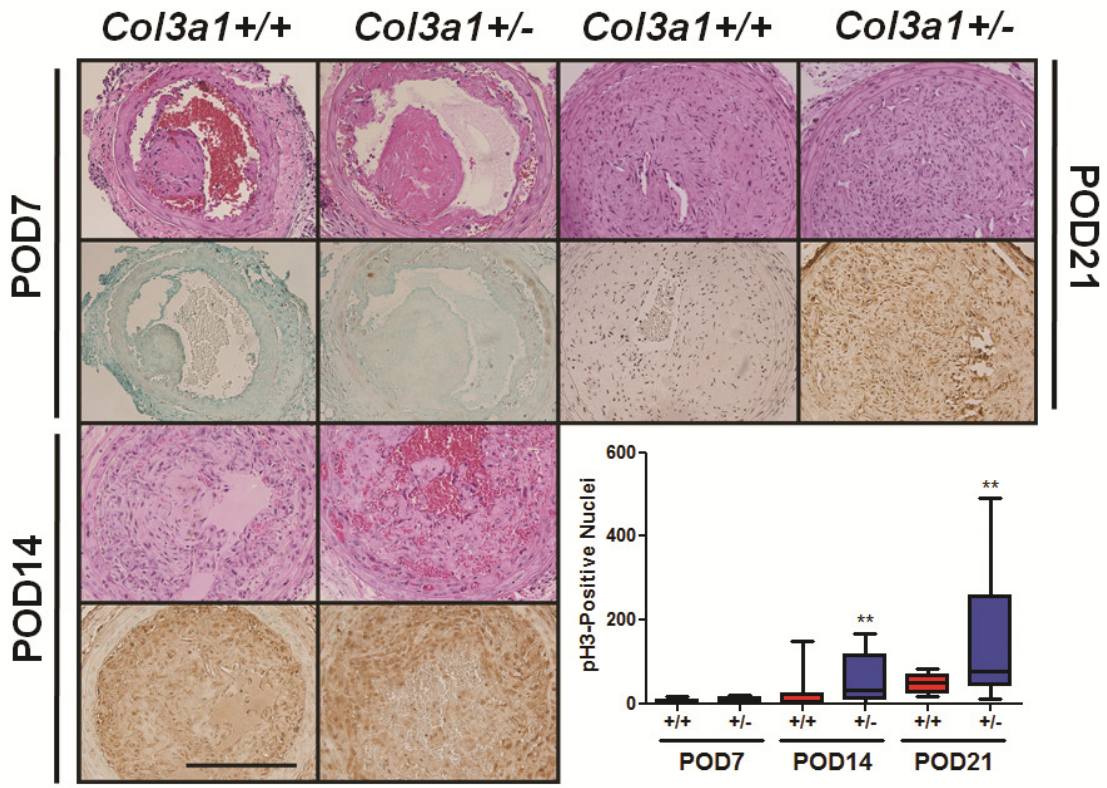

Figure 2.19. Number of proliferative myofibroblasts in occlusive thrombi at 7, 14, and 21 days after carotid ligation. Thrombi were immunoprobed with an antibody directed against the proliferative marker, phospho-histone3 (pH3). Counts revealed significantly higher numbers in mutant arteries at POD14 and POD21 but not in POD7. Note that the mean numbers progressively increase with time in mutant thrombi but peak at POD14 and regress by POD21 in wild-type thrombi.

Discussion

Low baseline expression of *Col3a1* in uninjured carotid arteries, when compared to dramatic situational upregulation in response to injury (Figure 2.9B), suggests that extant type III collagen contributes a relatively minor role in the maintenance of baseline arterial wall function. Although haploinsufficient mice do express lower message levels at baseline (Figure 2.9A), this difference is negligible compared to the differences likely unmasked by injury, as rapid upregulation we have observed in normal injury responses would quickly outpace maximal expression rates in *Col3a1*$^{+/-}$ tissues. These observations predict that differential *Col3a1* expression and succeeding production of

type III collagen exerts its influence more consequentially during active arterial remodeling than at relative rest in a mature vessel. This would help explain the discrepancy between the clinical effects of type III collagen deficiency on long-lived haploinsufficient mice grossly indistinguishable from wild-type littermates in a protected laboratory environment[15] and human patients with mutations variably impinging on type III collagen secretion invariably suffering complications and premature death[9].

Histologic features present in occlusive resolving thrombi from injured mutant arteries at POD 21 in Figures 2.10 and 2.12, as well as occlusive thrombi in injured mutant *and* wild-type arteries at POD13 in Figure 2.13, closely resemble features of healing granulation tissue[75], including dense myofibroblast populations within a newly synthesized and expanding matrix. This commonality between genotypes, at least at POD14, suggests a physiologic component to formation and growth of occlusive thrombus, as very little thrombus was detected proportional to the lengths of arteries at POD 7 (Figure 2.13, Table 2.2). Pathology arises, however, as wild-type thrombi regress and disappear by POD21, leaving behind residual neointimal scars, while mutant thrombi continue to expand. Thus, a critical checkpoint determining the transition between proliferative granulation tissue formation and contraction and maturation of scar tissue is not reached on time with insufficient production of type III collagen. Considering increased burdens of inflammatory cells and climbing levels of proliferation in resident myofibroblasts, these data offer the first hint that myofibroblast behavior when lacking the ability to secrete required levels of type III collagen orchestrate ineffective thrombus resolution that mimics fibroproliferative pathology.

Notably, thrombus burden is equal between genotypes at POD14, although significant differences in macrophages within the thrombi and neovessels within the media already emerge. This would specifically implicate the *content of the matrix* as the driving force behind the retention of macrophages and pro-angiogenic signaling that these cells would promote, resulting here in the localization of cells positive for the CD31 marker of endothelial precursor cells within the medial channels[82,83]. Whether the matrix produced by *Col3a1* mutant cells actively attracts and retains more macrophages from hypoxia and/or local factors secreted into the matrix or whether the properties of the matrix itself speeds or retards cell migration is yet unknown, although expression of the stromal cell-derived factor-1 (SDF-1) chemokine by perivascular myofibroblasts in proximity to active angiogenesis has been shown to be critical for the recruitment of bone marrow-derived circulating cells and the success of VEGF-programmed neoangiogenesis in adult tissues[83].

The linear continuity observed here between polar hotbeds of thrombus recanalization with segments containing neointimal lesions supports the concept that mature concentric neointimal scars originate from the successful confluence of such recanalizing channels (Figure 2.12 and 2.17). The orientation of neointimal lesions at the inferior, proximal pole of the resolving thrombus suggests that it represents the most mature phase of vascular wound healing, akin to an organized collagenous scar in healed skin. Perhaps with the normal resolution of thrombi by the timepoints at which investigators have examined neointimal lesions, this relationship has been largely ignored. In the original description of carotid ligation in mice, investigators purposely disposed of arterial segments through to contain residual thrombus before investigating

remote neointimal lesions[50]. Studies of thrombus organization (what few exist) discuss myofibroblasts and endothelial-lined recanalization, while studies of neointimal formation discuss smooth muscle cells alone, with the perception that neointimal hyperplasia is a phenomenon composed primarily of proliferation of local smooth muscle cells and reflected entirely in morphometric measurements of neointimal thickening[84]. Unfortunately, the distinction between myofibroblast and smooth muscle cells is subtle, with both cell types expressing smooth muscle-specific α-actin. Nonetheless, the data presented here where thrombus resolution is delayed is important for providing a novel paradigm from which to view and investigate neointimal formation: as a product of specialized cells behaving as hybrids of fibroblasts and smooth muscle cells, rather than one or the other, to enact thrombus resolution.

This study is not the first to describe thrombus resolution as a process embodying wound healing in the vasculature and a precursor process to neointimal formation. Investigators directly injuring arteries in pigs to induce stenotic neointimal formation identified an early thrombotic phase involving fibrin and platelets, an inflammatory and endothelial cell recruitment phase, and a proliferative phase in which "smooth muscle cells" migrate into and proliferate within fibrin-rich thrombi[65]. Authors take care to note that popular conceptions of neointimal proliferation and therapeutic strategies to inhibit the process fail to consider these upstream "humoral" and "cellular" events, specifically identifying the cellular production of extracellular matrix as a suitable target for modifying neointimal thickening[65].

Chapter 3: Dysfunctional Matrix Remodeling by Myofibroblasts from vEDS Patients and Type III Collagen-Deficient Mice

Introduction

Myofibroblasts: Regulators of Wound Healing

The myofibroblast is a cell type first isolated from granulation tissue, noted to possess composite synthetic properties of fibroblasts and contractile properties of SMCs[85]. The ability of fully differentiated myofibroblasts to contract results from the expression of *ACTA2*, which encodes the smooth muscle-specific isoform of α-actin (α-SMA) monomers that form contractile filaments similar to those observed in SMCs[86]. Quiescent fibroblasts require stimulation with transforming TGF-β1 to differentiate into myofibroblasts, and myofibroblast contraction initiates a positive feedback loop by stretch-based release of further active TGF-β1 from its latent form bound to the extracellular matrix[87-89].

However, TGF-β1 alone is not sufficient, as cellular expression of contractile α-SMA in response to TGF-β1 also requires *sustained* tensile resistance from the substratum the cell is attempting to contract, implicating α-SMA as a mechanosensitive protein[90,91]. In fact, bipolar cells and actin filaments align in planes parallel to a wound surface along the vector of greatest strain, i.e., along the long axis of a wound, rather than extending perpendicularly across its gaping width[92]. Cells replicate this alignment when cultured within a strained three-dimensional *in vitro* matrix lattice[93].

Myofibroblasts are the major actors in wound healing, essentially dictating the tipping point where the proliferative and tissue forming phase matures into the tissue remodeling and contraction phase. Almost all mature connective tissues exist under a native mechanical tension, even at rest, as demonstrated by the shrinking length or width of vessels, nerves, or punch biopsies of the skin upon dissection away from the body.

Thus, the volume of new and immature granulation tissue requires compaction to reestablish a "tension homeostasis," and this occurs as a function of both contractile force generated by the resident cells and the stiffness of the matrix they must contract. Myofibroblasts, which are both synthetic and contractile, modulate both parameters in turn[94].

Expression levels of α-SMA directly correlate with contractile force generated by myofibroblasts[95], and release of compacted matrix gels from the dishes and wells to which they have been originally tethered, thus neutralizing stress opposing cellular contraction within the tissue, allows measurement of the immediate shortening of the gel to reflect the relative contribution of active, energy-dependent contraction[96]. However, myofibroblasts do not contract indefinitely in granulation tissue to maintain tension (a process that would require untenable energy input). Instead, they introduce tension by semi-permanently remodeling the *arrangement* of newly synthesized matrix. After contractile forces incrementally compact local fibers, cells structurally "lock" those fibers in place by yet unknown mechanisms to form a denser, stiffer material. This defines the distinction between *contraction* and *contracture*[97-99] (Figure 3.1). Not only deposition but, critically, the succeeding *rearrangement* of matrix re-establishes native stress shielding of cells residing in connective tissue. This term describes how the design properties of the arranged matrix allow it to bear tensile load preferentially over the myofibroblasts[93], after which cellular contraction is no longer necessary and α-SMA expression decays[97,100].

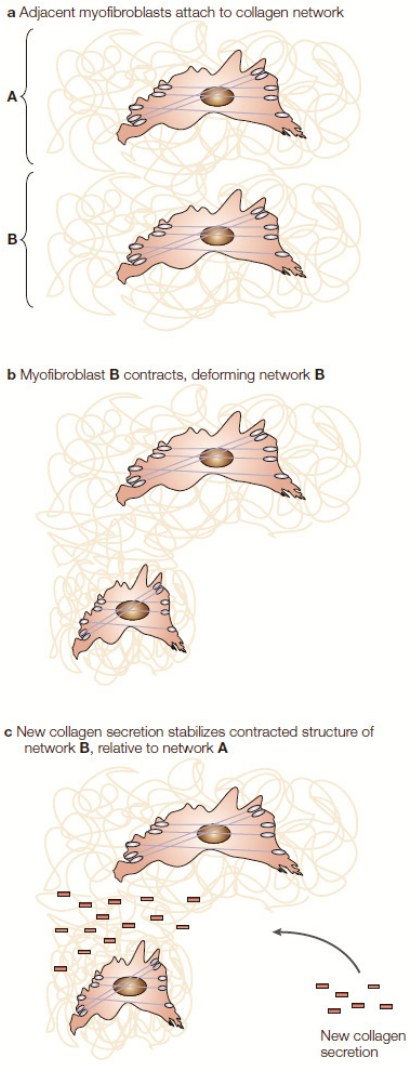

Figure 3.1. Model of extracellular matrix-remodeling phase of matrix contracture. Matrix contracture is mediated by myofibroblasts. How is the contractio of myofibroblasts translated into functional collagen-network shortening? The following working hypothesis serves to define some basic mechanisms. (*a*) Myofibroblasts are embedded in a collagen network. These cells bind to collagen fibrils through fibronexus adhesion complexes that are linked to intracellular stress fibers. (*b*) Cytoskeletal or signaling events in one of these myofibroblasts leads to stress-fiber contraction, which results in local matrix contraction, shortening, and bundling of the surrounding pericellular collagen network. As this is a local effect, its consequences are incremental, and affect at most a few surrounding cells and matrix. (*c*) New matrix components are added to stabilize the new collagen organization, relative to its neighbors. The addition of collagen would potentially increase collagen density and orientation. (*d*) The myofibroblast that contracted originally, as well as other surrounding myofibroblasts, can repeat the process so that this small incremental collagen-matrix remodeling can result in tissue contracture. Reprinted with permission from Nature Publishing Group [Myofibroblasts and mechano-regulation of connective tissue remodeling. Tomasek JJ, Gabbiani G, Hinz B, et al. *Nature Reviews Molecular Cellular Biology*. 2002].

Timing is everything, as the rate of effective remodeling not only determines the length of the window during which the strength of tissue is compromised but also the cumulative amount of energy input necessary to re-establish homeostasis. Thus, delayed rates of new type III collagen production likely alter the course of this process, as suggested by experiments explanting fetal skin fibroblasts from *Col3a1*$^{+/+}$, *Col3a1*$^{+/-}$, and *Col3a1*$^{-/-}$ littermates. Cells were seeded into type I collagen gels and allowed to contract and remodel the experimental matrix for 5 days. Disrupting the adhesion of the gels from the culture dishes to which they were tethered reveals a more effective shortening of the tissue by mutant fibroblasts. This active, cell-mediated contractile

response to release of tension implicates a higher dependence on cellular contraction for tissue compaction *prior* to release, and here the increasing dependence on contraction emerges as a function of the increasing genetic impediment to synthesizing new type III collagen (Figure 3.2).

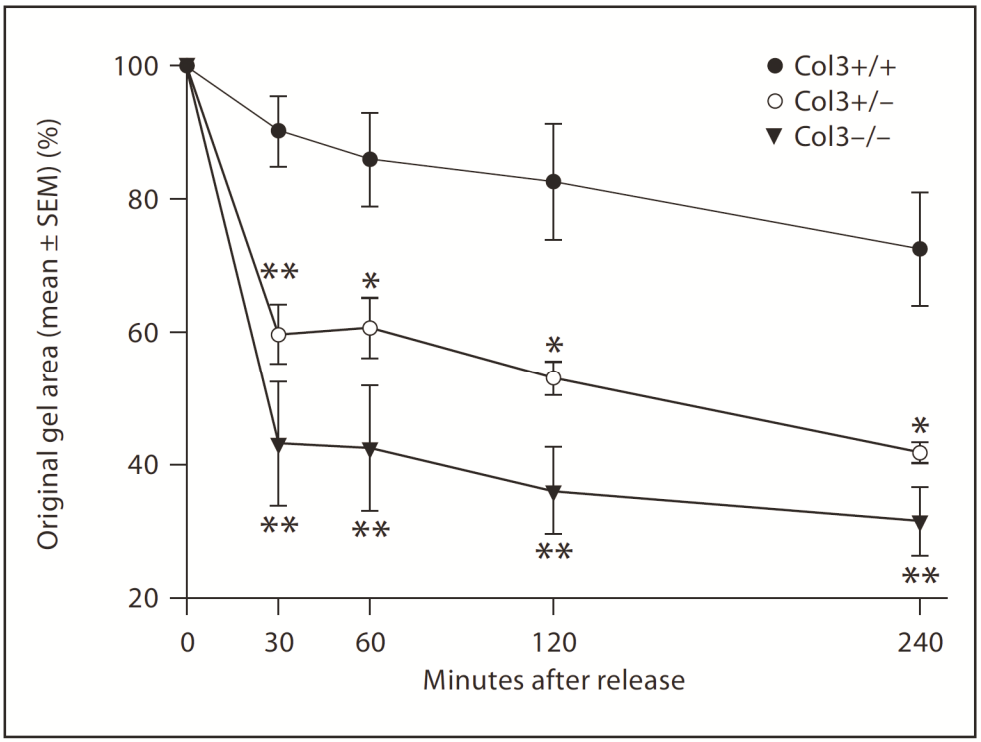

Figure 3.2. Collagen gel contraction by wild-type and type III collagen-deficient fetal (~E18.5) dermal fibroblasts. Wild-type and type III collagen-deficient fibroblasts were grown in attached collagen gels for 5 days. Stressed lattices were then released and the percentage of contraction calculated at 30, 60, 120, and 240 minutes post-release. Values represent means ± SEM. *Col3a1*$^{+/-}$ and *Col3a1*$^{-/-}$ values were found to be significantly different from *Col3a1*$^{+/+}$ values at all timepoints. Reprinted with permission from Karger Publishers [Diminished type III collagen promotes myofibroblast differentiation and increases scar deposition in cutaneous wound healing. Volk SW, Wang Y, Mauldin EA, et al. *Cells Tissues Organs*. 2010].

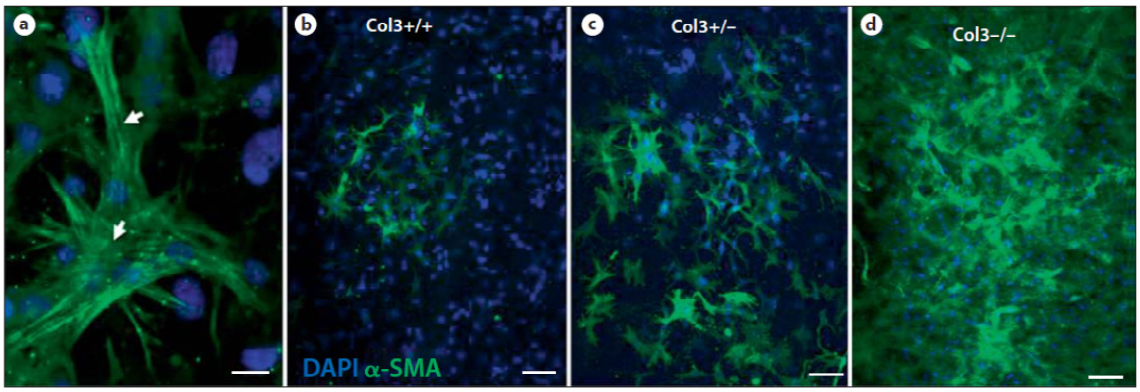

Figure 3.3. Increased α-SMA expression by type III collagen-deficient (*Col3a1*$^{+/-}$ and *Col3a1*$^{-/-}$) cells compared to wild-type (*Col3a1*$^{+/+}$) cells. Cells from all 3 genotypes, utilized in an attached fibroblast-populated collagen gell assay, were immunostained for α-SMA (green) and counterstained with DAPI (blue). (*a*) Myofibroblasts within collagen lattices were identifiied by α-SMA expression. α-SMA incorporation into stress fibers (arrows) could be visualized in cells from all 3 genotypes. (*b-d*) Representative images showing the percentage of myofibroblasts in cultures of *Col3a1*$^{+/+}$ (*b*), *Col3a1*$^{+/-}$ (*c*), and *Col3a1*$^{-/-}$ (*d*) cells are presented. Reprinted with permission from Karger Publishers [Diminished type III collagen promotes myofibroblast differentiation and increases scar deposition in cutaneous wound healing. Volk SW, Wang Y, Mauldin EA, et al. *Cells Tissues Organs*. 2010].

Staining tethered gels with fluorescent anti-α-SMA antibodies elucidates higher burdens of persistently α-SMA-expressing myofibroblasts in type III collagen-deficient cultures, in comparison with wild-type cultures (Figure 3.3), where α-SMA expression has possibly already peaked and receded secondary to stress-shielding via more effective remodeling of the matrix. Following full-thickness excisional punch biopsies in the skin of aged adult *Col3a1*$^{+/+}$ and *Col3a1*$^{+/-}$ mice (>1 year), type III collagen-deficient animals also demonstrate accelerated wound closure and significantly less wound area by 7 days, even for wounds created on the dorsal skull that were effectively splinted open by the tension of skin over bone. Immunohistochemical staining of wound cross-sections confirmed dramatically robust α-SMA expression in the granulation tissue of *Col3a1*$^{+/-}$ mice compared to wild-type mice[101] (Figure 3.4).

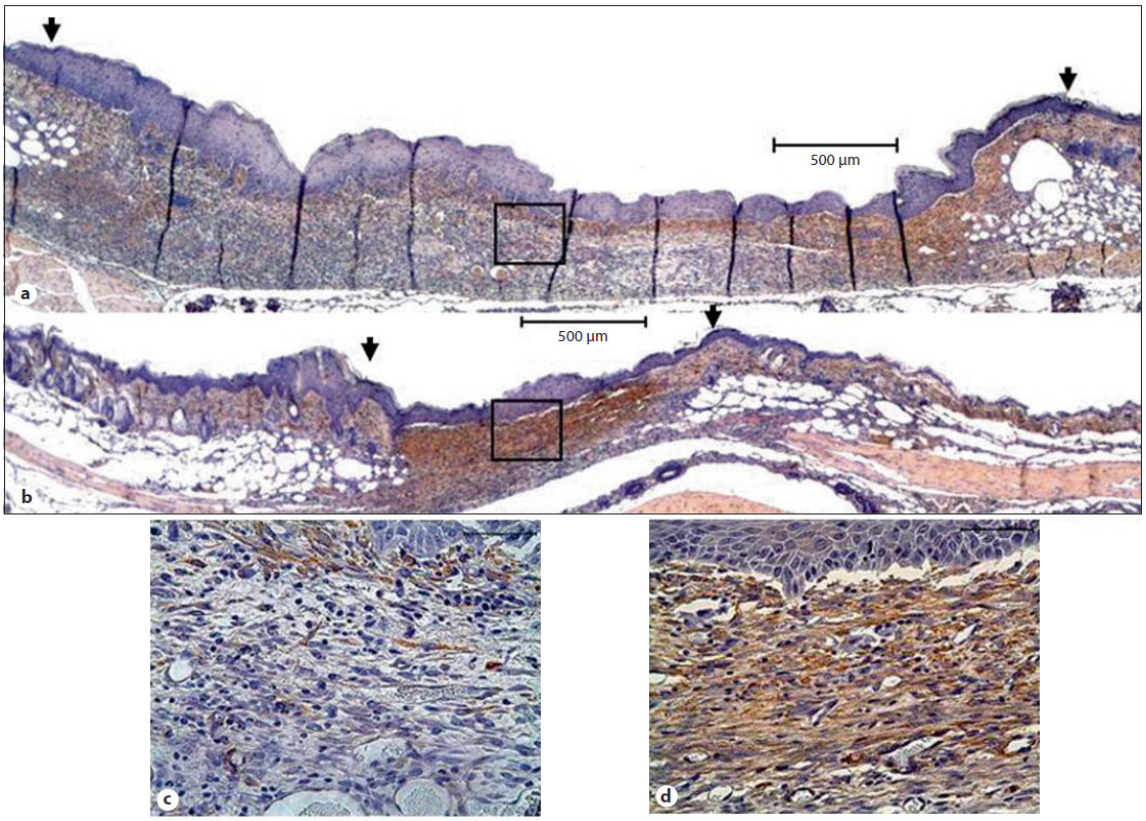

Figure 3.4. Wounds in aged type III collagen-deficient mice show increased wound contraction and granulation tissue α-SMA expression. Immunohistochemcial staining for α-SMA (brown) in representative wounds from *Col3a1*$^{+/+}$ (*a*) and *Col3a1*$^{+/-}$ (*b*) mice 7 days after wounding by excisional punch biopsy. Detailed views of the granulation tissue and overlying neoepithelium in wounds from *Col3a1*$^{+/+}$ (*c*) and *Col3a1*$^{+/-}$ (*d*) mice reveal increased α-SMA immunoreactivity in wounds from type III collagen-deficient mice (*Col3a1*$^{+/-}$) compared to wild-type mice. Reprinted with permission from Karger Publishers [Diminished type III collagen promotes myofibroblast differentiation and increases scar deposition in cutaneous wound healing. Volk SW, Wang Y, Mauldin EA, et al. *Cells Tissues Organs*. 2010].

The Role of Type III Collagen in Matrix Remodeling

Some speculate that matrix remodeling to restore tension homeostasis and stress shielding of cells may depend on the *de novo* production of type III collagen, which has been proposed to serve as a provisional matrix special to granulation tissue. Specifically, the temporary presence of type III collagen has been suggested to reduce the vulnerability theoretically arising from a situational breakdown of type I collagen cross-links to allow slipping of fibrils for compaction[98]. Soon after the original isolation

of the myofibroblast from granulation tissue, researchers investigating its synthetic products *in vivo* discovered a distinctly high proportion of type III (30-35%) within total collagen digested from granulation tissue, more resembling embryonic skin in relative collagen content than adult dermis. However, with the resorption of granulation tissue and the resolution of wound healing, this high proportion of type III collagen disappears simultaneously with the disappearance of α-SMA expression, and the vast majority of dermis collagen again consists of type I collagen[76]. In this way, the *content* of the matrix synthesized, namely the accumulating content of type III collagen, during the tissue formation phase may determine the ability of granulation tissue to progress to the final contraction and resolution phase of wound healing.

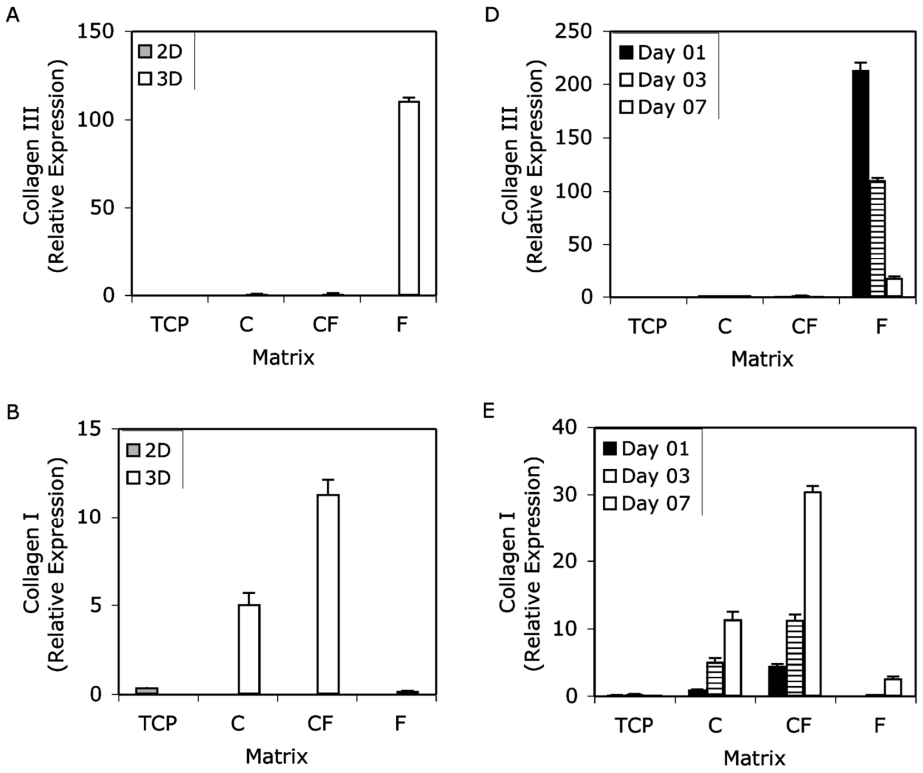

Figure 3.5. Gene expression of collagen type III α-chain (*A* and *D*) and collagen type I α-chain (*B* and *E*) over 7 days in culture. Results are normalized relative to 3D collagen on day 1. Two matrix geometries were used: two-dimensional monolayer culture (2D) and three-dimensional matrices (3D). The matrix materials used were tissue culture plastic (TCP), collagen (C), collagen-fibrin (CF), and fibrin (F). Panels *A* and *B* depict the effects of matrix geometry on matrix gene expression at day 3, which is representative of the temporal data. Panels *D* and *E* show the effects of matrix composition in 3D systems over time in culture. RT-PCR results were normalized to GAPDH expression at each timepoint and for each matrix condition. Results are expressed as the mean ± SEM. Reprinted with permission from Taylor & Francis [2D and 3D collagen and fibrin biopolymers promote specific ECM and integrin gene expression by vascular smooth muscle cells. Hong H, Stegemann JP. *Journal of Biomaterials Science, Polymer Edition.* 2008].

Indeed, seeding fibroblasts and SMCs into different three-dimensional matrix polymers, which are compacted from hydrated hemispheres into flattened disks within 24 hours, elicits differential production of new matrix. Seeding cells into a fibrin lattice resembling a fresh thrombus induces robust early expression of *Col3a1* that attenuates over 7 days[102]. Seeding cells into a lattice with a 1:1 ratio of fibrin and collagen to model a partially remodeled thrombus elicits weak expression of *Col3a1* but more robust and increasing expression of *Col1a1* over 7 days, suggesting a positive feedback for type

I collagen production as type I collagen begins to accumulate[102] (Figure 3.5D and E). Scanning electron microscopy images acquired 4 weeks after seeding fibroblasts in fibrin matrices visualize this initial ramping of local fibrillar collagen production[103]

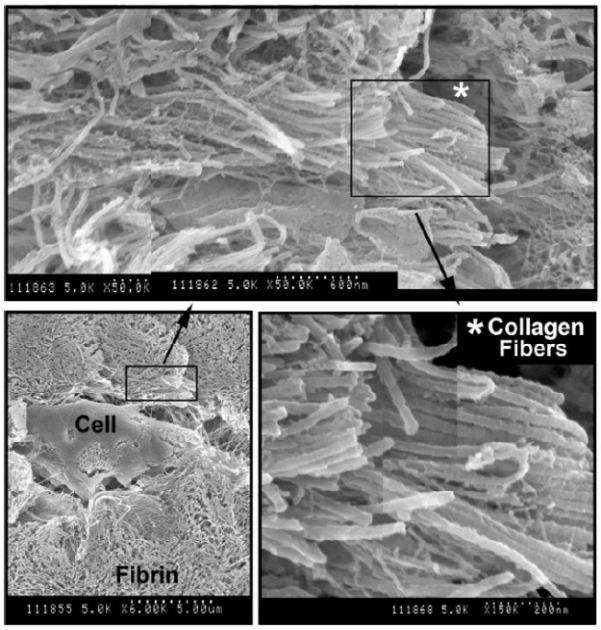

Figure 3.6. Representative scanning electron microscopy images of fibroblast-remodeled fibrin construct after 4 weeks. Depicted in the bottom left image is a cell embedded in the fibrin matrix. By week 4, the emergence of collagen fibril bundles embedded in the fibrin matrix becomes more apparent. In the top image, collagen parallel fibril bundles can be identified from the surrounding fibrin by the parallel bundling. The asterisk shows the location of the magnified region on the bottom right. Collagen fibrils in the interior were always identified near cellular material. Reprinted with permission from Springer [Initial fiber alignment pattern alters extracellular matrix synthesis in fibroblast-populated fibrin gel cruciforms and correlates with predicted tension. Sander EA, Barocas VH, Tranquillo RT. *Annals of Biomedical Engineering*. 2011].

(Figure 3.6). Nonetheless, *Col1a1* expression by cells within pure type I collagen lattices only modestly increases over 7 days, implicating a negative feedback dampening of synthesis by collagen accumulation that has reached a certain threshold[102] (Figure 3.5E). It is striking that none of this dynamic expression is observed in cells grown in monolayers on two-dimensional matrix substrates, suggesting not only that three-dimensional interaction with matrix ligands induces distinct signaling through cell-

surface receptors but also that tensional forces developing in tethered and compacted matrices provide additional, critically amplified stimuli (Figure 5.5A and B).

Deranged collagen fibrils in vEDS patients and *Col3a1*$^{-/-}$ mice have already demonstrated the necessity of type III collagen for normal, uniformly organized type I collagen fibrillogenesis. Both *in vitro* and *in vivo* basic studies of the actual formation of fibrils illustrate a more specific mechanism. In the developing metatarsal tendons of chick embryos, immature tendons show even distribution of type I and type III collagen and uniformly small fibrils. During a period of rapid development of fibrils, however, the two types of collagens segregate between the fascicle (high type I collagen) and investing connective tissue compartments (high type III collagen), where fascicular fibrils are larger and the fibrils in sheaths remain small until type III collagen levels eventually disappear, such that levels of type III collagen negatively correlate with developing fibril diameter[104].

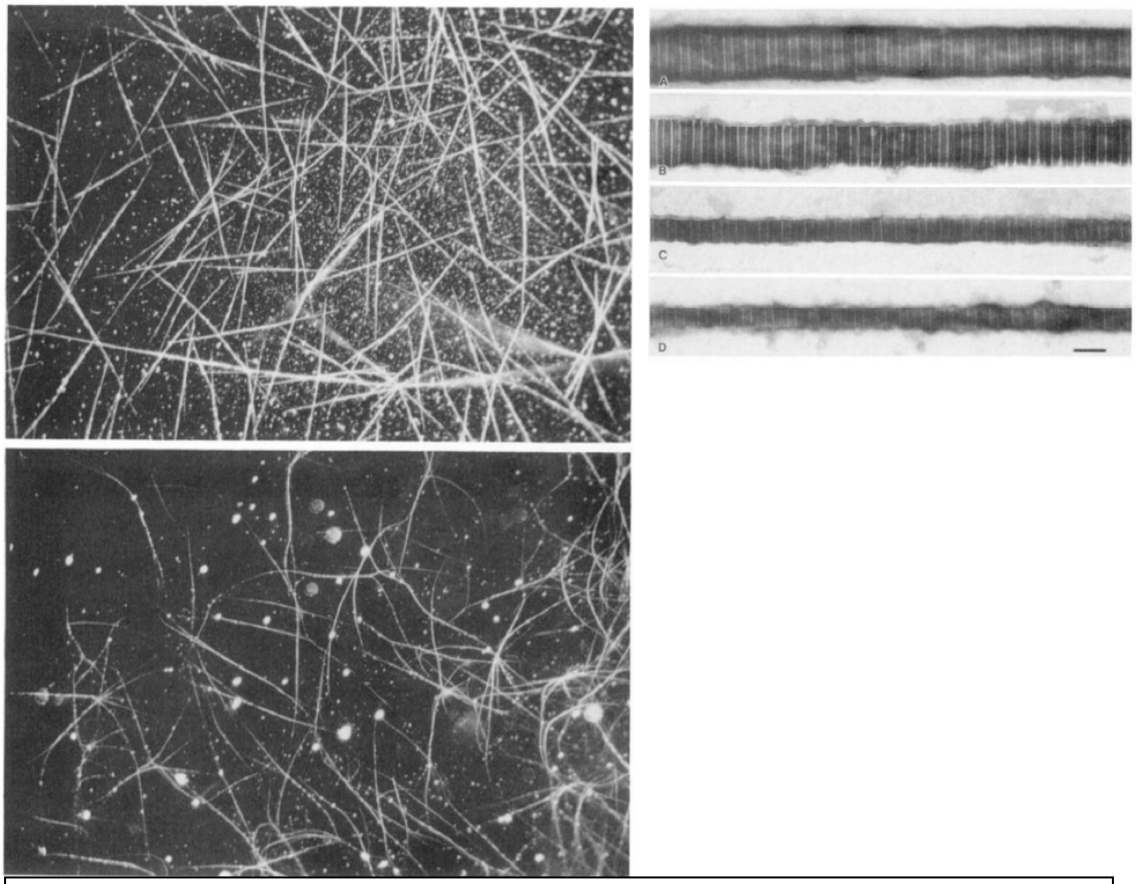

Figure 3.7. Morphometric analysis of collagen I fibrils and copolymer fibrils of pNcollagen III and collagen I by dark field and electron microscopy. Control collagen I fibrils were generated by cleaving pCcollagen I with C-proteinase, and copolymers were generated by cleaving procollagen III and pCcollagen I with C-proteinase. *Upper left*, Dark-field light microscopy of control collagen I fibers. *Lower left*, Dark-field microscopy of copolymer fibrils. The heterogeneous copolymer fibrils were longer and thinner and appeared more flexible than the control fibers of collagen I. *Upper right*, Control collagen I fibril (*A*), copolymer generated from an initial molar ratio of 0.5:1 (*B*), 1:1 (*C*), and 2:1 (*D*) of III: I. Reprinted with permission from The American Society for Biochemistry and Molecular Biology [Copolymerization of pNcollagen III and collagen I. Romanic AM, Adachi E, Kadler KE, et al. *Journal of Biological Chemistry*. 1991].

In vitro cell-free systems demonstrate that partially-cleaved type III procollagen (type III pNcollagen) copolymerizes with type I collagen when they are both newly and simultaneously cleaved from type III procollagen and type I pCcollagen, respectively. The presence of type III pNcollagen increases lag for incorporation of type I collagen into fibrils, lowering the maximum rate and decreasing the steady-state concentration of type I collagen incorporated. Again, relative proportions of type III pN collagen

negatively correlated with fibril diameter, with the resulting copolymer fibrils demonstrating greater flexibility (Figure 3.6). The kinetics of assembly best fit a model in which type III pNcollagen coats the circumference of developing fibers except at the growing tips[105].

Stress Shielding, Apoptosis, and Fibrocontractive Disease

Resolution of granulation tissue following tissue compaction involves a drop in cellularity and vascularity of the scar through incremental apoptosis of myofibroblasts and neovessels. The same is true for the cellularity of neointimal lesions with maturity over time[106]. When apoptosis fails to occur following wound healing, hypertrophic scars, keloids, or disfiguring contractures can develop as α-SMA-expressing cells continue to proliferate and generate granulation tissue even after wound closure. Indeed, fibrocontractive diseases of many organs involve the inappropriate and prolonged activity of dysregulated myofibroblasts[98,79].

The co-occurrence of stress shielding, loss of α-SMA expression, and apoptosis in maturing granulation tissue, as well as efforts to experimentally release splinted wound tension and resulting observations of acutely marked apoptosis in the newly unstressed granulation tissue[107], has led to the notion that loss of mechanical tension may provide the signal to initiate programmed cell death[108-110]. This notion is consistent with the long clinical experience of surgeons, who note that wounds bearing tension develop hypertrophic scars. In fact, externally applied mechanical loads to wounds (splints) during the early proliferative phase of healing inhibit apoptosis for several weeks afterward and were sufficient to induce hypertrophic scars in experimental animals. The

increased volume of granulation tissue corresponded to increased cellularity and not to increased production of collagen per individual cell, which statistically equaled that in unloaded tissue[111].

As the regulation of myofibroblast behavior appears exquisitely sensitive to mechanical interactions with their surrounding matrix, and as diminutive levels of type III collagen may possibly promote more rigid and less flexible matrix, for the second aim of this project, we seek to confirm dysregulation of myofibroblast activity in type III collagen-deficient tissues. In injured *Col3a1*$^{+/-}$ mouse arteries, we confirm impaired synthesis of type III collagen by α-SMA-positive myofibroblasts in resolving thrombi at POD14, compared to wild-type levels, alongside evidence of increased type I collagen deposition in mutant tissues, which progresses by POD21 to deranged remodeling of wider collagen fibers on average within neointimal lesions from mutant arteries. By seeding human dermal fibroblasts from vEDS patients with missense mutations of various inefficiency at secreting type III collagen into thrombus-mimicking fibrin gel constructs, we unmask abnormally high transcription of *ACTA2*, the gene encoding α-SMA, and abnormally delayed transcription of both *COL3A1* and *COL1A2*, one of the genes encoding type I collagen. We also visualize the deposition and rearrangement of collagen by these cells over time, discovering that type III collagen-deficient cultures are dramatically impaired in their ability to remodel collagen networks within stressed lattices.

Methods

Nonlinear Optical Microscopy of Collagen in Post-Injury Tissues

From our cohort of POD14 index slides as described in Chapter 2, we identified arterial segments with morphology consistent with the proliferative phase of vascular wound healing, including dense myofibroblast cellularity, expanding matrix production, and relatively high macrophage burdens. From our cohort of POD21 index slides, we identified arterial segments containing the apical neointimal lesion within an individual artery, i.e., the lesion representing the highest proportional occlusion of the artery lumen. Here we emphasize that extent of occlusion in the apex does not hold particular biological relevance to our investigation of remodeling in granulation tissue except to provide the greatest allowable area for image sampling within an individual segment. Apices were often situated near the center of axially oriented lesions, providing a reliable criterion by which to choose slides comparable across individual arteries.

We selected unstained slides that correspond to neighboring index slides containing suitable morphology ($N = 5$ *Col3a1*$^{+/+}$ slides from 1 artery, 5 *Col3a1*$^{+/-}$ slides from 1 artery at POD14; and 5 *Col3a1*$^{+/+}$ slides from 5 arteries, 7 *Col3a1*$^{+/-}$ slides from 7 arteries at POD21). Slides and tissues were deparaffinized and rehydrated by immersion in xylenes followed by immersion in a graded alcohol series. Tissue sections were then submerged in PBS until ready for imaging by nonlinear optical microscopy, or NLOM.

NLOM is an imaging technique designed for the specific visualization of collagen fibers within a wet, biologically intact tissue. The optical engineering of the custom-built, laser-based system has been described previously[112]. Relevant to data acquisition for the current experiments, NLOM captures two spectrally distinct signals, two-photon excited fluorescence (TPF) produced by resident cell cytoplasm and second-

harmonic generation (SHG) produced by the highly-ordered and birefringent molecular structure of fibrillar collagen[113,114]. Overlay of the two signals acquired from one tissue through a 40x objective (via customized software openly available, see http://biomed.tamu.edu/tml) spatially relates tissues or cell bodies and processes with their extracellular matrix.

At the time of imaging, tissues remained submerged under PBS on the slide through the use of hydrophobic ink to encircle the sections. The 40x aqueous objective was centered over the neointimal lesions and the images scanned by the laser in one plane to generate both TPF and SHG signal images. At high power, it quickly became obvious that SHG signal from abundant adventitial collagen saturated the sensitivity of the imaging software to neointimal fibers. We carefully situated tissues so that a standardized field of view captured by the software only contained neointimal or medial signals. The field of view (FOV) is defined by the software in computational units of 1 to 2.5, increasing in value with increase in power, and here we mostly utilize FOV 2.0 to image entire sections and FOV 1.5 to limit field to neointima. FOV is correlated with actual distance through the electronic regulation of movements of the microscope stage on the order of microns, with scale bars obtained through comparison of repeated images obtained after moving the stage a precise distance.

It also became obvious that the diameter and density of collagen fibers, much like cell density visible on H&E, varies locally within an individual artery segment. In order to reflect local diversity in the quantification of SHG, we captured images by semi-randomly centering the field of view over segments of the neointima in each slide, producing between 4 and 8 images per slide depending on the available neointimal area.

For each image, NLOM quantified a mean SHG signal intensity in arbitrary units within a region-of-interest (ROI) drawn to solely encompass neointima. Mean signal intensity arises as a function of not only the presence of collagen fibers within the ROI but also of the diameter of those individual fibers. Because the signal intensity measurement reflects autoregulation by the software to maximize imaging sensitivity, we took painstaking care to optimize focus of the objective onto the plane of the tissue to achieve maximum signal. We then normalized each mean neointimal intensity value to the mean intensity of an ROI drawn around the SHG signal generated by the internal elastic lamina, which we assume to be relatively constant and unaffected by genotype.

Similar to index slides sampled along the length of harvested arteries, each image represented highly localized phenomena, rather than phenomena uniformly distributed across the neointima, and presented information that was more unique than similar, even among images taken from the same arterial section. Thus, images were not treated as "technical" replicates, as they did not cluster in regard to an individual slide. To avoid under-representing the variance in the dataset by calculating a mean neointimal/elastin intensity ratio per slide and subsequently calculating a mean of mean intensity ratios per genotype, we calculated mean intensity ratios ± standard deviation based on the total number of images per genotype at POD21 ($N = 57$ *Col3a1*$^{+/+}$ images, 31 *Col3a1*$^{+/-}$ images). The complete set of intensity ratios were graphed as individual data points to reflect their near normal distributions. To determine statistically significant differences between the means, we performed an unpaired Student's *t* test. As POD14 tissues were more dynamic along the length of arteries and between arteries, it was not possible to

choose comparable morphologies from every mouse artery, and so statistical hypothesis testing was underpowered.

Histochemical and Immunohistochemical Evaluation of Matrix

As SHG reflects signal from all fibrillar collagen, including both type I and type III, we aimed to tease apart tissue expression of type I and type III collagen more specifically with immunohistochemical analysis. This more blunt technique only identifies the presence of absence of matrix antigen within a field and offers poor estimation of relative content between the two genotypes, although correlation between expression and morphology provides information about the biological circumstances of expression.

Tissues were prepared prior to incubation with antibody as described in Chapter 2 with routine HIER. Slides were incubated with mouse antibodies directed against mouse type I collagen (Abcam, Cambridge, MA) and mouse type III collagen (Biogenex, Fremont, CA) for 1 hour at room temperature. The specificity of structures stained with anti-collagen I antibody correlated to images obtained with NLOM, and the specificity of anti-collagen III antibody was confirmed through *Col3a1+/-* artery sections serving as negative controls. Slides were photographed and presented at 40x magnification, unless otherwise specified.

Broader histochemical assay of insoluble matrix, celullar, and mucinous components within sections was obtained through Movat pentachrome stain, by routine techniques. Pentachrome stains muscular material red, fibrinous material and blood

bright red, nuclei and elastin black, proteoglycans and ground substance blue, and collagen yellow.

Explant of Dermal Fibroblasts from Human vEDS Patients and Col3a1 *Mutant Fetal Mice*

Aliquots of dermal fibroblasts from human patients with vEDS and documented *COL3A1* missense mutations of relatively high severity (G769R, G832R, and G1021R) were a gift of Dr. Peter H. Byers of the Collagen Diagnostic Laboratory and Department of Pathology at the University of Washington. Dermal fibroblasts from healthy human control subjects (sex-matched and age-matched to within 10 years of age of patients at time of harvest) were obtained by our laboratory following informed consent in accordance with IRB approval of recruitment protocols. Fibroblasts were originally explanted from the dermis of punch biopsies obtained from the skin of the medial upper arm and cultured to form expansible cell lines. Briefly, explant involved dipping tissue into ethanol, PBS, and complete DMEM before scraping away epidermis and subcutaneous fat, transferring remaining dermis into new tissue culture dishes, and mincing in fresh DMEM. Sterile glass coverslips are placed to anchor minced tissue pieces and promote the adhesion and outgrowth of dermal fibroblasts, which are subsequently trypsinized and expanded within culture flasks by routine cell culture techniques. Cells are maintained with complete DMEM supplemented with 10% fetal bovine serum (Atlanta Biologicals) and 100U/ml penicillin, 100µg/ml streptomycin, and 250ng/ml amphotericin B (Gibco).

Since neonatal *Col3a1*$^{-/-}$ mouse pups survive until birth but rarely survive to weaning, much less into adulthood[15], we opted to generate *Col3a1*$^{+/+}$, *Col3a1*$^{+/-}$, and *Col3a1*$^{-/-}$ dermal fibroblast lines from fetal mouse tissues. We chose fetal tissues rather than embryonic fibroblasts, as fetuses have reached the age past which scarless wound healing (e.g., at E15) transitions to adult-type repair with scarring (at E18)[115]. We mated a pair of *Col3a1*$^{+/-}$ adult mice to generate offspring representing all possible genotypes. Following observation of a vaginal plug to suggest fertilization at E0.5, we anesthetized the pregnant female and sacrificed via thoracotomy on E18.5. We dissected out the uterus under sterile conditions and submerged in sterile PBS. In a dish, we dissected away the uterine wall to reveal four fetuses ~22mm in axial length, confirming age at E18. Fetuses were separated into individual dishes and skin harvested, minced, and anchored by sterile coverslips for establishment of cell lines and maintained using the same media as described above. Residual tissues were collected for genotyping to probe for both *Col3a1* and *Neo* alleles[80], and results demonstrated a litter yielding 1 *Col3a1*$^{+/+}$ cell line, 1 *Col3a1*$^{+/-}$ cell line, and 2 *Col3a1*$^{-/-}$ cell lines.

Fibroblast Culture in Three-Dimensional Fibrin Gels

We chose to seed fibroblasts within attached fibrin gel hemispheres, so that TGF-β1- stimulated contraction would decrease thickness but not shorten diameter of the *in vitro* tissue, thereby increasing tension. Furthermore, culture within a fibrin matrix allows for the unambiguous observation of *de novo* collagen synthesis[98,103,116,117]. We scored circles on the plastic surfaces of 35-mm wells in tissue culture plates and 35-mm dishes by tracing 22-mm diameter glass coverslips with a diamond-tipped pencil before

sterilizing under UV irradiation for 20 minutes. We reconstituted bovine plasma type IV fibrinogen (Sigma) in sterile phosphate-buffered saline at 2.5mg/ml and supplemented with 4mg/ml 6-aminocaproic acid (ACA, Acros Organics) to inhibit degradation of polymerized fibrin matrices by residual plasmin activity, and we sterilized the solution by 0.22µm vacuum filtration (Millipore). We also reconstituted 1000U bovine plasma thrombin (Sigma) in solutions of 0.1% bovine serum albumin (Sigma) for mixture with fibrinogen solution just prior to plating to give final concentrations of 0.1U thrombin/mg fibrinogen.

After trypsinizing fibroblasts from hyperconfluent culture in 75cm^2 flasks, we suspended pellets of 5 x 10^5 human fibroblasts or 2 x 10^5 fetal mouse fibroblasts in 1ml fibrinogen solution and mixed with 50µl thrombin solution before plating 1ml hemispheres of clotting fibrin within scored tissue culture wells and dishes. Hemispheres were then carefully incubated at 37°C for 30 minutes in a humidified incubator to allow complete polymerization of the fibrin lattice. Immediately afterward, the gels were fed with DMEM freshly supplemented with 10% fetal bovine serum (Atlanta Biologicals), 100U/ml penicillin, 100µg/ml streptomycin, and 250ng/ml amphotericin B (Gibco), 50µg/ml ascorbic acid (Sigma), and 4mg/ml ACA (Acros Organics) and impregnated with 10ng/ml recombinant human TGF-β1 immediately before use (R&D Systems) to stimulate the resident cells with a pulse of TGF-β1 and establish the day 0 timepoint.

Plate wells and dishes were subsequently (1) fixed with 4% paraformaldehyde or 10% buffered formalin for 10 minutes and stored wet in PBS and protected from light at 4˚C or (2) aspirated of media, washed with 2ml PBS, and dry frozen at -80˚C after

precisely 1 day, 3 days, 7 days, or 14 days for (1) imaging of cellular morphology and organization of collagen and (2) homogenization in TRI reagent and RNA extraction, respectively. In the meantime, media was replaced on Mondays, Wednesdays, and Fridays with complete DMEM freshly prepared as above, excepting the addition of TGF-β1. For control samples to establish baseline RNA levels, pellets simultaneously formed from identical numbers of fibroblasts were washed in 2ml PBS and immediately lysed in 1ml TRI reagent and frozen at -80˚C on day 0 without ever being exposed to three-dimensional fibrin or to TGF-β1 stimulation.

Nonlinear Optical Microscopy of Collagen in Three-Dimensional Gel Cultures

After fixation of gels containing either human dermal myofibroblasts or mouse fetal dermal myofibroblasts at days 1, 3, 7, and 14, slides and gels were subjected to NLOM. Fixed discoid gels of 22mm diameter and submerged in PBS were situated under the aqueous objective so that the laser penetrated the central axis where the gel was thickest. Images were acquired at FOV 1.0 in planes first intersecting the apical surface and then incrementally penetrating at 10μm-stepwise depths until reaching the floor of the dish. Cells extending above and below the plane of the image were captured by multiple images. In general, cells were clearest and most numerous in the plane equidistant between the apex and the floor, and images most demonstrative of cell behavior and matrix interaction are presented here.

Sequence Description	5' to 3' Sequence	Product Size		Sequence Description	5' to 3' Sequence	Product Size
Homo GAPDH Fwd	AAGGTGAAGGTCGGAGTCAAC	102		Mus GAPDH Fwd	AGGTCGGTGTGAACGGATTTG	123
Homo GAPDH Rev	GGGGTCATTGATGGCAACAATA			Mus GAPDH Rev	TGTAGACCATGTAGTTGAGGTCA	
Homo ACTA2 Fwd	CAGGGCTGTTTTCCCATCCAT	81		Mus ACTA2 Fwd	CCTGCTCTGCCTCTAGCAC	154
Homo ACTA2 Rev	ACGTAGCTGTCTTTTTGTCCC			Mus ACTA2 Rev	GGCCAGGGCTACAAGTTAAG	
Homo COL3A1 Fwd	CAGGGAACAACTTGATGGTG	131		Mus COL3A1 Fwd	CCATTTGGAGAATGTTGTGC	155
Homo COL3A1 Rev	AAGCAGAGCGAGAAGTAGCC			Mus COL3A1 Rev	AGACCTGGTTGTCCTGGAAG	
Homo COL1A1 Fwd	GTGCGATGACGTGATCTGTGA	119		Mus COL1A1 Fwd	AATGGAGATGATGGGGAAGCT	139
Homo COL1A1 Rev	CGGTGGTTTCTTGGTCGGT			Mus COL1A1 Rev	CATCCAAACCACTGAAGCCTC	
Homo COL1A2 Fwd	GAGCGGTAACAAGGGTGAGC	92		Mus COL1A2 Fwd	CTCTGCAACACAAGGAGTCTG	137
Homo COL1A2 Rev	CTTCCCCATTAGGGCCTCTC			Mus COL1A2 Rev	CCCTTTCGTACTGATCCCGAT	
Homo TGFB1 Fwd	GGAAACCCACAACGAAATCT	205		Mus TGFB1 Fwd	GGTGCTCGCTTTGTACAACA	140
Homo TGFB1 Rev	GAGGTATCGCCAGGAATTGT			Mus TGFB1 Rev	TCTCATAGATGGCGTTGTTGC	
Homo ITGA1 Fwd	AGAATGCAGCACTCAACTGG	173		Mus ITGA1 Fwd	ACCGGCTTCAGTGCTCATTA	148
Homo ITGA1 Rev	TGAACTCATGGGTCACGTTT			Mus ITGA1 Rev	TCATCTTGGTGGGCTCAGTT	
Homo ITGA2 Fwd	CGCTCAGTCAAGGCATTTTA	223		Mus ITGA2 Fwd	GACTTTCCAGACTGTGCAGC	125
Homo ITGA2 Rev	CATGTGGCAGTGGATAGGTC			Mus ITGA2 Rev	CTGCTTTCTCCGTGGGTTTC	
Homo ITGB1 Fwd	CAGGGGAAAATGGAAGAAAA	207		Mus ITGB1 Fwd	ACTGGTCCATGTCTAGCGTC	113
Homo ITGB1 Rev	ACTTGGGACTTTCAGGGATG			Mus ITGB1 Rev	CATGTCTCACAAGTTGGCCC	
Homo MMP1 Fwd	TTGCCGACAGAGATGAAGTC	111		Mus MMP1A Fwd	AATGTTCCCCAGTTACACGTG	132
Homo MMP1 Rev	GGAAGCCAAAGGAGCTGTAG			Mus MMP1A Rev	CATGGATGTGGTGTTGTTGCA	
Homo MMP2 Fwd	TTCCTGGGCAACAAATATGA	131		Mus MMP2 Fwd	CCCAGAAAAGATTGACGCTGT	178
Homo MMP2 Rev	AACAGGCTGTACCCTTGGTC			Mus MMP2 Rev	ACTCCAGTTAAAGGCAGCATC	
Homo MMP9 Fwd	CCGGACCAAGGATACAGTTT	148		Mus MMP9 Fwd	GAGACGGGTATCCCTTCGAC	166
Homo MMP9 Rev	CATTCACGTCGTCCTTATGC			Mus MMP9 Rev	TGACATGGGGCACCATTTGAG	

Table 3.1. Forward and reverse primer sequences utilized for quantitative PCR assay. Detection of SYBR green fluorescence was used to derive relative transcript levels of the genes listed. Sequences presented in 5' to 3' orientation.

Plates containing three-dimensional gel cultures were dry frozen at -80˚C at the appropriate timepoint as above, and once all day 1, day3, and day 7 plates had been collected, gels were thawed on ice and thoroughly scraped from plates using plastic cell lifters and 0.5ml TRI reagent. Reagent and solid tissues were then each transferred into individual round-bottom tubes already containing 0.5ml TRI reagent for a combined volume of ~1ml TRI reagent per gel. For the remainder of RNA extraction, gels were effectively treated as tissues homogenized with a protocol identical to that described for harvested arteries in Chapter 2, except that gels each yielded sufficient RNA to be homogenized separately as individual biological replicates rather than pooled. Samples homogenized in TRI reagent were then grouped alongside thawed day 0 samples of cell

pellets lysed in 1ml TRI reagent for further RNA extraction following manufacturer's instructions (Sigma).

Reverse transcription of cDNA samples was performed using identical methods to those described in Chapter 2, although one cDNA sample was generated per biological replicate rather than pooled. Quantitative PCR was performed on a Roche LightCycler 480 instrument using primers designed in-house for mouse and human *GAPDH*, *COL3A1*, *COL1A1*, *COL1A2*, *ACTA2*, *TGFB1*, *MMP1*, *MMP2*, *MMP9*, *ITGA1*, *ITGA2*, and *ITGB1* (Table 3.1) and reagents available in the LightCycler 480 SYBR Green I Master kit (Roche) according to manufacturer's instructions. Again, quantification of target gene expression normalized to internal control gene expression (*GAPDH*) related message levels from day 1, day 3, and day 7 gels to baseline levels in an equivalent mass of RNA derived from day 0 cell pellets according to the Comparative C_T method[81].

Gel experiments were repeated three separate times for both three mouse and three human cell lines that differentially secrete type III collagen based on genotype, and samples from gels plated at the same time for the same experiment were analyzed relative to each other. We calculated mean fold-changes in gene expression ± standard deviations from the three biological replicates for each of the cell lines at each of the timepoints relative to baseline message levels in the type III collagen-sufficient cell lines at day 0. As we were interested in the differential expression of target genes over time as a function of *COL3A1* genotype, we performed a two-way analysis of variance for mean fold-changes between samples and post-test analyses between pairs of cell lines harvested at the same timepoint. Statistical calculations were carried out on GraphPad

software, and error bars represent standard error of the mean between measurements derived from technical and biological replicates. We concluded statistically significant differences in expression when $p < .05$.

Results

Thrombi remodeled by actin-positive myofibroblasts, resulting in differential collagen production durring active resolution and formation of mature neointimal lesions.

We attempted to determine whether differential burdens of thrombi or neovessels at POD21, when contrasts were most pronounced, could be correlated with any molecular differences in the extracellular matrix of the neointima between *Col3a1*$^{+/+}$ or *Col3a1*$^{+/-}$ arteries. We restricted our investigation to matrix deep to the internal elastic lamina, including matrix within residual occlusive thrombi and within more mature neointimal lesions, since any tissue present must have arisen in response to carotid ligation and involved *de novo* synthesis of type III collagen.

Thus, we chose arterial segments both from areas near the center of unresolved thrombi and from the apex of neointimal lesions for initial histochemical analysis by Movat pentachrome stain. Most relevant to the matrix content is the distinction between "muscular" cell bodies in red, collagenous matrix in yellow, and mucinous ground substance in blue. Despite similar appearance by hematoxylin and eosin stain, Movat stain reveals a subtle pattern of patches of collagen accumulation around the outermost edges of *Col3a1*$^{+/+}$ thrombus, relative to the more mucinous matrix in the interior. Matrix is less differentiated In *Col3a1*$^{+/-}$ thrombus and more categorically yellow

(Figure 3.8). Cell density in *Col3a1*$^{+/-}$ thrombus is striking, consistent with significantly higher numbers of proliferative pH3-positive cells identified in Chapter 2.

As histochemical stains provide relatively nonspecific information, we sought to hone our analysis of collagen content by imaging slides with nonlinear optical miscroscopy (NLOM) of second harmonic generation (SHG), which derives images of intact fibrillar collagen microstructure *in situ* and corresponds mean signal intensity within a region of interest to the number and diameter of fibers present[112,118]. Images confirmed the relatively increased accumulation of collagen in outer patches of undulating collagen fibers in the *Col3a1*$^{+/+}$ thrombus. The *Col3a1*$^{+/-}$ thrombus similarly contains undulating fibers but in a more uniform distribution and a much reduced intensity (Figure 3.8).

We subjected the same POD21 thrombus slides imaged by NLOM, which does not alter tissues, to immunoprobing with anti-α-SMA antibody, and all slides contained positive cells suggestive of myofibroblast differentiation. Interestingly, neointimal lesions also stain broadly positive for α-SMA, consistent with the notion that neointimal lesions originate from the myofibroblast-mediated process of thrombus resolution. In these mature lesions, Movat pentachrome identifies more uniform matrix composition in neointima from each of the two genotypes, although extracellular blue shading implies that *Col3a1*$^{+/+}$ segments contain a more mucinous matrix, while more yellow coloring indicates that *Col3a1*$^{+/-}$ segments contain a more collagenous matrix (Figure 3.8).

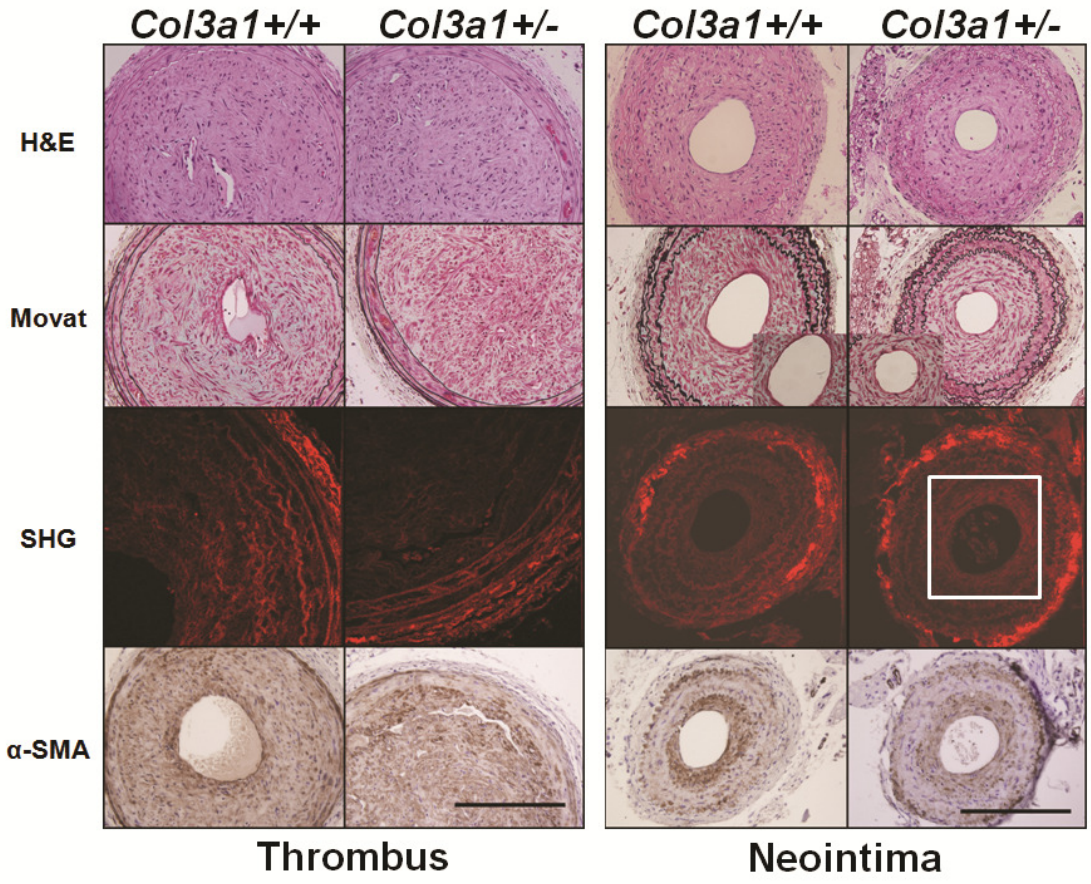

Figure 3.8. Qualitative analysis of matrix produced by resident myofibroblasts in resolving thrombi and in mature neointimal lesions at 21 days post-injury. Slides are presented in distal-to-proximal orientation from top-to-bottom of the figure. On hematoxylin and eosin stain (H&E), wild-type and mutant arteries appear similar. However, Movat pentachrome exposes differential matrix synthesis in thrombus and neointima. Red denotes muscular fibers, blue denotes ground substance, and yellow denotes collagen. Wild-type thrombus exhibits ground substance localized centrally, while collagenous patches are restricted to the periphery, which was confirmed by enhanced second harmonic generation (SHG) intensity (red pseudo-color) produced by collagen in the periphery and attenuation of signal near the recanalizing lumen. Matrix in type III collagen-deficient thrombus is more diffusely yellow on Movat and lacks the well-delineated fibers on SHG signal seen in wild-type thrombus. In more mature neointima, Movat staining of wild-type matrix is diffusely blue, while collagen III-deficient matrix is diffusely yellow. Insets at 100x compare differential matrix stains side-by-side. White box on SHG signal in collagen III-deficient neointima highlights paradoxically enhanced intensity of collagen fibers circling the lumen. Positive staining for α-SMA in all slides confirms that tissue within the limits of the internal elastic lamina is synthesized by fibromuscular cells, suggesting that these newly formed tissues share a common cellular origin. Note that the most intense α-SMA staining in wild-type thrombus occurred in a pattern opposite to that of collagen signal by SHG and Movat stain.

To investigate the qualitative evidence on Movat that mutant cells produce a more collagenous matrix by the time thrombus resolution matures into neointima, we

again imaged neointimal lesions with NLOM to specifically visualize collagen organization in relation to genotype. Signal interference from the expectedly high collagen content in adventitia drowns out SHG in the neointima somewhat, but a relatively intense signal is detectable in a band pattern of undulating and honeycombing collagen fibers circumscribing the lumen in both genotypes, although to a greater degree in *Col3a1*$^{+/-}$ lesions. This honeycombing pattern of matrix within the neointima by late timepoints has been described previously[53].

Quantification of nonlinear optical microscopy signal reveals significantly higher mean intensity of collagen signal in Col3a1$^{+/-}$ *neointima and wider variance in fiber width.*

To test the hypothesis that impaired production of type III collagen leads to disproportionately high overall collagen accumulation in neointimal scars, we imaged apical neointimal lesions chosen from the arteries of 5 *Col3a1*$^{+/+}$ and 6 *Col3a1*$^{+/-}$ mice. We restricted the field of view of the NLOM software to the neointima, thereby excluding any saturating interference from adventitia, while applying the same field to each segment. Even within any given neointima, the tissue displayed regional variation in signal intensity. We captured multiple images from each section (N = 31 *Col3a1*$^{+/+}$, 57 *Col3a1*$^{+/-}$ total images), semi-randomly positioning the field to sample all quadrants of neointimal tissue.

From each of the captured images, we applied a region of interest mask over the neointima to derive a mean neointimal SHG intensity, which we then normalized to the intensity derived from a mask including only a portion of the internal elastic lamina (Figure 3.9A). Immunohistochemical analysis of type III collagen has produced no

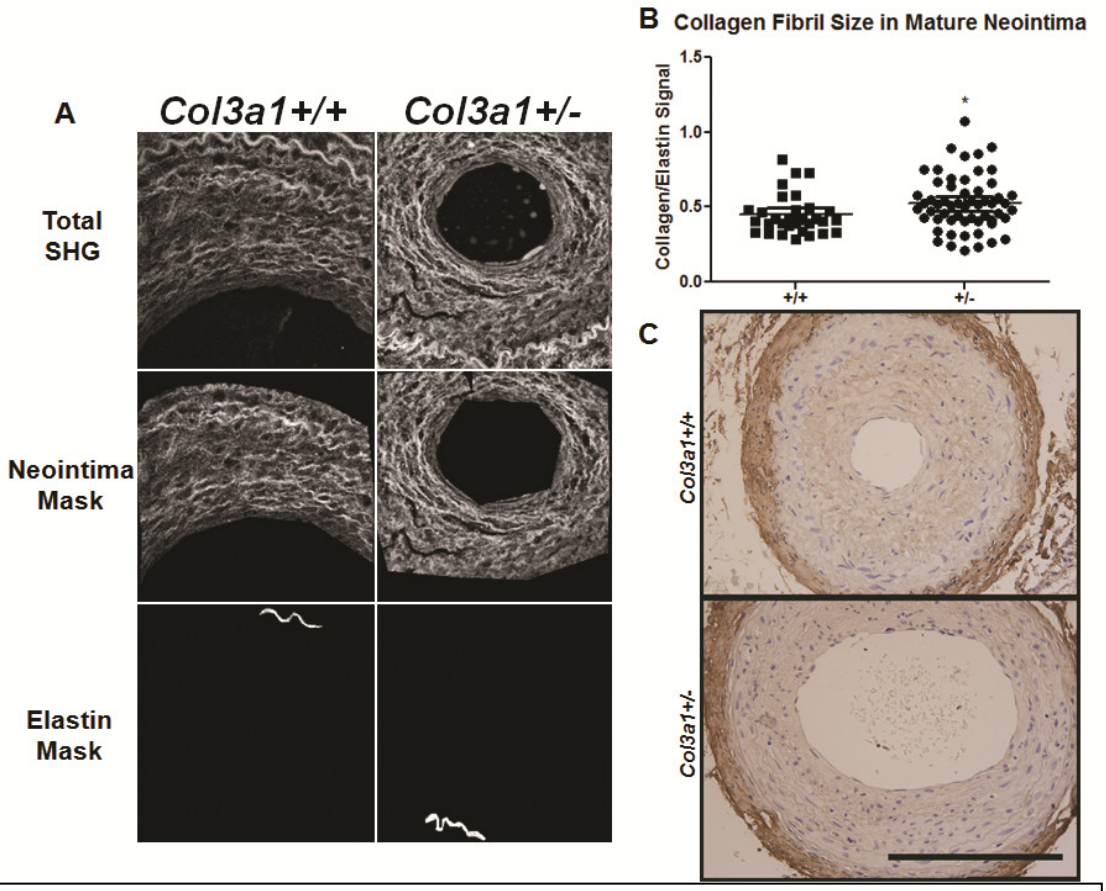

Figure 3.9. Type I collagen content within neointimal lesions negatively correlates with *Col3a1* gene dose. (*A*) NLOM microscopy (FOV 1) was used to visualize fibrillar collagen within mature neointimal lesions and intensities quantified by normalizing mean SHG intensity within the region of interest to mean intensity derived from a segment of the internal elastic lamina. (*B*) Intensity ratios were plotted from each image to depict regional variation within lesions observed at high power. Normalized SHG generated by mutant neointima was significantly more intense that that in wild-type tissue, and wider spread of values suggests greater variation in fibril diameter in mutant lesions. (*C*) Immunostaining for type I collagen produced a honeycomb-shaped signal identical to SHG images, which was limited to the neointima and absent in the arterial media, confirming that mature neointimal collagen largely consists of type I fibers.

positive stains within mature neointimal lesions in our hands (data not shown). Thus, to determine whether SHG signal at POD21 neointima was generated from type I collagen, we immunoprobed arterial sections containing prominent neointima, which showed positivity in the identical honeycombing pattern described above. Notably, this signal was limited to the neointima and did not extend into the arterial media, suggesting differential behavior in response to injury between the two tissues (Figure 3.9C).

By comparing the mean collagen/elastin signal ratios from the pooled images for each genotype, we confirmed a significantly increased mean intensity in *Col3a1*$^{+/-}$ neointimal lesions (Figure 3.9B, $p = .0408$) and a trend toward wider variance in mutant lesions ($p = .0668$). The algorithm from which NLOM signal intensity is derived produces higher intensities both from more numerous fibrils and from thicker collagen fibrils, so these data are consistent with multiple descriptions of increased mean thickness of collagen fibrils, as well as greater variability in fibril thickness, both in *Col3a1* knockout mice[15] and in human vascular Ehlers-Danlos syndrome patients[9].

Impaired synthesis of type III collagen in the proliferative phase of thrombus resolution is associated with early increases in SHG.

As the dramatic increase in proportional type III collagen content occurs temporarily during granulation tissue formation and is subsequently resorbed with maturation of wound healing[76], we sought to detect type III collagen production in tissues from our POD14 cohort of index slides displaying morphology resembling proliferating and expanding granulation tissue. It was at this timepoint that type III collagen-deficient arteries first began to show significantly increased incidence of neoangiogenesis, so we sought to more clearly associate differential type III collagen production in the expanding matrix with pathological changes.

In wild-type vascular granulation tissue at 14 days after injury, type III collagen production was abundant by immunohistochemical probe. By comparison, haploinsufficient tissues conspicuously lacked type III collagen within their matrix, despite similar appearance to wild-type tissues on H&E stain. NLOM of slides from the

same POD14 cohort demonstrated an opposite effect of type III collagen deficiency on the intensity of SHG. Normalized collagen/elastin SHG in resolving thrombi was greater in mean intensity in *Col3a1* mutant tissues as compared to wild-type tissues (0.6615±0.31 vs. 0.4505±0.14; N = 5 $Col3a1^{+/+}$, 5 $Col3a1^{+/-}$ sections), which is even more striking considering that little of the signal was generated by type III collagen. However, differences in intensity were underpowered and not significant (p = .2063).

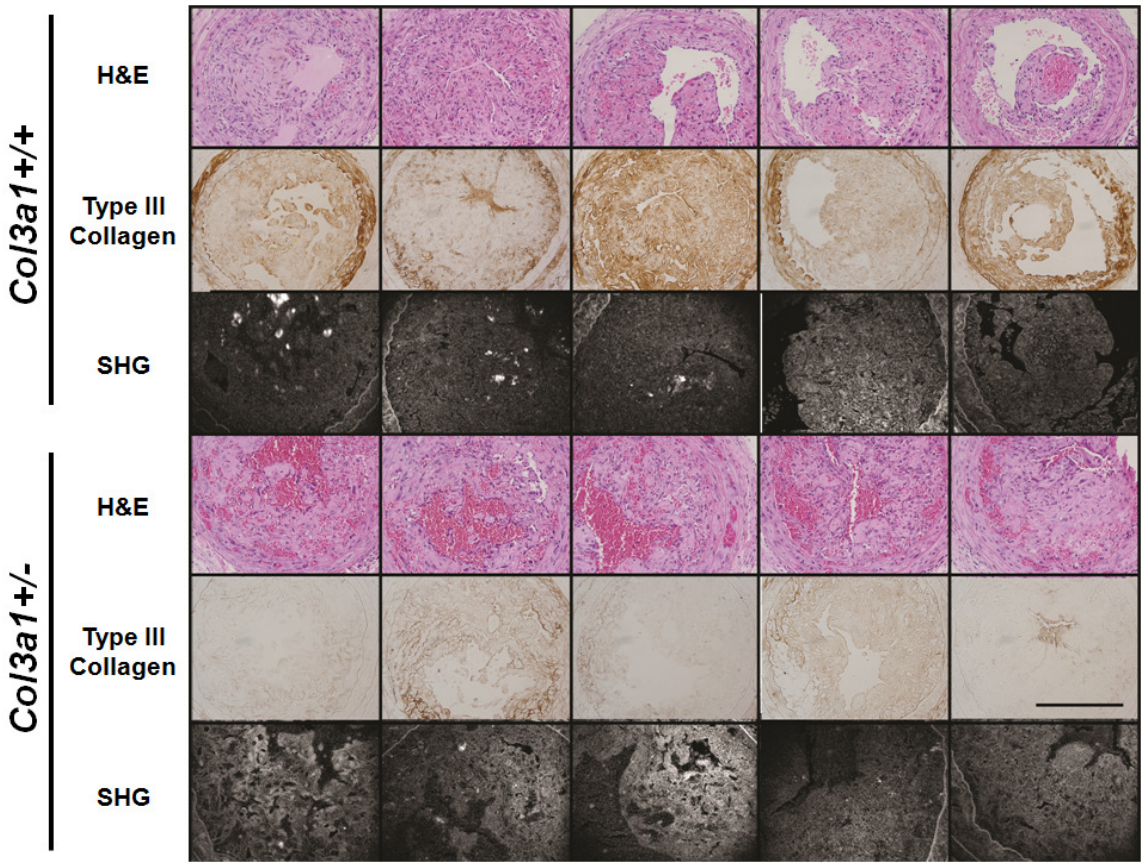

Figure 3.10. Type III collagen content and SHG collagen signal in vascular granulation tissue 14 days after injury. Resolving thrombi that resemble granulation tissue in wild-type arteries express abundant type III collagen, in comparison to $Col3a1^{+/-}$ tissues. A counterstain was not applied in order to allow for unambiguous signal differences between genotypes. SHG from NLOM investigation of artery sections paradoxically reveal increased signal for collagen in $Col3a1^{+/-}$ thrombi, suggesting that signal was generated largely by type I collagen. Note that SHG appears more in a diffuse field in all sections at POD14, in contrast to more discrete fibers observed at POD21.

Impaired synthesis of type III collagen during the remodeling of three-dimensional fibrin gels alters the mechanism of gel compaction following TGF-β1 stimulation.

To clarify the effects of delayed secretion of type III collagen on wound healing, especially in the context of thrombus resolution, we chose an *in vitro* model exploiting primary fibroblast cell lines seeded within three-dimensional stabilized fibrin lattices tethered to the tissue culture dish as a gelled hemisphere. Once the cultures gelate, the cells are stimulated with TGF-β1 (10 ng/ml) to simulate the conditions of fibroblasts recruited into platelet- and/or inflammatory cell-rich thrombi. Over time, the evolution of tensional forces that develop as these cells remodel the fibrin matrix provide further stimulation. Furthermore, not only does the fibrin gel construct better model a primitive thrombus than a collagen gel and stimulate *Col3a1* expression[102], it also allows for unambiguous observation of synthesis and rearrangement of *new* collagen by NLOM imaging.

We compared dermal fibroblasts isolated from human patients with *COL3A1* missense mutations of various impact on fibroblast secretion of type III collagen[9] with those from age-matched controls, as well as murine fetal dermal fibroblasts isolated at E18 from *Col3a1*$^{+/+}$, *Col3a1*$^{+/-}$, and *Col3a1*$^{-/-}$ littermates. All cell lines successfully contract the volume of their gel matrix from a hemisphere to a flattened disc by 24h and are grossly indistinguishable. Gels were fixed after 1d, 3d, 7d, and 14d and imaged by NLOM for TPF and SHG to observe the production and organization of fibrillar collagen by local cells over time. By day 3, only the slightest traces of collagen were visible, mostly in control, type III collagen sufficient cell lines (data not shown). However,

collagen was clearly visible in all cultures by day 7, and emerging differences in the accumulated levels and structural configuration of that collagen were most obvious by day 14.

In the control, type III collagen sufficient cultures, both in normal human and *Col3a1*$^{+/+}$ cells, resident fibroblasts secreted collagen at levels generating a more intense signal than levels produced by mutant cells. In fact, the intensity of signals generated by fibrillar collagen appears to decrease with the increasing severity of mutations in *COL3A1* in human cells (as mutations nearest to the C-terminus are associated with lower type III collagen secretion; Figures 3.11 and 3.12) and decrease with reducing gene dose of *Col3a1* in mouse cells (data not shown). Although fibrillar collagen includes both type I and type III collagen, the magnitude of signal differences between mutant and control cultures suggests a suppressive effect by mutations on the production of type I collagen, above and beyond their more direct effects on the secretion of type III collagen (Figures 3.11 and 3.12).

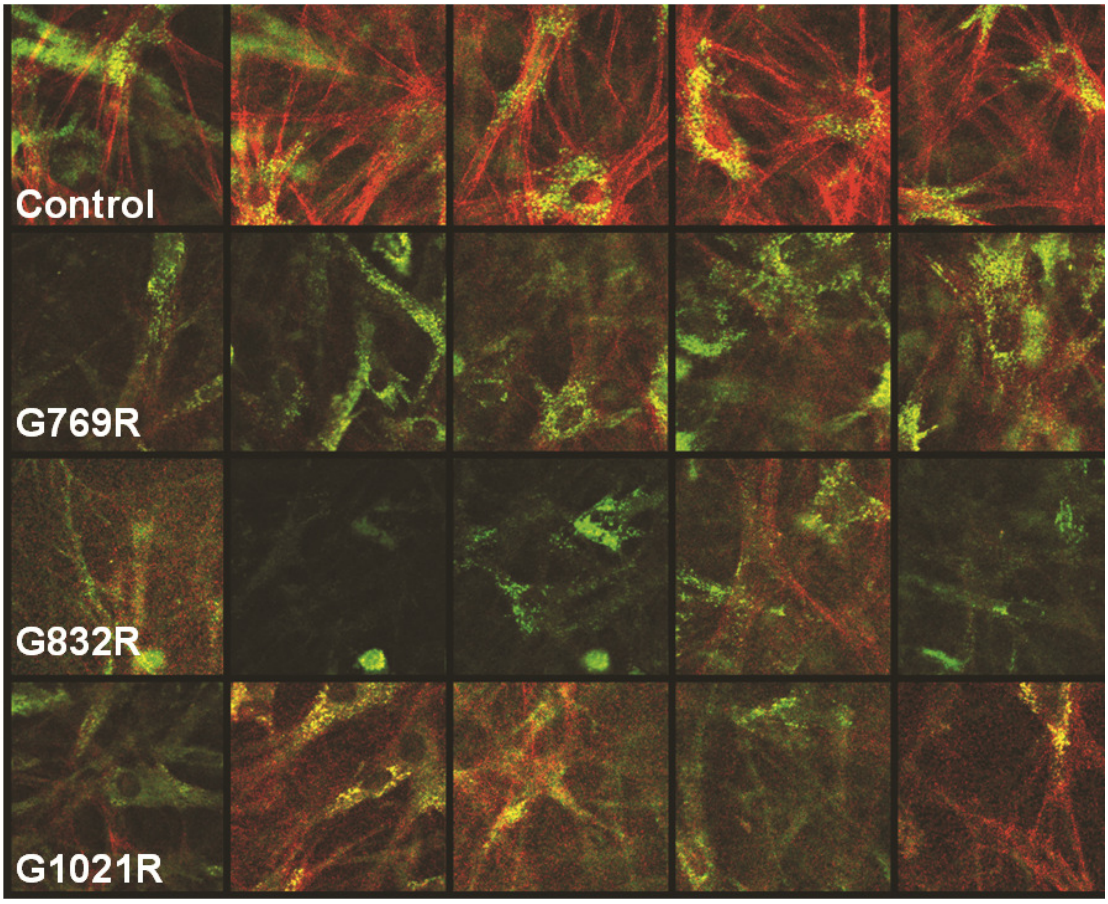

Figure 3.11. Remodeling of newly synthesized collagen as a function of *COL3A1* genotype after 7 days in three-dimensional culture. By 7 days, control cells have already organized radiations producing more intense collagen matrix SHG signal, which extend outward in a network from compact cell bodies. Human vEDS patient cells display initial formation of radiations in genotypes less detrimental to type III collagen secretion (G769R and G832R), but cell bodies are more extended and spindled and seemingly more numerous as severity of genotype/phenotype correlation increases, seen at the most extreme in G1021R cultures.

Furthermore, resident cells appear to have arranged the collagen fibers present in cultures at day 7 and day 14 differently as a function of relative type III collagen production. Control cells extend radiations of collagen fibers outward from their relatively compact cell bodies, while cultures harboring the most severe mutations (G1021R) only contain collagen fibers thinly sheathing lengthy, extended cell bodies and processes. Remaining cultures occupy this structural spectrum from compact cells/radiating collagen to extended cells/collagen sheaths as a function of their

genetically-mediated rate of secretion of new type III collagen into the matrix over time (Figures 3.11 and 3.12).

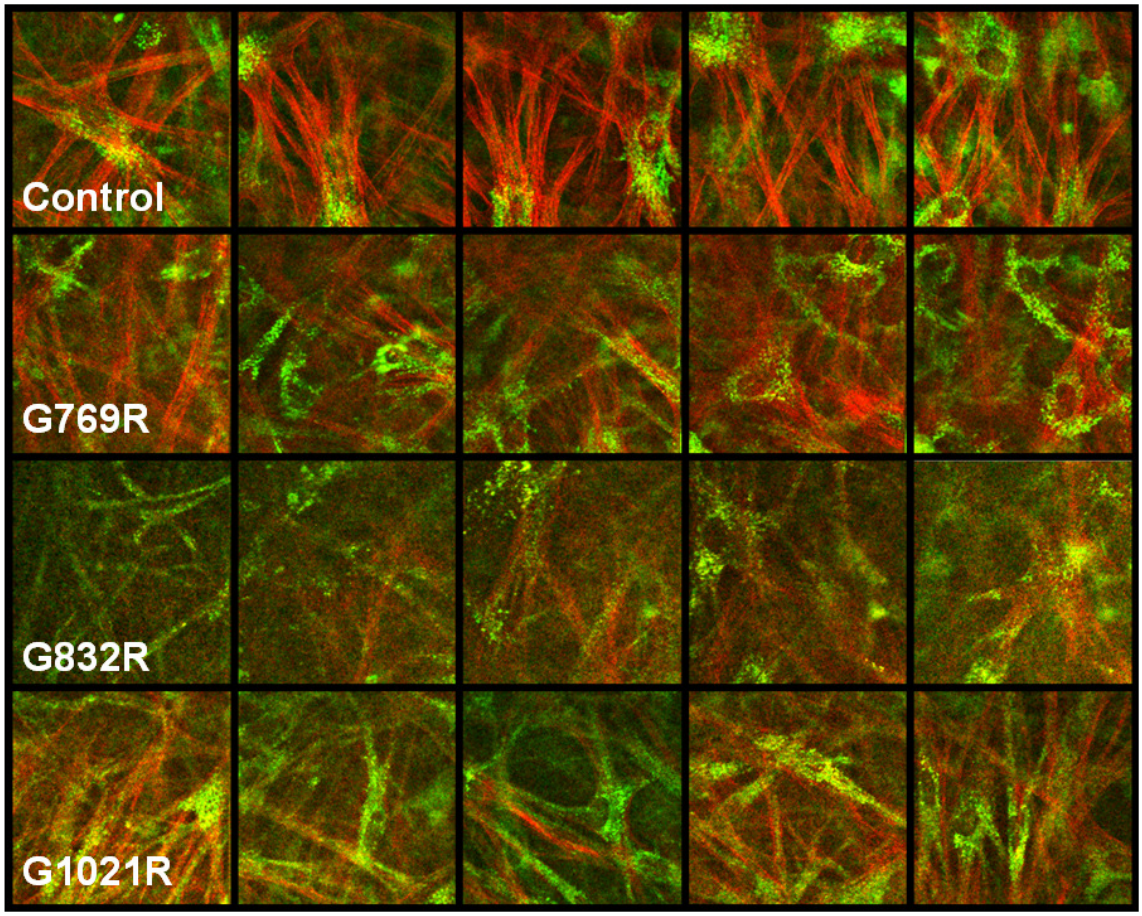

Figure 3.12. Remodeling of newly synthesized collagen as a function of *COL3A1* genotype after 14 days in three-dimensional culture. By 14 days, organized radiations produced by control cells become thicker and more numerous per cell, increasing intensity of SHG signal. Human vEDS patient cells display further thickening of radiations and cell body compaction in a spectrum varying by genotype/phenotype correlation with rate of type III collagen secretion (top to bottom). In the most severely affected and most type III collagen-deficient cultures (G832R and G1021R), cells form only meager radiations, and most signal remains localized in a sheath around more numerous cell bodies and extended bipolar processes.

Impaired synthesis of type III collagen during the remodeling of three-dimensional fibrin gels inhibits transcription of COL3A1, *COL1A1*, and *COL1A2 but disinhibits transcription of ACTA2.*

Quantitative PCR analysis assayed the relative transcription of genes responsible for the major fibrillar collagens in the extracellular matrix, *COL3A1*, *COL1A1*, and *COL1A2*, as the seeded cells remodeled the three-dimensional construct over time. In addition, we assayed transcription of *ACTA2*, which encodes the α-SMA protein most responsible for myofibroblast cellular contraction. Results demonstrate significantly upregulated message levels of *ACTA2* by days 3 and 7 in the cultures remodeled by cells with the most severe genetic impediment (G1021R) to type III collagen secretion (Figure 3.13). On the other hand, vEDS patient cells express lower message levels of genes encoding type I collagen compared to control cells, which was significant for both patient cell lines at days 3 and/or 7 for *COL1A2* expression but not for *COL1A1*. Surprisingly, vEDS patient cells also expressed significantly lower levels of *COL3A1* at days 3 and 7, as missense mutations in *COL3A1* perturb type III collagen secretion downstream of transcription and pose no threat to transcription efficiency (Figure 3.13).

On the other hand, myofibroblasts from all lines display similar expression

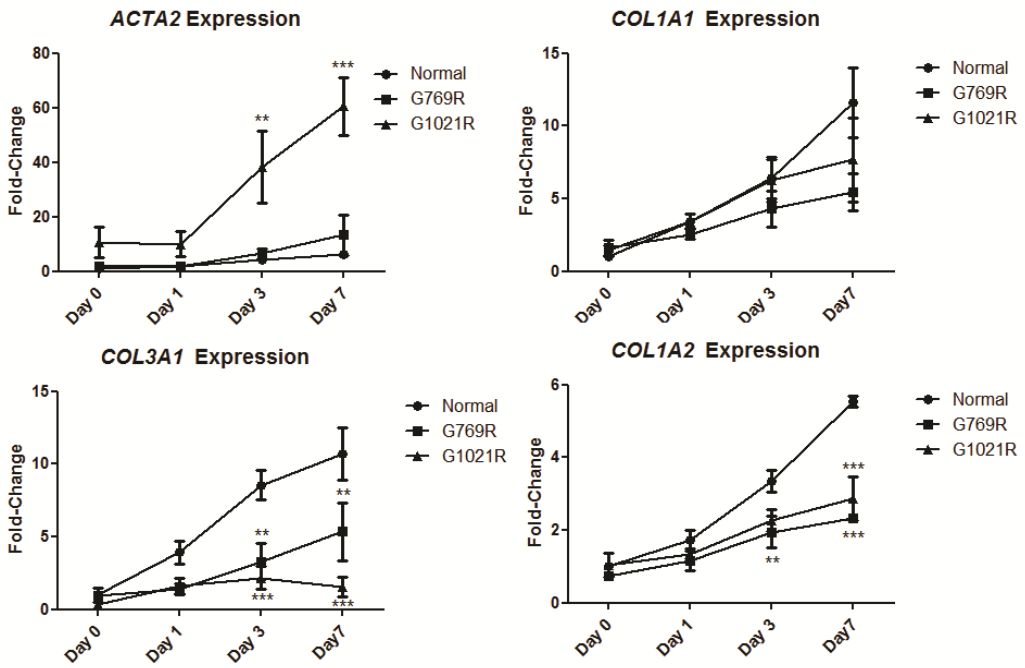

Figure 3.13. Expression of genes controlling new collagen synthesis and contraction of three-dimensional matrix in cultures of myofibroblasts following TGF-β1 stimulation. Myofibroblast cultures from vEDS patient cell lines show significantly less upregulated expression of genes encoding fibrillar extracellular matrix proteins (*COL3A1* and *COL1A2*) by days 3 and 7, compared to normal control myofibroblasts, but the most severe mutation (G1021R) in patient cells confers significantly upregulated *ACTA2* expression by the same timepoints, compared with control cultures. **, $p < .01$; ***, $p < .001$.

of genes necessary for production of α1β1 and α2β1 integrin receptors that mediate outside-in signal transduction from the matrix, in particular via ligand binding by unique motifs present on type III collagen[119], and display similar expression of *TGFB1* necessary for further secretion of TGF-β1 into the matrix. One exception to this is the highly significant increased upregulation of *ITGA2* ($p < .001$) 1 day after stimulation by cells with an intermediately severe genotype (G769R). Otherwise, expression of *TGFB1* and *ITGA2* similarly increases after 1 day but again returns to baseline by day 3 and remains there at day 7 in all cells. Expression of *ITGA1* and *ITGB1* commonly and steadily increases among all cell lines (Figure 3.14).

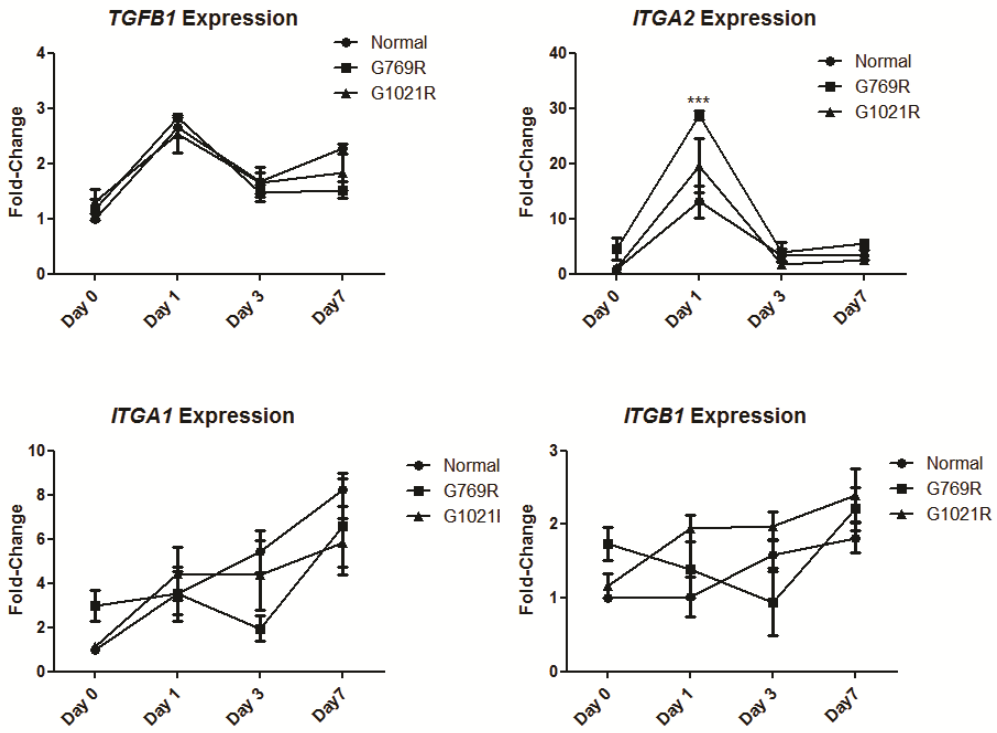

Figure 3.14. Expression of genes encoding proteins that mediate outside-in matrix signal transduction in response to TGF-β1 stimulation. Patient cells upregulate genes encoding TGF-β1 and α1β1 and α2β1 integrins known to interact with binding sites on type III collagen similarly to upregulation by normal control cells, with the exception of highly significant enhanced expression of *ITGA2* by G769R cells at day 1. ***, $p < .001$.

Lastly, expression of genes encoding matrix-digesting enzymes collagenase (MMP-1) and matrix metalloproteinase-9 (MMP-9) robustly increases at day 1 in response to TGF-β1 but occurs similarly within all cell cultures, while expression of the gene encoding matrix metalloproteinase-2 (MMP-2) remains negligible (Figure 3.15).

Data from cultures of mouse fetal dermal fibroblasts showed similar trends in expression to the human myofibroblast cultures above, although differential expression by mutant genotypes was not significant. One notable exception to this was the replication of significantly increased ($p < .05$) expression of *Itga2* by *Col3a1*$^{+/-}$ myofibroblasts, cells harboring an intermediate *Col3a1* gene dose, 1 day after TGF-β1 stimulation (data not shown).

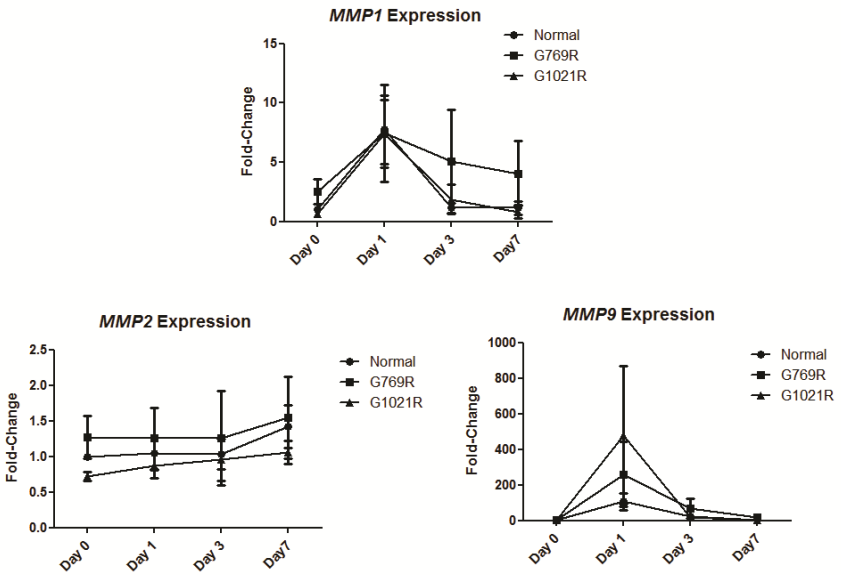

Figure 3.15. Expression of genes encoding matrix-digesting enzymes in response to TGF-β1 stimulation. All lines similarly demonstrate robust upregulation of *MMP1* and *MMP9* at day 1 after TGF-β1 stimulation before returning to baseline at day 3, while expression of *MMP2* remains flat throughout.

Discussion

We noted previously that neointimal lesions when present were always situated at or just beyond the poles of resolving thrombi, which, on the basis of the migrating wave-like progression of thrombus resolution, suggests that they represent the most mature phase of arterial wound healing. Thus, they resemble a residual cutaneous scar and likely possess the collagenous matrix most maturely organized since the eliciting injury. Here we present evidence that formation of a mature neointimal scar in type III collagen-deficient arteries in response to injury involves production of deranged collagen by resident myofibroblasts (Figure 3.9). Furthermore, this derangement occurs within the timeframe that collagen acquires a more ordered structure through active remodeling by these fibroblasts, which is apparent when comparing the discrete fibrous shape of SHG signal at POD21 to the more diffusely distributed signal at POD14 (Figure 3.10). Although it is not explicitly clear that an increased mean intensity of SHG as

measured by NLOM is directly proportional to increased collagen mass within the tissue, the relationship between signal and individual fiber diameter implies a higher mean diameter of collagen fibrils and a wider variance in diameters. This is consistent with a defining feature of fibrosis: *disorganized* and highly-crosslinked collagen deposition[120].

The discrepancy between SHG signal produced by type III collagen-deficient tissues, where signal is enhanced, and that produced by type III collagen-deficient cell cultures, where signal is lacking, likely results from the difference in relative density of myofibroblasts involved between the remodeling of the tissue and remodeling of the gel construct. Again, timing is everything. Neointimas in *Col3a1*$^{+/-}$ tissues are organized at late timepoints, after 21 days, by cells derived from those in preceding thrombi, which we have shown to contain a significantly abnormal density of proliferating myofibroblasts when compared with wild-type thrombi (Figure 2.19). Experimental constructs of type III collagen-deficient gels instead begin with the same number of cells as wild-type control gels and were only followed for 14 days.

In addition, increased α-SMA expression, as would occur from in increased number of actively contracting myofibroblasts, directly correlates with increased contractile tension within a remodeled tissue[95], and sustained tension further upregulates α-SMA expression[90,91]. Thus, the lack of sufficient ramping of tension could explain the failure to elicit differential expression of *Acta2* or matrix genes in mouse gel constructs at late timepoints, when gels contained less than half the number of myofibroblasts that were seeded into human cultures. In fact, significantly increased early *Itga2* expression by cells with intermediately severe mutations at early timepoints was preserved between species.

As suggested by our quantitative PCR results from human cultures, on the other hand, mechano-sensitive feedback from growing tension in the matrix is one of the driving forces behind transcriptional regulation of collagen production. Cells from all genotypes generally show similar TGF-β1-mediated early transcription events in the first day of culture, before *ACTA2* expression even begins to rise (Figures 3.13, 3.14, and 3.15). However, events occurring between 3 and 7 days, long after the original TGF-β1 pulse, involve deposition and organization of new insoluble extracellular matrix, as observed in NLOM images from remodeling gels (Figures 2.11 and 3.12). It is the feedback from deposition and reorganizing activity by cells in this time period that correlates with the emergence of differential transcription of genes encoding matrix proteins by mutant cultures (Figure 3.13).

The effect of tension and collagen accumulation on transcriptional regulation of matrix production was most obvious in the regulation of *COL3A1* expression by human myofibroblasts. Unlike mutant cells from mice, where haploinsufficiency of the allele determines a maximum rate of transcription at half the rate of wild-type cells, missense mutations in humans do not impede initial transcription but only the maximum rate of post-translational secretion of structurally altered proteins from the endoplasmic reticulum. So the fact that we observe differential expression of *COL3A1* at late timepoints as a function of genotype in human cultures suggests that *COL3A1* expression is sensitive to feedback dependent on the rate of secretion of new type III collagen.

In vitro experiments generating copolymers of type I and type III collagen have determined that the relative content of each at the time of fibrillogenesis determines the

rate of fibril extension, the diameter of resulting fibrils, and the flexibility of those fibrils[105], so it is likely that sluggish production of new type III collagen alters the material properties of the total matrix produced, possibly providing some type of feedback to suppress the further upregulation of *COL3A1* and *COL1A2* and promote the compensatory upregulation of *ACTA2* (Figure 3.13).

Some hint of such a mechanism comes from the concept of stress-shielding in mature connective tissue, where cells are shielded from external loads on the tissue by the mechanical properties of the organized matrix they construct. That is, even after an original matrix volume has been compacted into a higher density, the cells themselves no longer have to bear the load of resisting tension their own cellular contraction[94]. This could explain the simultaneously compact bodies of control cells in NLOM images and the plateau reached in *ACTA2* expression after 7 days in culture (Figures 3.11 and 3.13).

Images of mutant cultures, on the other hand, demonstrate an inability of cells within a type III collagen deficient matrix to construct a stress-shielding connective tissue on the same timecourse as normal, type III collagen sufficient cultures, such that burden of tensional loads may instead fall on the contractile myofibroblasts themselves and on the energy required to maintain that contraction for a longer period of time. This prediction of increased reliance on contraction is borne out by images of extended myofibroblasts in the absence of a matrix shield and the simultaneous excess in *ACTA2* expression observed in these cultures after 7 days (Figures 3.11 and 3.13). Rather than waste the energy of indefinite contraction, a programming switch to forego present matrix production to instead initiate proliferation and generate more cellular actors within the tissue before reattempting matrix production could be yet another way that

mutant cells cope with an untenable tensional load. If this cycle continuous without cells ever achieving stress-shielding of tension due to the inflexible matrix they inevitably produce, a fibroproliferative contracture could plausibly result[94].

Chapter 4: Altering the Course of Thrombus Resolution Alters the Incidence of Vascular Defects Following Injury

Introduction

In-Stent Restenosis and the Development of Drug-Eluting Stents

With the advent of endovascular interventions to restore patency of arteries occluded by arterial diseases like atherosclerosis, the development of restenosis of the lumen following balloon angioplasty or stent placement poses a substantial impediment to successfully alleviating ischemia[121], despite however much thickening adaptively decreases stress on injured walls. Stents improve upon angioplasty through the device's permanent geometric resistance to diameter-reducing remodeling of the arterial media, a homeostatic response to decreased flow as discussed in Chapter 2. However, restenosis as a consequence of neointimal hyperplasia persists, affecting virtually all treated patients, with 7% suffering total occlusion and 30% suffering partial "proliferative" occlusion that extends beyond the axial length of the stent[122].

Cytostatic strategies to reduce the activation and proliferation of neointimal cells in response to vascular injury and inflammatory stimuli thus include the local administration of rapamycin (also known as sirolimus) by coated stents, in theory to replicate rapamycin's *in vitro* check of vascular SMC S phase entry by maintaining levels of $p27^{Kip1}$ cyclin-dependent kinase inhibitor. At 3 and 7 days after placement of stents, local rapamycin delivery led to lower protein levels in whole vessel lysates of the proliferative markers proliferating cell nuclear antigen (PCNA) and phosphorylated retinoblastoma protein (pRb) by 60% and 50%, respectively, and higher levels of $p27^{Kip1}$. By 28 days, use of sirolimus corresponded with a ~50% reduction in stenosis in

both pigs and humans on histological images in comparison to arteries stented with bare metal[84,121,123-125] (Figure 4.1).

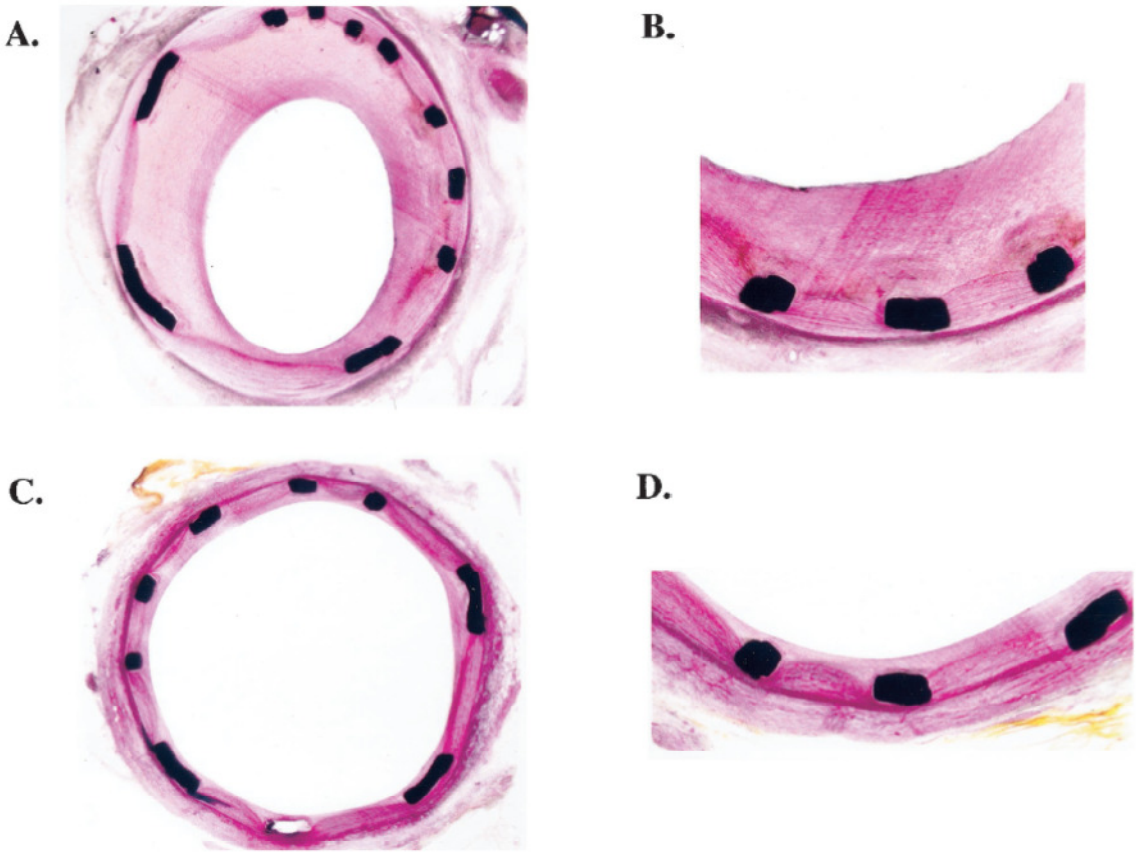

Figure 4.1. Low- and high-power photomicrographs 28 days after oversized stent placement in normal porcine coronary arteries. *A* and *B* (high power) are a bare metal stent with neointimal formation typical for degree of strut-induced medial injury. *C*, Rapamycin-coated stent has significantly less neointima vs. bare metal stent despite a similar degree of vessel injury. High-power photomicrograph of rapamycin-eluting stent (*D*) demonstrates neointima consisting of SMCs and proteoglycans. Notice strut-induced focal medial compression without medial necrosis or intimal hemorrhage. Reprinted with permission from Wolters Kluwer Health [Stent-based delivery of sirolimus reduces neointimal formation in a porcine coronary model. Suzuki T, Kopia G, Hayashi S, et al. *Circulation*. 2001].

However, attributing these results to such a straightforward antiproliferative mechanism deserves reconsideration. We presented evidence in Chapters 2 and 3 that the development of neointimal lesions *requires* and emerges as only the final stage of several in the process of thrombus resolution and vascular wound healing. Studies of

neointimal thickening following rapamycin, like those above, have largely failed to fully investigate the link to early thrombosis-related events, instead relating molecular analyses at early timepoints to histological morphometry at later timepoints and incorrectly assuming that these metrics gauge an identical and linear outside-in proliferative process[84,123]. It is possible that rapamycin may not directly inhibit the proliferation of neointimal cells as surmised but may instead fundamentally alter the course of critical upstream inflammatory events.

Rapamycin as an Immunomodulator

Rapamycin/sirolimus is a natural product macrolide extracted from microorganisms in the soil of Easter Island (site of the extinct Rapanui civilization). It was originally celebrated as an immunosuppressant preventing acute rejection of transplantated allografts on par with cyclosporin and tacrolimus, which impede T cell activation and subsequent proliferation by specifically inhibiting calcineurin-dependent transcriptional upregulation of cytokines like IL-2 and their receptors[126, 127]. However, rapamycin, though similar in macrolide structure to tacrolimus, has no effect on cytokine production but instead alters intracellular signaling elicited by IL-2 receptor agonism to block T cell proliferation. Rapamycin arrests the G1-to-S-phase progression by interrupting the decline of $p27^{Kip1}$ and rise of $p21^{Cip1}$ cyclin-dependent kinase inhibitors as above, but this inhibitory effect is not limited to T cells or even to IL-2 signaling but likely extends to growth-factor-mediated cell behavior more generally[127,128].

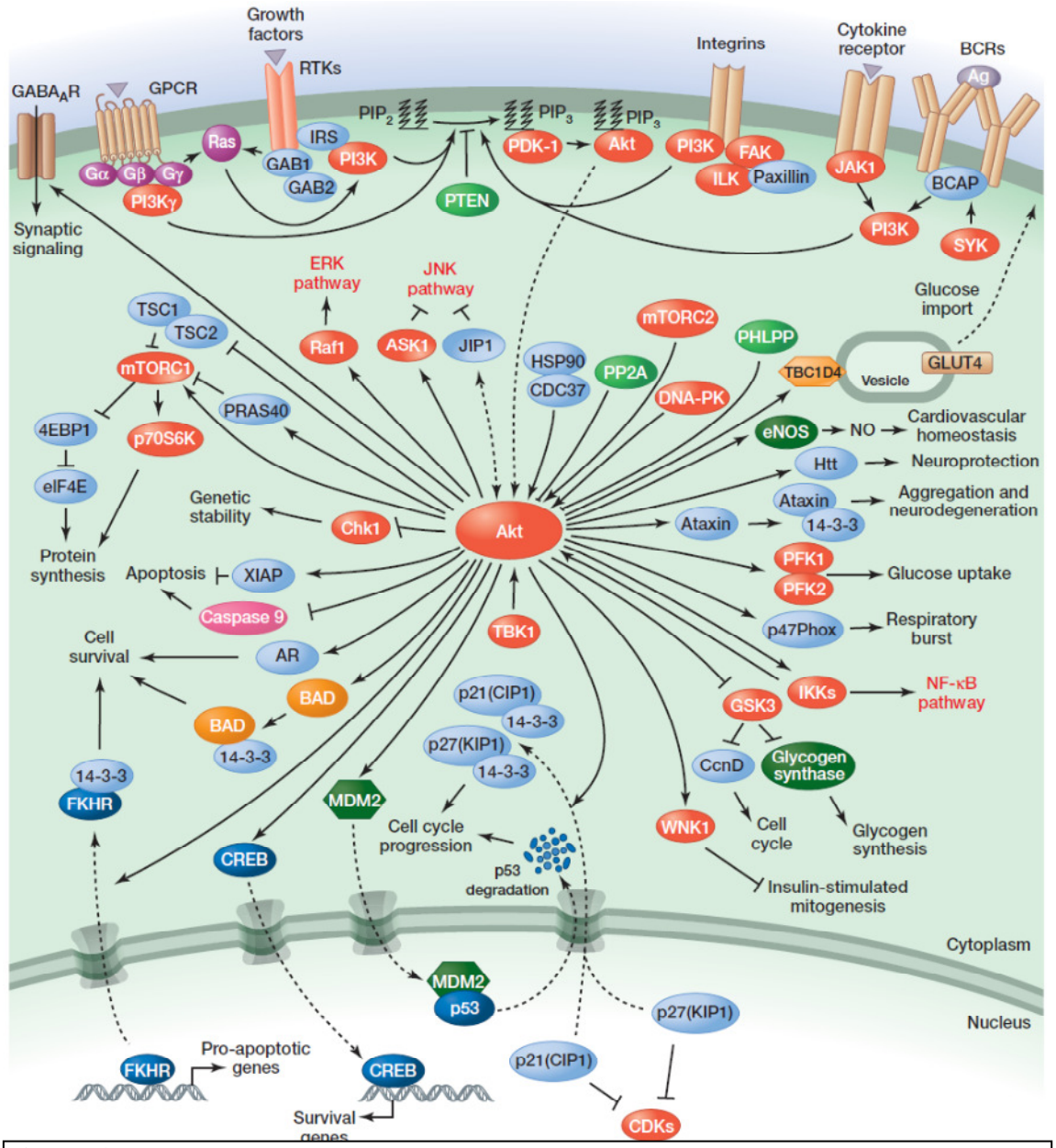

Figure 4.2. Signaling events activating Akt and cellular functions regulated by Akt. Reprinted with permission from Cold Spring Harbor Laboratory Press [PI3K-PKB/Akt Pathway. Hemmings BA, Restuccia DF. *Cold Spring Harbor Perspectives in Biology*. 2012].

Rapamycin mediates its effects on signaling by inhibiting the kinase activity of mammalian target of rapaymycin (mTOR) within the broader context of the PI3K/Akt pathway (Figure 4.2), which helps explain its pleiotropic effects. The diversity of cell functions regulated via the highly conserved PI3K/Akt signaling cascade includes proliferation, survival, growth, metabolism, migration, and angiogenesis, earning a massive amount of attention from researchers, and rapamycin is a useful tool for

studying the mTOR-dependent wing of this pathway[129-131]. Not surprisingly considering this spectrum of behaviors, much of the discussion has been stimulated by the preponderance of cancer-associated mutations that impinge on this pathway, and rapamycin and its derivatives have even been auditioned as anti-neoplastic agents[132].

However, just as unchecked cell proliferation is necessary but not sufficient for carcinogenesis, the cell behavior targets of rapamycin include but are by no means limited to cell proliferation. Although rapamycin prevents IL-2-mediated T cell proliferation and acute cell-mediated allograft rejection much like cyclosporin, it also clearly outperforms cyclosporin in preventing *chronic* allograft rejection. Chronic rejection, unlike acute rejection, occurs through: 1) increasingly antibody- and activated macrophage-mediated inflammatory mechanisms, 2) the familiar occlusive vascular pathology of neointimal hyperplasia, and 3) interstitial fibrosis of the graft. So it appears that a broader mechanism extending beyond antiproliferative effects may account for the efficacy of rapamycin in attenuating both late rejection *and* neointimal hyperplasia[133-136].

Transplant biology offers an excellent disease model linking the chronic dysregulation of wound healing and fibroproliferative pathology described in Chapter 3 with problematic vascular remodeling. For our purposes here, it especially highlights the primary initiating roles of inflammatory cell migration into and chronic stimulation from within a new tissue, without negating a role for cell proliferation[137]. An elegant study transplanting mouse carotid arteries into the circulation of recipients deficient for various chronic inflammatory scenarios (i.e, no acquired immunity at all, no B cells or humoral immunity, no CD4+ T cells, or no macrophages) showed that each of these

models completely fails to develop neointimal thickening, unlike control recipients of the same background strain[138] (Figure 4.3).

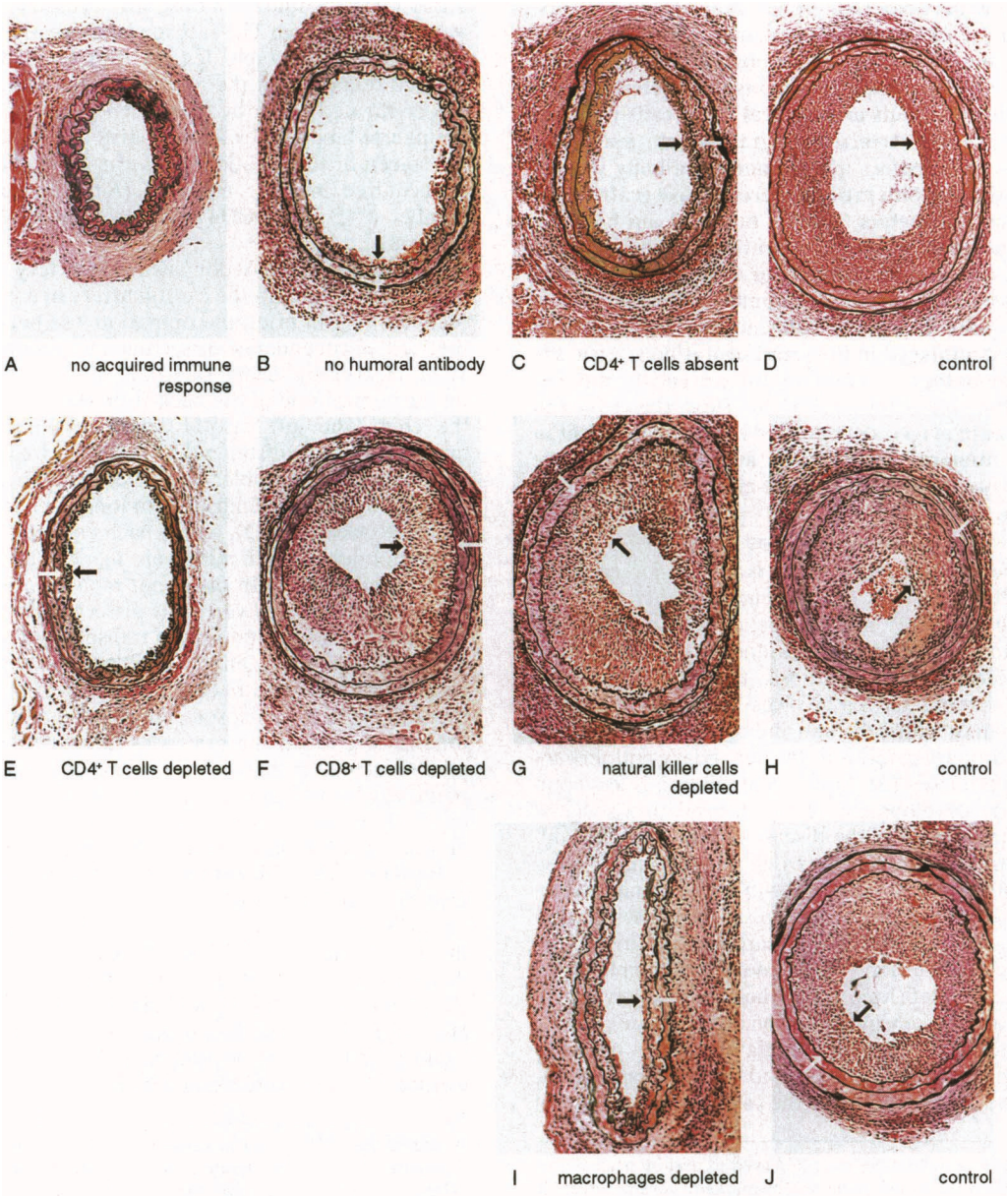

Figure 4.3. Selected sections from mouse carotid artery loops allografted into strains whose immunologic features are described in the panels. The neointima extends between the internal elastic lamina (Verhoeff's elastin stain) and the vessel lumen (between arrows in *B-J*; there is no neointima in *A*). (*A*) *Rag2*$^{-/-}$, (*B*) μMT$^{-/-}$, (*C*) CD4$^{-/-}$, (*D*) B6129F2/J control for *A-C*. (*E*) MHC II$^{-/-}$, (*F*) MHC I$^{-/-}$, (*G*) bg^{3}/bg^{3}, (*H*) C57BL/6J control for *E-G*. (*I*) *op/op*, (*J*) op/+ control for *op/op*. Reprinted with permission from the National Academy of Sciences of the United States of America [Immunologic basis of transplant-associated arteriosclerosis. Shi C, Lee W-S, He Q, et al. *Proceedings of the National Academy of Sciences*. 1996].

It follows that rapamycin could produce similar effects, as the PI3K/Akt pathway regulates chemotaxis and migration[139,140]. In fact, rapamycin potently inhibits chemotaxis and chemokinesis of phagocytic neutrophils in response to granulocyte-macrophage colony-stimulating factor[141]. Everolimus, an mTOR inhibitor derived from rapamycin for oral administration, similarly prevents both transplant vasculopathy in human patients and stent restenosis in atheroma-prone animal models. This prompted investigators to determine that it broadly inhibits human macrophage chemotaxis toward monocyte chemoattractant protein-1 and multiple other attractants *in vitro*[142]. Only minimal evidence from transplant studies extends rapamycin's blunting of chemotaxis to macrophages[143], but rapamycin clearly impedes macrophage phagocytosis of antibody-coated structures, most likely through inhibition of mTOR/p70S6 kinase-dependent organization of cytoskeletal actin[144].

Regardless, studies of neointimal thickening in $p27^{Kip1-/-}$ mice following direct mechanical injury to femoral arteries have already identified excessive infiltration of bone marrow-derived inflammatory cells, not fibrocellular proliferation, as the *primary* cause. As proof, researchers determined that bone marrow transplant from $p27^{Kip1-/-}$ donors prior to injury was sufficient to confer neointimal thickening onto wild-type mice. However, occlusive fibrocellular hyperplasia in $p27^{Kip1-/-}$ recipients of wild-type and $p27^{Kip1-/-}$ bone marrow still exceeded all other groups, suggesting that the unchecked proliferation of non-hematopoietic cells migrating into the intima downstream of inflammatory signals was also involved[145]. Thus, the most parsimonious interpretation of the fact that rapamycin elevates cellular $p27^{Kip1}$ is that, where neointimal hyperplasia progresses as an extension of vascular wound healing, the

suppressive effect of rapamycin more likely hinges on its suppression of early inflammatory cell migration, long before it can act by suppressing the proliferation of secondarily-arriving neointimal cells. The distinction is crucial, if vascular wound healing depends as much on a thrombotic nidus for inflammatory stimulation as our data would suggest, because rapamycin's protective effect against neointimal formation may simultaneously be its deadly effect against thrombus resolution.

Impairment of Wound Healing by Rapamycin

A blunting of inflammatory infiltrate by rapamycin is consistent with extensive evidence that rapamycin pathologically impairs wound healing, as successful wound healing requires macrophage infiltration (see Chapter 2). This has, not incidentally, limited rapamycin's clinical usefulness. Following transplantation in humans, rapamycin has been associated with severe complications like venous thromboembolism, dehiscence of graft anastomoses or sternal closures, gastroduodenal ulcers and hemorrhage, and deep surgical wound infections, among others[146,147,148].

Rapamycin-eluting stents significantly reduce restenosis when compared to bare-metal stents, as measured both by angiographic metrics and incidence of repeat invasive revascularization, for the first 9 months following percutaneous coronary intervention[149], earning approval by the Federal Drug Administration and widespread adoption into clinical practice. However, subsequent clinical practice also allowed broader perspectives on outcomes from much larger treatment cohorts (N = 8146 and 6033 vs. N = 1058) over a longer period of time (3 years vs. 270 days), revealing an unexpected

number of recipient patients who paradoxically survive without restenosis only to die from late stent thrombosis[150] (Figure 4.4). These events are rare but as devastating as the disease they are meant to prevent, and the risk of death from drug-eluting stents (coated

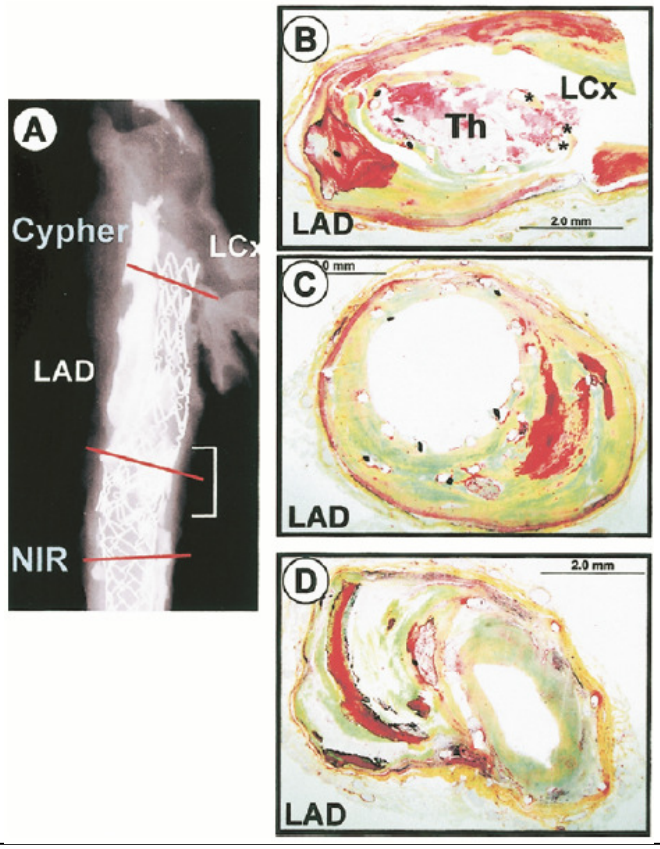

Figure 4.4. Mechanisms of late stent thrombosis in ostial and bifurcation stenting. (*A* to *D*) Radiograph and histologic sections (Movat pentachrome) from a 77-year old man who had two stents placed in the native left anterior descending coronary artery (LAD) for stable angina 450 days before sudden cardiac death. (*A*) Radiograph of the LAD with two stents in place, a proximal rapamycin-eluting (Cypher) and a distal bare-metal stent (NIR). The Cypher stent struts (*) protrude into the ostium of the left circumflex artery (LCx). (*B*) Section taken from the proximal Cypher stent, which is totally occluded by a platelet-rich thrombus while distally it is patent (*C*) with minimal neointimal tissue. The NIR stent (*D*) in the distal LAD demonstrates 50% in-stent area stenosis consisting of neointimal tissue composed of smooth muscle cells in a proteoglycan/collagen matrix with absence of fibrin. Reprinted with permission from Elsevier [Pathology of drug-eluting stents in humans: delayed healing and late thrombotic risk. Joner M, Finn AV, Farb A, et al. *Journal of the American College of Cardiology*. 2006].

in either rapamycin or paclitaxel, both antiproliferative agents) first significantly exceeds that for bare-metal stents after 6 months. Risk of thrombosis steadily increases from there, without sign of diminishing, at the rate of 0.6% per year and occurs unpredictably despite antiplatelet therapy[151,152].

Pathological evaluation of affected arteries at autopsy following fatal thrombosis show proximal occlusive platelet-rich thrombi but distally patent segments in areas within rapamycin-eluting stents, while "control" sections in areas within bare-metal stents demonstrate stenotic but stable neointimal thickening[150] (Figure 4.4). Fibrin deposits were found overlaying struts even in nonoccluded, rapamycin-stented segments from patients dying from unrelated causes, such that delayed healing prevented any growth of an endothelialized barrier between the vascular wall and the lumen[150] (Figure 4.5).

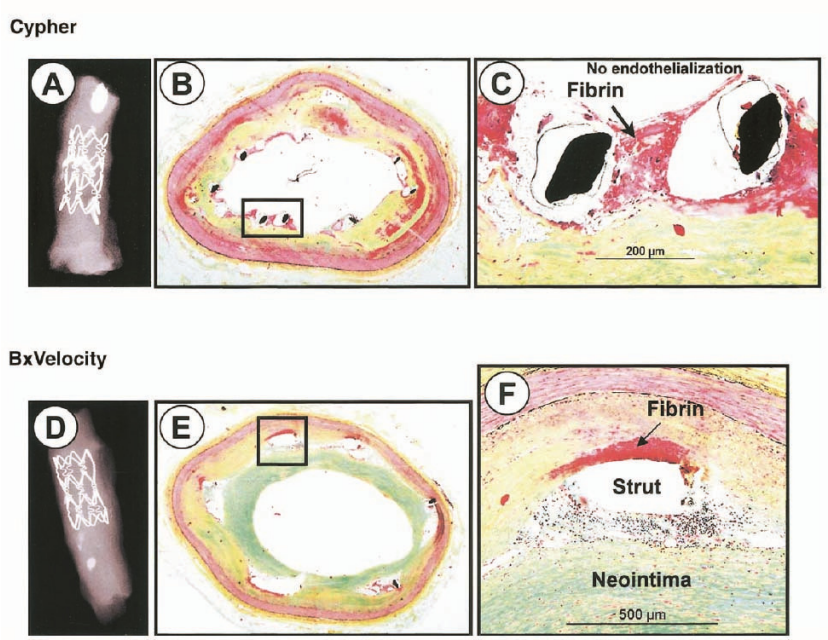

Figure 4.5. A 65-year old man suffered traumatic injury to the head resulting in death. This patient had received two stents in the LAD, a proximal Cypher and a distal Bx Velocity (bare-metal) 15 months before death, which were found to be patent at autopsy. (*A*) (Cypher) and (*D*) (Bx Velocity) are radiographs of the stented LAD segment. All sections have been stained with Movat pentachrome. (*B*) Histologic section of the Cypher stented artery showing minimal coverage of the struts by fibrin. (*C*) High-power magnification showing peri-strut fibrin with rare endothelial cells but no luminal thrombus, whereas inflammation and smooth muscle cells are only rarely observed. (*E*) Section of the Bx Velocity stent. There is abundant neointimal tissue consisting of smooth muscle cells in a proteoglycan matrix and an overlying endothelium. (*F*) High-power section of the boxed area in *E*. Lymphocytes are present around the stent strut with minimal fibrin underneath the strut. The luminal surface of the stent is covered by smooth muscle cells in a proteoglycan/collagen rich matrix. Reprinted with permission from Elsevier [Pathology of drug-eluting stents in humans: delayed healing and late thrombotic risk. Joner M, Finn AV, Farb A, et al. *Journal of the American College of Cardiology*. 2006].

The number of struts without an overlying neointimal layer positively correlated with the number of struts covered by platelet-rich thrombi, suggesting that the neointima and its endothelial barrier were actually thrombo-protective. Thus, investigators conclude that, while preventing the neointima from thickening may prevent relative ischemia due to decreased flow, the total extent of neointimal suppression does *not* suffice as a parameter by which success of clinical intervention is based. *Total* occlusion of flow by thrombosis more often occurs in the presence of rapamycin, as determined by

clinical data[151,152], and in the *absence* of endothelial-lined neointima, as determined by histological analysis, so further refinements to intravascular intervention must balance these risks[64].

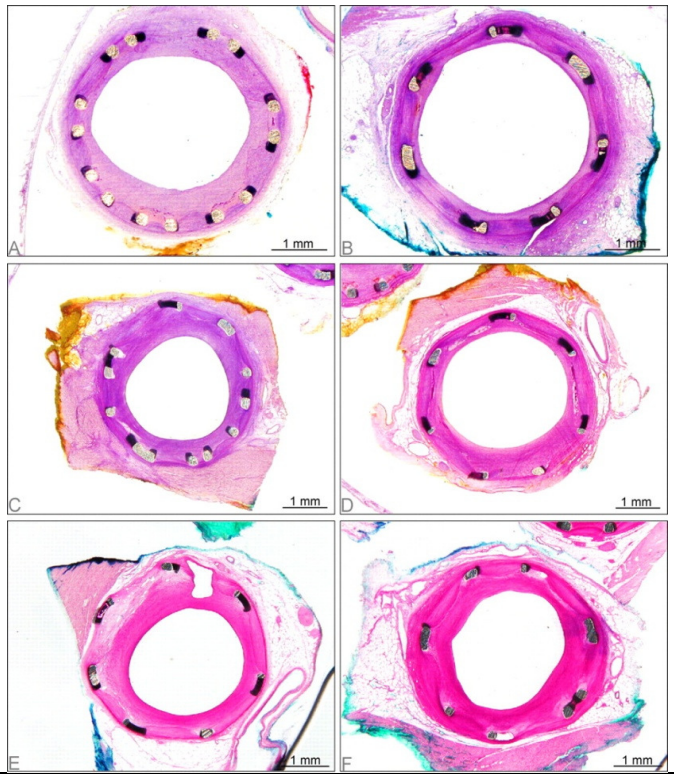

Figure 4.6. Low power photomicrographs at 30, 60, 90, and 180 days after placement of control and rapamycin-eluting stents in porcine coronary arteries. At 30 days, neointimal area is greater with bare metal (*A*) as compared to the rapamycin stent (*B*). At 90 and 180 days, neointimal area and morphology are similar for bare metal (*C*, 90 days and *E*, 180 days) and rapamycin stents (*D*, 90 days and *F*, 180 days). Metachromatic stain. Reprinted with permission from Oxford University Press [Long-term effects of polymer-based, slow-release, sirolimus-eluting stents in a porcine coronary model. Carter AJ, Aggarwal M, Kopia GA, et al. *Cardiovascular Research*. 2004].

Furthermore, evidence from pig models uncommonly followed out until very late timepoints (60, 90, and 180 days) belie the fact that rapamycin-eluting stents merely *delay* the onset of arterial inflammation and neointimal hyperplasia, eventually achieving thickness similar to that in bare-metal stents. Neointima developed in response to bare metal stents, on the other hand, had stabilized in thickness by these late timepoints.

Most surprisingly, at these late timepoints protein levels of cell cycle-inhibiting $p27^{Kip1}$ *and* the cycling marker PCNA in whole tissue lysates were elevated in rapamycin-stented arteries over bare-stented arteries, either refuting original theories that rapamycin acts by inhibiting cycling of the resident neointimal cells[153,154] (Figure 4.6) and/or possibly demonstrating a confound of extrapolating neointimal events from whole tissue samples.

Given the immunostatic properties of rapamycin and its ability to retard wound healing from progressing beyond the initial inflammatory phase, for the final aim of the current study we sought to pharmacologically alter the course of thrombus resolution prior to the functioning of mutant myofibroblasts to confirm the necessity of dysregulated myofibroblast activity for the development of vascular defects in mutant arteries. We systemically administered rapamycin to *Col3a1*$^{+/+}$ and *Col3a1*$^{+/-}$ mice daily for 14 post-operative days following carotid ligation so that we might immobilize thrombus resolution prior to the myofibroblast-driven proliferative phase. By delaying the downstream recruitment of and onset of deranged collagen synthesis by *Col3a1*$^{+/-}$ myofibroblasts, we sought to normalize the incidence of medial neovascularization observed between wild-type and mutant arterial segments at POD21. This would imply that myofibroblast activity, including production of deranged collagen matrix, is necessary for the emergence of vascular defects in type III collagen-deficient mice, and that the appearance of blood-filled vascular channels occurs through the active process of remodeling following injury rather than as a complication of baseline arterial fragility.

We also hypothesize that prevention of initial thrombus formation may improve the incidence of medial neovascular defects in the walls of *Col3a1*$^{+/-}$ arteries and

possibly identify a therapeutic avenue for vEDS patients. However, our original data involved the use of ketoprofen for pain control in the first two post-operative days, and ketoprofen possesses a potent antiplatelet activity equivalent to aspirin[155,156,157]. Thus, we opted to investigate the influence of ketoprofen over the incidence of medial defects at POD21 by repeating carotid ligations but switching pain control methods to the administration of buprenorphine, an opioid narcotic. We expect that buprenorphine will further prolong thrombus resolution and exaggerate differences in the incidence of defects in mutant mice.

Methods

Administration of rapamycin following injury by carotid ligation.

Carotid ligation was performed exactly as described originally in Chapter 2, this time with 4 *Col3a1*$^{+/+}$ mice and 4 *Col3a1*$^{+/-}$ mice subsequently receiving rapamycin daily for the first post-operative 14 days. Rapamycin dissolves poorly in aqueous solution, so powder was dissolved into DMSO at a concentration of 25mg/ml. At the time of treatment, rapamycin/DMSO solution was freshly diluted 1:10 into PBS just before subcutaneous injection into the animal, so that the drug could not precipitate out of the injectate. The resulting injected dose, administered for the first time at 4 hours after the conclusion of the procedure and daily after that, was a total of 2mg/kg. For vehicle-treated controls (N = 5 *Col3a1*$^{+/+}$ mice; 5 *Col3a1*$^{+/-}$ mice), animals were administered an equivalent volume of DMSO based on weight to their counterparts in the rapamycin-treated arm, which was freshly diluted 1:10 just before injection over an

identical timecourse. Mice recovered from surgery over a similar timecourse as before, losing and regaining weight within the first 7 post-operative days without any excessive rates of death in comparison with mice from the original untreated experiments.

All mice were sacrificed on POD21 and their carotid arteries processed as described in Chapter 2. Histological analysis, by an identical method of counting the presence or absence of occlusive thrombus and presence or absence of media-occupying neovessels for each index slide, was performed. Results between rapamycin- and vehicle-treated groups from each genotype were analyzed by constructing 2x2 contingency tables and applying Fisher's exact test. Tables were first constructed to compare effects of genotype under the condition of each treatment, and a second round of tables was constructed to compare effects of treatment on each of the genotypes.

Administration of buprenorphine following carotid ligation.

In this experiment, 4 *Col3a1*$^{+/+}$ mice and 9 *Col3a1*$^{+/-}$ mice received carotid ligation, and we merely switched the prescribed analgesic for pre- and post-operative pain relief in rodents from 5mg/kg ketoprofen (administered as pre-operative analgesia and twice daily for the first two post-operative days) to 0.1mg/kg buprenorphine (administered as pre-operative analgesia and twice daily for the first two post-operative days). All subsequent post-operative care was identical to the original experiments in Chapter 2, although we observed no animal deaths before scheduled sacrifice at POD21 in this cohort, likely due to superior pain control by buprenorphine. Carotid arteries

were harvested, processed into index slides, and the resulting pathology analyzed again identically to methods described in Chapter 2.

Results

Rapamycin treatment profoundly retards thrombus resolution, similarly affecting both genotypes.

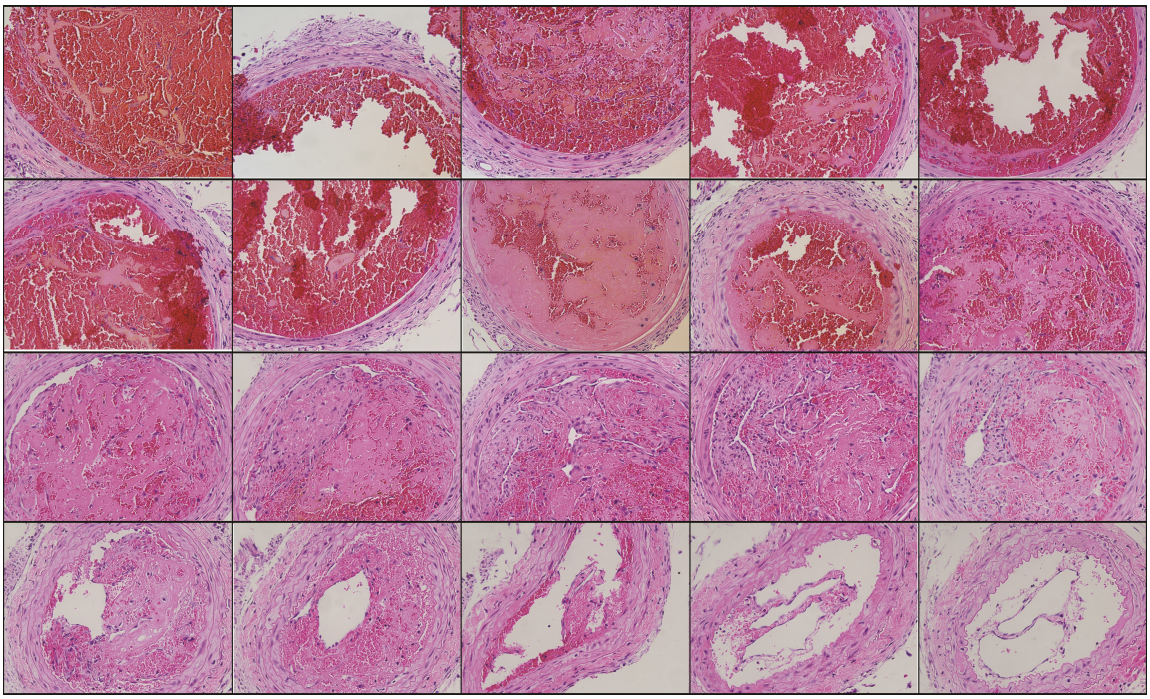

Figure 4.7. Rapamycin profoundly retards thrombus resolution through 21 days in wild-type mice. At the distal poles of residual thrombus, clotted red blood cells are streaked only partially by pink, acellular fibrin, although migration of neutrophils, macrophages, and fibroblasts into fibrin tracts is apparent by inspection of characteristic morphology of these cell types. As fibrin deposition increases further down the arterial axis, cell migration intensifies, and invaginating clefts lined by endothelial cells appear. Further down still, clefts coalesce into centrally recanalized channels. The profuse cellularity observed previously at POD14 in areas displaying similar morphology from both genotypes was largely attenuated under the influence of rapamycin.

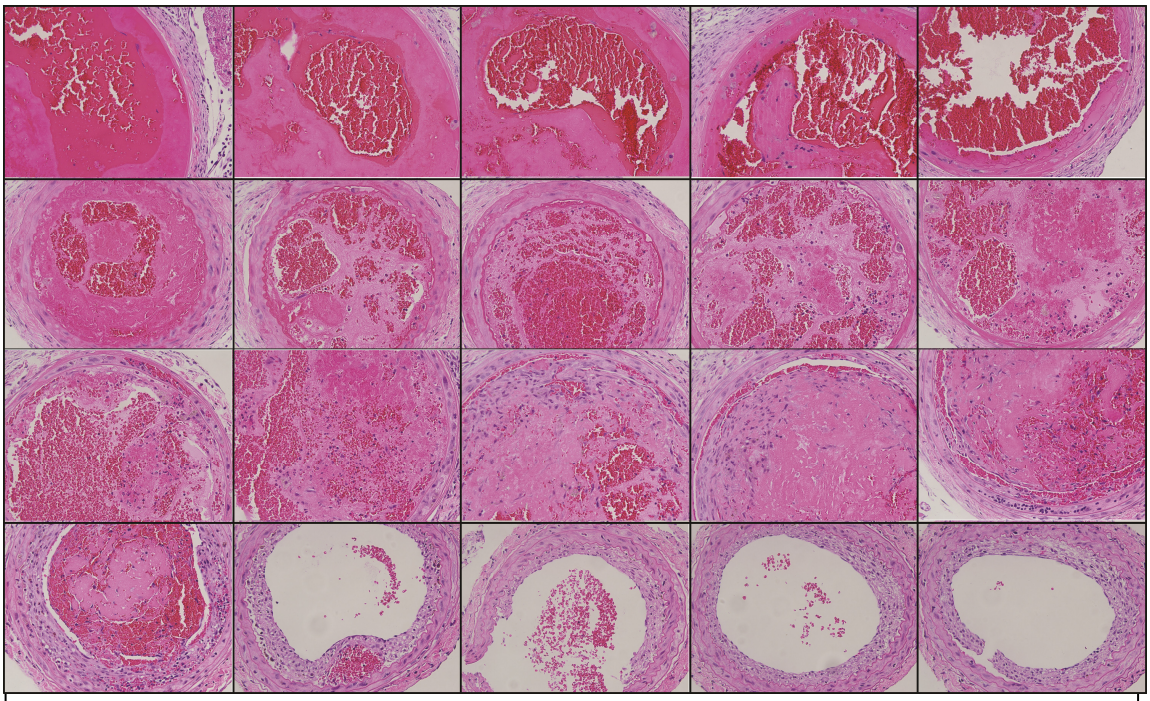

Figure 4.8. Rapamycin profoundly retards thrombus resolution through 21 days in type III collagen-deficient mice. At the distal poles of residual thrombus, clotted red blood cells are matted only partially by pink, acellular fibrin, although migration of neutrophils, macrophages, and fibroblasts into fibrin swaths is apparent by inspection of characteristic morphology of these cell types. As fibrin deposition increases further down the arterial axis, cell migration intensifies, and invaginating clefts lined by endothelial cells appear. Further down still, occlusive thrombi are resorbed into the neointima lining the recanalized lumen. The profuse cellularity observed previously at POD14 in areas displaying similar morphology from both genotypes was largely attenuated under the influence of rapamycin. However, unlike the wild-type artery above, neointimal formation still occcurs at the proximal poles in type III collagen-deficient segments.

By creating a cohort of index slides from rapamycin-treated animals and from vehicle-treated animals, we found no morphological difference between vehicle-treated animals and untreated animals from experiments in Chapter 2 (data not shown). Slides from rapamycin-treated animals, on the other hand, demonstrate vividly altered morphology that similarly affects all arteries regardless of genotype (Figures 4.7 and 4.8). The most salient feature of a common pathology is the impediment to migration of all cell types present, including neutrophils with polymorphic nuclei, macrophages with abundant cytoplasm, and spindled fibroblasts, and the suppression of remodeling despite

high burdens of inflammatory cells in both groups. As a result, large fields of fibrin remain unremodeled into a more collagenous matrix, as had been instead seen in more densely cellular thrombi from untreated artery segments in Chapter 2. However, small areas of neointimal formation are present at the proximal poles of mutant arteries (Figure 4.8), while wild-type arteries display endothelial lining of fibrinous collars encircling the lumen (Figure 4.7). This feature was previously described in wild-type arteries at POD14 just distal to proper neointimal formation (Figure 2.16), so it appears to be a precursor lesion to neointimal hyperplasia. Here, the dropout of fibrinous material from the collar in sections of Figure 4.7 is due to artifact introduced during serial sectioning, as the material was likely not sturdy enough to stand up to the microtome blade.

Rapamycin treatment equalizes the incidence of neovessels occupying the arterial media.

Trial	Measure	+/+ Pos	+/+ Neg	+/- Pos	+/- Neg	p-value
Rapamycin	Thrombus	49	18	51	29	.2869
N=4,4	Neovessels	4	63	5	75	1.000
Vehicle	Thrombus	31	69	28	76	.5403
N=5,5	Neovessels	6	94	15	89	**.0644**
	Thrombus	.0001		.0001		
	Neovessels	1.000		**.0961**		

Table 4.1. Rapamycin significantly increases thrombus burden in both genotypes but equalizes the incidence of neovascularizatioin.

The most obvious and consistent similarities between all arterial segments regardless of genotype is the heavy burden of occlusive thrombus and the striking simultaneous absence of vascular channels penetrating the arterial media. By statistical

analysis of arterial segments, no differences were detected in the number of segments containing unresolved thormbi between the genotypes under rapamycin treatment (p = .2869), and no differences were detected in the number of segments containing media-penetrating neovessels (p = 1.000; Table 4.1). On the other hand, statistical analysis of segments from vehicle-treated mice replicated the higher incidence of neovessels in mutant artery segments (although the analysis was underpowered and not statistically significant, p = .0644) without convincingly replicating the higher thrombus burden in mutant segments compared to wild-type segments (p = .5403).

However, by comparing artery segments from rapamycin-treated animals to those from vehicle-treated animals reveals an extremely significant increase in occlusive thrombus burden affecting both genotypes equally (p = .0001 in both cases). Nonetheless, rapamycin has no effect on the relative absence of neovessels observed in wild-type segments but confers a clear trend in the reduction of neovessels in mutant segments (p = .0961).

Buprenorphine increases incidence of thrombus and neovessels in wild-type artery segments but attenuates them in mutant artery segments following carotid ligation.

Trial	Measure	+/+ Pos	+/+ Neg	+/- Pos	+/- Neg	p-value
POD21 Ketoprofen	Thrombus	6	71	25	91	**0.0289**
N=8,9	Neovessels	1	76	17	99	**0.0016**
Buprenorphine	Thrombus	20	56	17	150	**0.0019**
N=4,9	Neovessels	8	67	11	156	0.3051
	Thrombus	**.0025**		**.0105**		
	Neovessels	**.0169**		**.0412**		

Table 4.2. Buprenorphine transfers the predisposition for thrombosis from mutant artery segments to wild-type artery segments, equalizing the risk for neovascularization.

Despite our hypothesis that buprenorphine would exaggerate residual thrombus burden in *Col3a1*$^{+/-}$ artery segments, we instead found that narcotic analgesics improved the resolution of thrombus and the incidence of neovessels in comparison with ketoprofen, a non-steroidal anti-inflammatory drug (NSAID) acting nonselectively on the cyclo-oxygenase-mediated production of prostaglandin E_2. On the other hand, ketoprofen appeared to be protective against residual thrombus burden and neovascularization in wild-type artery segments (Table 4.2).

Discussion

The discrepancy between statistically ambiguous thrombus burden in arteries from vehicle-treated mutant animals (p = .5403) and differential thrombus burden in mutant arteries from the original data (p = .0289) reflects that thrombus burden has not been as thoroughly sampled here as in Chapter 2. However, the data available here, where artery segments are already numerous enough to come very close to achieving statistical significance for the increased incidence of neovessels in mutant arteries (p =

.0644) supports the hypothesis that the thrombus itself does not attract circumstances promoting neoangiogenesis. Rather, the properties of the specifically altered matrix produced by type III collagen-deficient cells seem to be necessary for pathologic neovascularization.

Otherwise, rapamycin successfully neutralizes neovascularization in all arteries following injury, regardless of genotype. However, the equally undesirable result of significantly enhanced burden of unresolved thrombus in arteries regardless of genotype is not a suitable therapeutic tradeoff. This result is consistent with clinical experience that rapamycin-eluting stents promote occlusive thrombosis, even in altered flow states far less dramatic than induced here[151,152]. At the same time, our pathological slide series demonstrates that rapamcyin severely retards thrombus resolution but does not neutralize it entirely, as neointimal lesions still form in arteries from treated animals, albeit at thicknesses smaller than those seen previously in Chapter 2. These data are consistent with longer-term animal studies showing that rapamycin only delays the progression of neointimal hyperplasia, which eventually reaches thicknesses on par with injured arteries in untreated animals[153]. This calls into question the therapeutic benefit of drug-eluting stents vs. bare-metal stents, when drug-eluting stents may improve stenosis by radiographic measurements but do not necessarily improve long-term survival by impeding resolution of fibrin deposits and increasing risk for snowballing occlusive thrombogenesis.

One interesting note from the literature examining the usefulness of rapamycin-eluting stents is the polarized regard by which different researchers approach the study of neointimal proliferation. Studies celebrating rapamycin's prevention of neointimal

hyperplasia discuss stenosis from neointimal formation as clear-cut pathology to be reduced[84,121,123-125], while studies implicating rapamycin for the increased risk of thrombogenesis decry the impaired healing[64,150,158], as defined by a lack of neointimal coverage growing over stent struts. It is interesting to consider why neointimal thickening occurs in the first place in response to injury, considering the vascular mechanics afforded by wall thickening and by the material properties afforded by circumferential matrix remodeling within the new tissue, as we have observed using NLOM. Obviously a balance between essential healing and girding of injured structures with sufficient patency of the lumen to maintain appropriate blood flow to downstream organs is more desirable than either extreme. The data presented by this project, by linking immunity- and myofibroblast-mediated thrombus resolution, neointimal formation, and matrix production, provides a new paradigm within which to optimize therapeutic regulation of arterial wound healing.

In regards to our trial of buprenorphine in comparison with earlier experiments utilizing ketoprofen, it appears that its antiplatelet effects may outweigh the anti-inflammatory effects within wild-type arteries following injury, decreasing the extent of thrombus generation and extension and thus preventing succeeding thrombus resolution. In mutant arteries, however, a baseline predisposition to impaired thrombus resolution and tendency even for excessive thrombus growth and extension likely overcomes any benefit from reduced initial thrombus nidus. Instead, ketoprofen's anti-inflammatory effects may impede arterial wound healing even further in an effect smaller than that of rapamycin but just large enough to blunt the benefits of pro-neovascularization signalineg by inflammatory cells and extend the presence of neovessels beyond a

timeframe in which they are useful. This result is important for guidance of patient care, as arterial injury and progression to clinical complications like dissection in vulnerable populations often involves a painful component, and use of commonly available NSAIDs to treat the symptoms of pain may precipitate clinical progression.

Chapter 5: Discussion

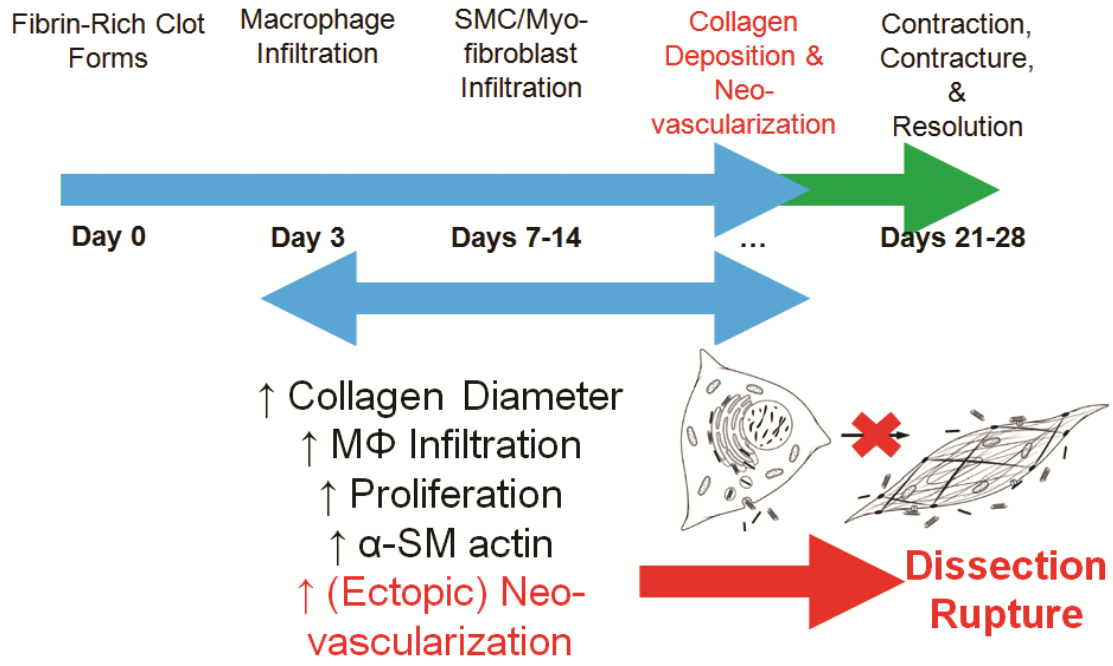

Figure 5.1. Model of fibroproliferative vascular wound healing resulting from deficient secretion of type III collagen following injury.

Fibroproliferative vascular wound healing in vEDS patients?

Together, the data presented in this dissertation strongly argue for a pathological process at work in type III collagen-deficient arteries that more closely resembles predisposition to fibroproliferative disease following tissue injury than to the inherent "tissue fragility" often touted to explain the clinical complications of vEDS patients[159]. According to our results, thrombus resolution proceeds normally until the proliferative phase, where recruited myofibroblasts that secrete insufficient levels of type III collagen generate deranged matrix within an expanding granulation tissue, which then accumulates greater numbers of macrophages in association with increased myofibroblast proliferation, expression of contractile α-SMA, and incidence of ectopic neovascularization. Rather than the tapering of myofibroblast activity and progression to the final contraction and resolution phase characteristic of normal wound healing, the

type III collagen-insufficient tissue appears to enter into a smoldering cycle resembling disorganized and unchecked contracture (Figure 5.1).

This novel model of pathogenesis would reconcile many perplexing clinical features of the disease, as discussed in Chapter 2, with the vascular mechanics of arterial wall integrity, as discussed in Chapter 1. The fact that neovessels persistently traverse the medial layer bears structural significance for wall integrity in that these abnormal defects threaten to disrupt the normally even distribution of wall stress in elastic arteries as afforded by their lamellar architecture[33]. Thus, these channels could increase the risk of localized structural failure under situational bouts of increased wall stress, possibly culminating in the blood-filled inter- or intralayer false lumina of arterial dissection or, worse, complete wall rupture. This possibility is consistent with a predisposition to dissection or rupture *despite* only rarely noted premonitory weakening of wall tensile strength by arterial dilation[159], as is more commonly and consistently observed in other syndromes associated with artery dissection, like Marfan syndrome or Loeys-Dietz syndrome[29]. In this way, spontaneous artery rupture or dissection is not spontaneous at all but more accurately an overexuberant response on the part of tissue to covert injury.

This would also explain the clinical benefit of celiprolol[14], which as a beta-blocker prevents spikes in arterial wall stress by restricting blood pressure within a stable range, and the clinical failure of celiprolol to actually alter the severe course of complications once they have been initiated by breakthrough injury. The benefit of celiprolol despite a physiologic effect opposite to what had been hypothesized (i.e., the observed increase in mean blood pressure rather than a predicted lowering to theoretically reduce stress on thin and overly weak arteries[14]) underscores the misleading

nature of studying uninjured tissues in this disease. Physiological parameters measured at baseline, which guided the design of this trial, apparently provide no predictive value for risk of complication.

The longevity of the "tissue fragility" hypothesis[4,160] obscures the assumptions inherent to its logic, which include the assumption that type III collagen is necessary for arterial wall strength, which has never been directly proven by mechanical testing. Another assumption is the notion that wound healing suffers in vEDS patients because the matrix in the organ wall is weaker[13,14]. Here we demonstrate the likelihood that the matrix is actually stiffer, which is a conclusion long available from classic studies that first characterized structurally enlarged fibers[9], essentially stiffer fibers considering the biochemistry of rigidly crosslinked polymers[2], in the skin. This stiffness in the tissue is critical to pathology such that weakness emerges from the inability of myofibroblasts to effectively remodel stiffer tissue when necessary and must instead rely on their own inherently unreliable contraction[98]. Thus, the scenario we are constructing here of fibroproliferative pathology is paradoxical in that less matrix protein of one type leads to stiffer bundles of another matrix protein, and that remodeling myofibroblasts take longer to achieve stress-shielding, leading to a prolonged inflammatory granulation tissue, one defining component of which--neovascularization--may confer the *coups de grace* of true tissue fragility.

Despite the bias that pervades the tissue fragility hypothesis for vEDS patients, observations made in a separate, less classifiable population further support a clinching role for transmural neovascularization in the precipitation of vascular catastrophes. Patients suffering from strokes at a premature age caused by cervical artery dissection

already possess strong phenotypic overlap with vEDS patients[16,39], but studies of their connective tissue reveal further overlap in that abnormally structured collagen fibrils, including increased diameters, as well as irregularly contoured surfaces or absent banding patterns on electron microscopy, were observed in the skin. Furthermore, immunogold labeling of type I and type III collagen on electron microscopy is *increased* in abnormal sections of tissue[161].

Since the initiation of this project, clinical researchers in this same group obtained biopsies from superficial temporal arteries distant from the site of earlier cervical artery dissection. Examination of the tissue revealed pathologic changes in association with dissection that were common to all patients examined. These changes were limited to the arterial media and adventitia, rather than appearing in the form of an intimal tear as canonized in clinical dogma. Rather, researchers identified the abnormal appearance of capillary neoangiogenesis penetrating the medial layer of vascular wall and evidence of primary intramural microhematoma[162-164]. As these changes were identified in arteries *other* than the sites of dissection, this new data suggests that patients prone to spontaneous dissection and stroke possess an inherent and systemic arteriopathy in the form of an abnormally increased burden of focal defects and, critically, *not* in the form of a diffuse weakness attributable to the baseline elastic properties of the vasculature[162-164] (Figure 5.2).

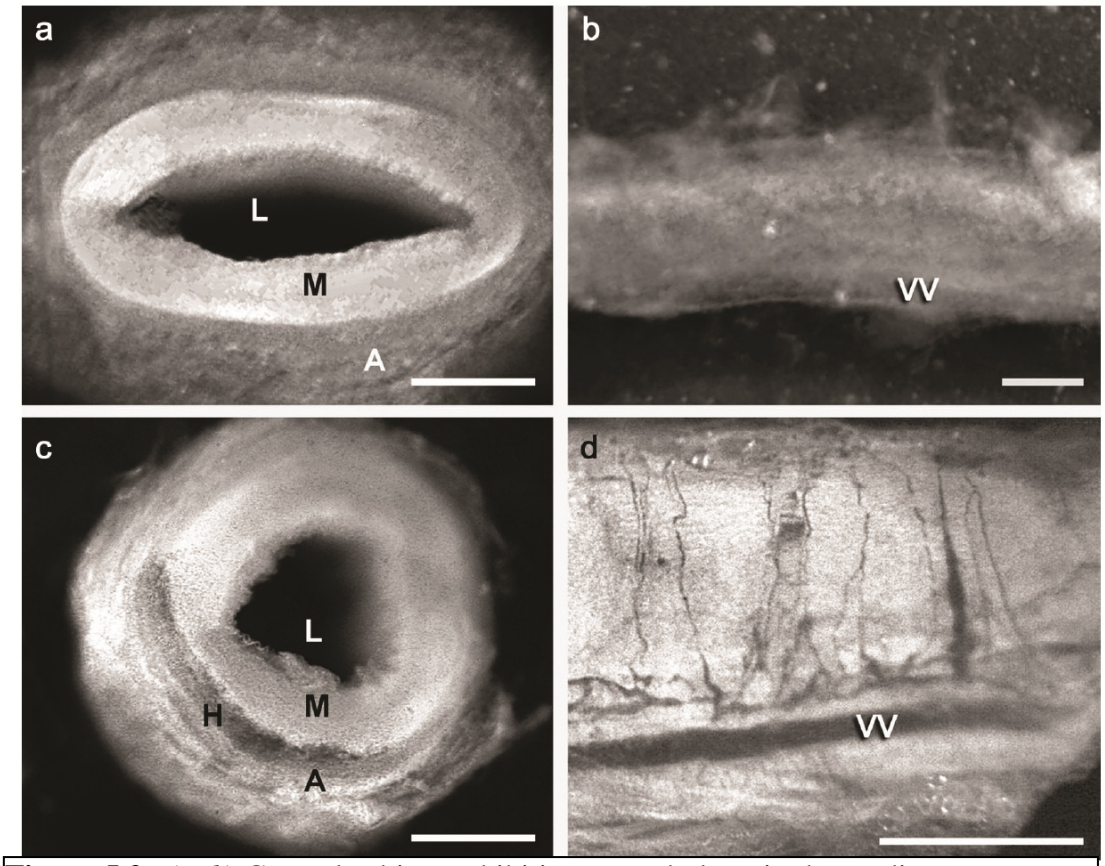

Figure 5.2. (*a, b*) Control subject exhibiting no pathology in the media or adventitia. (*c,d*) Patient with prior history of spontaneous cervical artery dissection demonstrating (*c*) a sickle-shaped microhematoma along the medial/adventitial border and (*d*) severe capillary neoangiogenesis. Reprinted with permission from Lippincott Williams & Wilkins [The outer arterial wall layers are primarily affected in spontaneous cervical artery dissection. Volker W, Dittrich R, Grewe S, et al. *Neurology*. 2011].

The benefit of this information is synergistic with that provided in the current project, in that these studies associate neoangiogenesis with a prior, defined history of risk for breach of arterial wall integrity. The most important contribution of this project is the *causative* link between an initiating injury, which we experimentally induced, and the subsequent pathologic inflammatory and fibroproliferative events involving deranged matrix production that *precipitate* this neoangiogenesis. In our animal model, uninjured mice otherwise appear identical to wild-type littermates in longevity, gross arterial wall histology, and even arterial wall strength[15,36].

Future Directions

As this study hinges on the events occurring in the neointima, a vanishingly small tissue contained within an elastic artery, a vastly different tissue whose relative size threatens to wash out or confound any changes on whole-tissue biochemical assays, exploitation of sophisticated NLOM imaging was critical to the conclusions at which we have arrived. Above and beyond the simple mass of total collagen within a whole tissue as measured by biochemical digestion, or the relative density visualized as a field of collagen among histological structures via qualitative histochemical stains, NLOM allowed us the direct and quantifiable observation of intact collagen fibers and the structural parameters that determine their emergent mechanical properties. These include fiber size and micro-orientation within the extracellular network in relation to the resident cells responsible for their synthesis and remodeling, which more realistically reflects the *composite* material properties of a dynamic tissue than dry collagen mass alone[98,165]. Although electron microscopy allows the visualization of collagen fibers, NLOM, unlike electron microscopy, provides field of view at the biologically-relevant level of histological structure rather than single-cell ultrastructure, which is more useful for making conclusions about the mechanical forces impinging on resident cells and the mechanical properties acquired by the tissue as an effect of responsive remodeling[98,112].

Further studies to test the hypothesis that impaired rates of type III collagen secretion lead to remodeling of a stiffer tissue could involve NLOM and a "bioreactor" cell culture system developed by our collaborator, Alvin T. Yeh, PhD[166]. Seeding of mutant fibroblast cell lines into fibrin gels molded in a cruciate formation allows for

rigging the gel to force transducers along two axes after the period of time over which the cells remodel the matrix. Tension measurements to determine acquired stiffness of the synthesized and organized matrix could dissect apart the contributions to mechanical properties inherent the matrix itself from those generated by cellular contraction, if measurements were made both before and after disruption of cellular contractile filaments. Thus, the hypothesis that weakness of type III collagen-deficient matrix originates in the excessive reliance on contraction by myofibroblasts and the failure of stress-shielding, as suggested by our imaging, could be tested experimentally.

Other areas for future research include a more careful analysis of the conditions for myofibroblast apoptosis in our fibrin gel constructs. Correlation between stress shielding and programmed cell death[108], or the lack thereof, would help explain not only the persistently dysregulated proliferation of myofibroblasts in resolving thrombi but also the oxygen and nutritional needs demanded by a constantly remodeling granulation tissue and the prompting of persistent angiogenesis of fragile neovessels, much in the nature of a growing tumor[167]. If stress shielding is truly the tipping point that initiates apoptosis, *COL3A1* mutant cells may never be able to overcome the challenges they face in remodeling the matrix they synthesize.

Exciting but still controversial research on the role of bone marrow-derived circulating "fibrocytes" in inflammatory and fibroproliferative pathology could open new therapeutic options for vEDS patients and for patients vulnerable to sCAD[168]. It has already been suggested that bone marrow-derived cells contribute to the bulk of cells within neointimal lesions observed at relatively late timepoints following intravascular injury[169]. Although studies performed since then have determined that the original

burden of cells derived from bone marrow regresses so that long-term neointima includes only locally-derived cells[170], we have shown in this project that the critical period for successful vs. pathologic vascular wound healing occurs much earlier. The period encompassing granulation tissue expansion by matrix synthesis and compaction by remodeling is mediated by fibrocellular neointima cells behaving more like myofibroblasts than like quiescent smooth muscle cells[74]. So it may not matter that bone marrow-derived fibrocytes disappear after maturation of neointima, in the paradigm of wound healing supported by this project. In fact, this may be expected and purposeful, if cells home to injured vessels and resulting thrombi, degrade fibrin and replace the lattice with collagenous matrix, compact that matrix to lock in suitable tissue strength to gird arteries weakened by injury, achieve tensional homeostasis and stress shielding, and then die by apoptosis. Considering that vascular wound healing depends so heavily on attracting circulating cells to a structure that itself is located in the circulation, it may even be more plausible that the most critical steps in wound healing be enacted by fibrocytes rather than by dedifferentiated smooth muscle cells, which would necessarily need to degrade their own matrix first in order to migrate inward from the wall.

The particularly exciting possibility raised by the pathological mechanisms elucidated in this project is the opportunity to replace circulating *Col3a1*$^{+/-}$ fibrocytes, and by extension the deranged matrix they would produce, with type III collagen-sufficient bone marrow transplant. If the disease model suggested by the data in this project is accurate, and if myofibroblasts responsible for wound healing in the arteries of vEDS patients could instead produce normal matrix with physiologic material properties,

then the predisposition to delayed thrombus resolution, fibroproliferative remodeling, and risk for vascular catastrophe may in fact be curable.

Reference List

(1) Reid AJ, Milewicz DM. Arteries, Smooth Muscle Cells, and Genetic Causes of Thoracic Aortic Aneurysms. In: Gary S.Hoffman, Cornelia M.Weyand, Carol A.Langford, Jorg J.Goronzy, eds. *Inflammatory Diseases of Blood Vessels*. 2nd ed. Wiley-Blackwell; 2012.

(2) Prockop DJ, Kivirikko KI. Collagens: molecular biology, diseases, and potentials for therapy. *Annu Rev Biochem* 1995;64:403-34.

(3) Myllyharju J, Kivirikko KI. Collagens and collagen-related diseases. *Ann Med* 2001 February;33(1):7-21.

(4) Beighton P, De Paepe A, Steinmann B, Tsipouras P, Wenstrup RJ. Ehlers-Danlos syndromes: revised nosology, Villefranche, 1997. Ehlers-Danlos National Foundation (USA) and Ehlers-Danlos Support Group (UK). *Am J Med Genet* 1998 April 28;77(1):31-7.

(5) Byers PH, Murray ML. Heritable collagen disorders: the paradigm of the ehlers-danlos syndrome. *J Invest Dermatol* 2012;132(E1):E6-E11.

(6) Byers PH. Ehlers-Danlos syndrome type IV: a genetic disorder in many guises. *J Invest Dermatol* 1995 September;105(3):311-3.

(7) Prockop DJ, Kivirikko KI. Heritable diseases of collagen. *N Engl J Med* 1984 August 9;311(6):376-86.

(8) Byers PH, Holbrook KA, Barsh GS, Smith LT, Bornstein P. Altered secretion of type III procollagen in a form of type IV Ehlers-Danlos syndrome. Biochemical studies in cultured fibroblasts. *Lab Invest* 1981 April;44(4):336-41.

(9) Smith LT, Schwarze U, Goldstein J, Byers PH. Mutations in the COL3A1 gene result in the Ehlers-Danlos syndrome type IV and alterations in the size and distribution of the major collagen fibrils of the dermis. *J Invest Dermatol* 1997 March;108(3):241-7.

(10) Pepin M, Schwarze U, Superti-Furga A, Byers PH. Clinical and genetic features of Ehlers-Danlos syndrome type IV, the vascular type [see comments]. *N Engl J Med* 2000 March 9;342(10):673-80.

(11) Pyeritz RE. Ehlers-Danlos syndrome. *N Engl J Med* 2000 March 9;342(10):730-2.

(12) Dobrin PB. Mechanical properties of arterises. *Physiol Rev* 1978 April;58(2):397-460.

(13) Boutouyrie P, Germain DP, Fiessinger JN, Laloux B, Perdu J, Laurent S. Increased carotid wall stress in vascular Ehlers-Danlos syndrome. *Circulation* 2004 March 30;109(12):1530-5.

(14) Ong KT, Perdu J, De BJ, Bozec E, Collignon P, Emmerich J, Fauret AL, Fiessinger JN, Germain DP, Georgesco G, Hulot JS, De PA, Plauchu H, Jeunemaitre X, Laurent S, Boutouyrie P. Effect of celiprolol on prevention of cardiovascular events in vascular Ehlers-Danlos syndrome: a prospective

randomised, open, blinded-endpoints trial. *Lancet* 2010 October 30;376(9751):1476-84.

(15) Liu X, Wu H, Byrne M, Krane S, Jaenisch R. Type III collagen is crucial for collagen I fibrillogenesis and for normal cardiovascular development. *Proc Natl Acad Sci U S A* 1997 March 4;94(5):1852-6.

(16) Schievink WI, Michels VV, Piepgras DG. Neurovascular manifestations of heritable connective tissue disorders. A review. *Stroke* 1994 April;25(4):889-903.

(17) Fleischmajer R, Perlish JS, Timpl R, Olsen BR. Procollagen intermediates during tendon fibrillogenesis. *J Histochem Cytochem* 1988 November;36(11):1425-32.

(18) Birk DE, Mayne R. Localization of collagen types I, III and V during tendon development. Changes in collagen types I and III are correlated with changes in fibril diameter. *Eur J Cell Biol* 1997 April;72(4):352-61.

(19) Lee D, Yuki I, Murayama Y, Chiang A, Nishimura I, Vinters HV, Wang CJ, Nien YL, Ishil A, Wu BM, Vinuela F. Thrombus organization and healing in the swine experimental aneurysm model. Part I. A histological and molecular analysis. *J Neurosurg* 2007 July;107(1):94-108.

(20) Wilson AJ, Gibson PR. Epithelial migration in the colon: filling in the gaps. *Clin Sci (Lond)* 1997 August;93(2):97-108.

(21) Salamonsen LA. Tissue injury and repair in the female human reproductive tract. *Reproduction* 2003 March;125(3):301-11.

(22) Fata JE, Ho AT, Leco KJ, Moorehead RA, Khokha R. Cellular turnover and extracellular matrix remodeling in female reproductive tissues: functions of metalloproteinases and their inhibitors. *Cell Mol Life Sci* 2000 January 20;57(1):77-95.

(23) Wagenseil JE, Mecham RP. Vascular extracellular matrix and arterial mechanics. *Physiol Rev* 2009 July;89(3):957-89.

(24) Kassab GS. Biomechanics of the cardiovascular system: the aorta as an illustratory example. *J R Soc Interface* 2006 December 22;3(11):719-40.

(25) Storkholm JH, Zhao J, Villadsen GE, Hager H, Jensen SL, Gregersen H. Biomechanical remodeling of the chronically obstructed Guinea pig small intestine. *Dig Dis Sci* 2007 February;52(2):336-46.

(26) MacDonald JA. Smooth muscle phenotypic plasticity in mechanical obstruction of the small intestine. *Neurogastroenterol Motil* 2008 July;20(7):737-40.

(27) Newby AC, Zaltsman AB. Molecular mechanisms in intimal hyperplasia. *J Pathol* 2000 February;190(3):300-9.

(28) Singer AJ, Clark RA. Cutaneous wound healing. *N Engl J Med* 1999 September 2;341(10):738-46.

(29) Loeys BL, Schwarze U, Holm T, Callewaert BL, Thomas GH, Pannu H, De Backer JF, Oswald GL, Symoens S, Manouvrier S, Roberts AE, Faravelli F, Greco MA, Pyeritz RE, Milewicz DM, Coucke PJ, Cameron DE, Braverman AC,

Byers PH, De Paepe AM, Dietz HC. Aneurysm syndromes caused by mutations in the TGF-beta receptor. *N Engl J Med* 2006 August 24;355(8):788-98.

(30) Oderich GS, Panneton JM, Bower TC, Lindor NM, Cherry KJ, Noel AA, Kalra M, Sullivan T, Gloviczki P. The spectrum, management and clinical outcome of Ehlers-Danlos syndrome type IV: a 30-year experience. *J Vasc Surg* 2005 July;42(1):98-106.

(31) Davis EC. Smooth muscle cell to elastic lamina connections in developing mouse aorta. Role in aortic medial organization. *Lab Invest* 1993 January;68(1):89-99.

(32) *Harrison's Principles of Internal Medicine*. 17th ed. McGraw-Hill Companies; 2008.

(33) Glagov S, Wolinsky H. Aortic wall as a 'two-phase' material. Nature 199[4893], 606-608. 8-10-1963.
Ref Type: Generic

(34) Caruso FS, Berger BM, Darragh A, Weng T, Vukovich R. Effect of celiprolol, a new beta 1-alpha 2 blocker, on the cardiovascular response to exercise. *J Clin Pharmacol* 1986 January;26(1):32-8.

(35) Plancke A, Holder-Espinasse M, Rigau V, Manouvrier S, Claustres M, Khau Van KP. Homozygosity for a null allele of COL3A1 results in recessive Ehlers-Danlos syndrome. *Eur J Hum Genet* 2009 November;17(11):1411-6.

(36) Cooper TK, Zhong Q, Krawczyk M, Tae HJ, Muller GA, Schubert R, Myers LA, Dietz HC, Talan MI, Briest W. The haploinsufficient Col3a1 mouse as a model for vascular Ehlers-Danlos syndrome. *Vet Pathol* 2010 November;47(6):1028-39.

(37) Schwarze U, Schievink WI, Petty E, Jaff MR, Babovic-Vuksanovic D, Cherry KJ, Pepin M, Byers PH. Haploinsufficiency for one COL3A1 allele of type III procollagen results in a phenotype similar to the vascular form of Ehlers-Danlos syndrome, Ehlers-Danlos syndrome type IV. *Am J Hum Genet* 2001 November;69(5):989-1001.

(38) Leistritz DF, Pepin MG, Schwarze U, Byers PH. COL3A1 haploinsufficiency results in a variety of Ehlers-Danlos syndrome type IV with delayed onset of complications and longer life expectancy. *Genet Med* 2011 August;13(8):717-22.

(39) Schievink WI. Spontaneous dissection of the carotid and vertebral arteries. *N Engl J Med* 2001 March 22;344(12):898-906.

(40) Schievink WI, Mokri B, O'Fallon WM. Recurrent spontaneous cervical-artery dissection. *N Engl J Med* 1994 February 10;330(6):393-7.

(41) North KN, Whiteman DA, Pepin MG, Byers PH. Cerebrovascular complications in Ehlers-Danlos syndrome type IV. *Ann Neurol* 1995 December;38(6):960-4.

(42) Debette S, Markus HS. The genetics of cervical artery dissection: a systematic review. *Stroke* 2009 June;40(6):e459-e466.

(43) Mokri B. Traumatic and spontaneous extracranial internal carotid artery dissections. *J Neurol* 1990 October;237(6):356-61.

(44) Norris JW, Beletsky V, Nadareishvili ZG. Sudden neck movement and cervical artery dissection. The Canadian Stroke Consortium. *CMAJ* 2000 July 11;163(1):38-40.

(45) Schievink WI. The treatment of spontaneous carotid and vertebral artery dissections. *Curr Opin Cardiol* 2000 September;15(5):316-21.

(46) Trosch RM, Hasbani M, Brass LM. "Bottoms up" dissection. *N Engl J Med* 1989 June 8;320(23):1564-5.

(47) Dragon R, Saranchak H, Lakin P, Strauch G. Blunt injuries to the carotid and vertebral arteries. *Am J Surg* 1981 April;141(4):497-500.

(48) Grau AJ, Brandt T, Buggle F, Orberk E, Mytilineos J, Werle E, Conradt, Krause M, Winter R, Hacke W. Association of cervical artery dissection with recent infection. *Arch Neurol* 1999 July;56(7):851-6.

(49) Gilden D, Cohrs RJ, Mahalingam R, Nagel MA. Varicella zoster virus vasculopathies: diverse clinical manifestations, laboratory features, pathogenesis, and treatment. *Lancet Neurol* 2009 August;8(8):731-40.

(50) Kumar A, Lindner V. Remodeling with neointima formation in the mouse carotid artery after cessation of blood flow. *Arterioscler Thromb Vasc Biol* 1997 October;17(10):2238-44.

(51) Schwartz SM, deBlois D, O'Brien ER. The intima. Soil for atherosclerosis and restenosis. *Circ Res* 1995 September;77(3):445-65.

(52) Wexler BC. Histopathological reactivity of carotid arteries of normotensive Sprague-Dawley vs spontaneously hypertensive rats to ligation injury. *Stroke* 1979 November;10(6):674-9.

(53) Buck RC. Intimal thickening after ligature of arteries: an electron-microscopic study. *Circulation* 1961;9:418-26.

(54) Brint S, Jacewicz M, Kiessling M, Tanabe J, Pulsinelli W. Focal brain ischemia in the rat: methods for reproducible neocortical infarction using tandem occlusion of the distal middle cerebral and ipsilateral common carotid arteries. *J Cereb Blood Flow Metab* 1988 August;8(4):474-85.

(55) Barone FC, Knudsen DJ, Nelson AH, Feuerstein GZ, Willette RN. Mouse strain differences in susceptibility to cerebral ischemia are related to cerebral vascular anatomy. *J Cereb Blood Flow Metab* 1993 July;13(4):683-92.

(56) Glagov S, Weisenberg E, Zarins CK, Stankunavicius R, Kolettis GJ. Compensatory enlargement of human atherosclerotic coronary arteries. *N Engl J Med* 1987 May 28;316(22):1371-5.

(57) Korshunov VA, Berk BC. Strain-dependent vascular remodeling: the "Glagov phenomenon" is genetically determined. *Circulation* 2004 July 13;110(2):220-6.

(58) Guyton JR, Hartley CJ. Flow restriction of one carotid artery in juvenile rats inhibits growth of arterial diameter. *Am J Physiol* 1985 April;248(4 Pt 2):H540-H546.

(59) Liu SQ, Tang D, Tieche C, Alkema PK. Pattern formation of vascular smooth muscle cells subject to nonuniform fluid shear stress: mediation by gradient of cell density. *Am J Physiol Heart Circ Physiol* 2003 September;285(3):H1072-H1080.

(60) Cunningham KS, Gotlieb AI. The role of shear stress in the pathogenesis of atherosclerosis. *Lab Invest* 2005 January;85(1):9-23.

(61) Wolberg AS, Aleman MM, Leiderman K, Machlus KR. Procoagulant activity in hemostasis and thrombosis: Virchow's triad revisited. *Anesth Analg* 2012 February;114(2):275-85.

(62) Kawasaki T, Dewerchin M, Lijnen HR, Vreys I, Vermylen J, Hoylaerts MF. Mouse carotid artery ligation induces platelet-leukocyte-dependent luminal fibrin, required for neointima development. *Circ Res* 2001 February 2;88(2):159-66.

(63) Yamashita A, Furukoji E, Marutsuka K, Hatakeyama K, Yamamoto H, Tamura S, Ikeda Y, Sumiyoshi A, Asada Y. Increased vascular wall thrombogenicity combined with reduced blood flow promotes occlusive thrombus formation in rabbit femoral artery. *Arterioscler Thromb Vasc Biol* 2004 December;24(12):2420-4.

(64) Finn AV, Nakazawa G, Joner M, Kolodgie FD, Mont EK, Gold HK, Virmani R. Vascular responses to drug eluting stents: importance of delayed healing. *Arterioscler Thromb Vasc Biol* 2007 July;27(7):1500-10.

(65) Schwartz RS, Edwards WD, Huber KC, Antoniades LC, Bailey KR, Camrud AR, Jorgenson MA, Holmes DR, Jr. Coronary restenosis: prospects for solution and new perspectives from a porcine model. *Mayo Clin Proc* 1993 January;68(1):54-62.

(66) Burnand KG, Gaffney PJ, McGuinness CL, Humphries J, Quarmby JW, Smith A. The role of the monocyte in the generation and dissolution of arterial and venous thrombi. *Cardiovasc Surg* 1998 April;6(2):119-25.

(67) Tsapogas MJ, Stirling GA, Girolami PL. Study on the organization of experimental thrombi. *Angiology* 1966 November;17(11):825-32.

(68) Schafer K, Konstantinides S, Riedel C, Thinnes T, Muller K, Dellas C, Hasenfuss G, Loskutoff DJ. Different mechanisms of increased luminal stenosis after arterial injury in mice deficient for urokinase- or tissue-type plasminogen activator. *Circulation* 2002 October 1;106(14):1847-52.

(69) Nosaka M, Ishida Y, Kimura A, Kuninaka Y, Inui M, Mukaida N, Kondo T. Absence of IFN-gamma accelerates thrombus resolution through enhanced MMP-9 and VEGF expression in mice. *J Clin Invest* 2011 July;121(7):2911-20.

(70) Modarai B, Burnand KG, Humphries J, Waltham M, Smith A. The role of neovascularisation in the resolution of venous thrombus. *Thromb Haemost* 2005 May;93(5):801-9.

(71) Martin P. Wound healing--aiming for perfect skin regeneration. *Science* 1997 April 4;276(5309):75-81.

(72) Khan R, Agrotis A, Bobik A. Understanding the role of transforming growth factor-beta1 in intimal thickening after vascular injury. *Cardiovasc Res* 2007 May 1;74(2):223-34.

(73) Tomasek JJ, Gabbiani G, Hinz B, Chaponnier C, Brown RA. Myofibroblasts and mechano-regulation of connective tissue remodelling. *Nat Rev Mol Cell Biol* 2002 May;3(5):349-63.

(74) Majesky MW, Lindner V, Twardzik DR, Schwartz SM, Reidy MA. Production of transforming growth factor beta 1 during repair of arterial injury. *J Clin Invest* 1991 September;88(3):904-10.

(75) Roberts AB, Sporn MB, Assoian RK, Smith JM, Roche NS, Wakefield LM, Heine UI, Liotta LA, Falanga V, Kehrl JH, . Transforming growth factor type beta: rapid induction of fibrosis and angiogenesis in vivo and stimulation of collagen formation in vitro. *Proc Natl Acad Sci U S A* 1986 June;83(12):4167-71.

(76) Gabbiani G, Le LM, Bailey AJ, Bazin S, Delaunay A. Collagen and myofibroblasts of granulation tissue. A chemical, ultrastructural and immunologic study. *Virchows Arch B Cell Pathol* 1976 August 11;21(2):133-45.

(77) Barger AC, Beeuwkes R, III, Lainey LL, Silverman KJ. Hypothesis: vasa vasorum and neovascularization of human coronary arteries. A possible role in the pathophysiology of atherosclerosis. *N Engl J Med* 1984 January 19;310(3):175-7.

(78) Farb A, Weber DK, Kolodgie FD, Burke AP, Virmani R. Morphological predictors of restenosis after coronary stenting in humans. *Circulation* 2002 June 25;105(25):2974-80.

(79) Desmouliere A, Badid C, Bochaton-Piallat ML, Gabbiani G. Apoptosis during wound healing, fibrocontractive diseases and vascular wall injury. *Int J Biochem Cell Biol* 1997 January;29(1):19-30.

(80) Stevenson K, Kucich U, Whitbeck C, Levin RM, Howard PS. Functional changes in bladder tissue from type III collagen-deficient mice. *Mol Cell Biochem* 2006 February;283(1-2):107-14.

(81) Schmittgen TD, Livak KJ. Analyzing real-time PCR data by the comparative C(T) method. *Nat Protoc* 2008;3(6):1101-8.

(82) Kim H, Cho HJ, Kim SW, Liu B, Choi YJ, Lee J, Sohn YD, Lee MY, Houge MA, Yoon YS. CD31+ cells represent highly angiogenic and vasculogenic cells in bone marrow: novel role of nonendothelial CD31+ cells in neovascularization and their therapeutic effects on ischemic vascular disease. *Circ Res* 2010 September 3;107(5):602-14.

(83) Grunewald M, Avraham I, Dor Y, Bachar-Lustig E, Itin A, Jung S, Chimenti S, Landsman L, Abramovitch R, Keshet E. VEGF-induced adult neovascularization: recruitment, retention, and role of accessory cells. *Cell* 2006 January 13;124(1):175-89.

(84) Suzuki T, Kopia G, Hayashi S, Bailey LR, Llanos G, Wilensky R, Klugherz BD, Papandreou G, Narayan P, Leon MB, Yeung AC, Tio F, Tsao PS, Falotico R, Carter AJ. Stent-based delivery of sirolimus reduces neointimal formation in a porcine coronary model. *Circulation* 2001 September 4;104(10):1188-93.

(85) Gabbiani G, Hirschel BJ, Ryan GB, Statkov PR, Majno G. Granulation tissue as a contractile organ. A study of structure and function. *J Exp Med* 1972 April 1;135(4):719-34.

(86) Eddy RJ, Petro JA, Tomasek JJ. Evidence for the nonmuscle nature of the "myofibroblast" of granulation tissue and hypertropic scar. An immunofluorescence study. *Am J Pathol* 1988 February;130(2):252-60.

(87) Desmouliere A, Geinoz A, Gabbiani F, Gabbiani G. Transforming growth factor-beta 1 induces alpha-smooth muscle actin expression in granulation tissue myofibroblasts and in quiescent and growing cultured fibroblasts. *J Cell Biol* 1993 July;122(1):103-11.

(88) Vaughan MB, Howard EW, Tomasek JJ. Transforming growth factor-beta1 promotes the morphological and functional differentiation of the myofibroblast. *Exp Cell Res* 2000 May 25;257(1):180-9.

(89) Wipff PJ, Rifkin DB, Meister JJ, Hinz B. Myofibroblast contraction activates latent TGF-beta1 from the extracellular matrix. *J Cell Biol* 2007 December 17;179(6):1311-23.

(90) Hinz B, Mastrangelo D, Iselin CE, Chaponnier C, Gabbiani G. Mechanical tension controls granulation tissue contractile activity and myofibroblast differentiation. *Am J Pathol* 2001 September;159(3):1009-20.

(91) Hinz B, Phan SH, Thannickal VJ, Galli A, Bochaton-Piallat ML, Gabbiani G. The myofibroblast: one function, multiple origins. *Am J Pathol* 2007 June;170(6):1807-16.

(92) Petroll WM, Cavanagh HD, Barry P, Andrews P, Jester JV. Quantitative analysis of stress fiber orientation during corneal wound contraction. *J Cell Sci* 1993 February;104 (Pt 2):353-63.

(93) Eastwood M, Mudera VC, McGrouther DA, Brown RA. Effect of precise mechanical loading on fibroblast populated collagen lattices: morphological changes. *Cell Motil Cytoskeleton* 1998;40(1):13-21.

(94) Brown RA, Prajapati R, McGrouther DA, Yannas IV, Eastwood M. Tensional homeostasis in dermal fibroblasts: mechanical responses to mechanical loading in three-dimensional substrates. *J Cell Physiol* 1998 June;175(3):323-32.

(95) Hinz B, Celetta G, Tomasek JJ, Gabbiani G, Chaponnier C. Alpha-smooth muscle actin expression upregulates fibroblast contractile activity. *Mol Biol Cell* 2001 September;12(9):2730-41.

(96) Tomasek JJ, Haaksma CJ, Eddy RJ, Vaughan MB. Fibroblast contraction occurs on release of tension in attached collagen lattices: dependency on an organized actin cytoskeleton and serum. *Anat Rec* 1992 March;232(3):359-68.

(97) Grinnell F, Ho CH. Transforming growth factor beta stimulates fibroblast-collagen matrix contraction by different mechanisms in mechanically loaded and unloaded matrices. *Exp Cell Res* 2002 February 15;273(2):248-55.

(98) Tomasek JJ, Gabbiani G, Hinz B, Chaponnier C, Brown RA. Myofibroblasts and mechano-regulation of connective tissue remodelling. *Nat Rev Mol Cell Biol* 2002 May;3(5):349-63.

(99) Wakatsuki T, Kolodney MS, Zahalak GI, Elson EL. Cell mechanics studied by a reconstituted model tissue. *Biophys J* 2000 November;79(5):2353-68.

(100) Darby I, Skalli O, Gabbiani G. Alpha-smooth muscle actin is transiently expressed by myofibroblasts during experimental wound healing. *Lab Invest* 1990 July;63(1):21-9.

(101) Volk SW, Wang Y, Mauldin EA, Liechty KW, Adams SL. Diminished type III collagen promotes myofibroblast differentiation and increases scar deposition in cutaneous wound healing. *Cells Tissues Organs* 2011;194(1):25-37.

(102) Hong H, Stegemann JP. 2D and 3D collagen and fibrin biopolymers promote specific ECM and integrin gene expression by vascular smooth muscle cells. *J Biomater Sci Polym Ed* 2008;19(10):1279-93.

(103) Sander EA, Barocas VH, Tranquillo RT. Initial fiber alignment pattern alters extracellular matrix synthesis in fibroblast-populated fibrin gel cruciforms and correlates with predicted tension. *Ann Biomed Eng* 2011 February;39(2):714-29.

(104) Birk DE, Mayne R. Localization of collagen types I, III and V during tendon development. Changes in collagen types I and III are correlated with changes in fibril diameter. *Eur J Cell Biol* 1997 April;72(4):352-61.

(105) Romanic AM, Adachi E, Kadler KE, Hojima Y, Prockop DJ. Copolymerization of pNcollagen III and collagen I. pNcollagen III decreases the rate of incorporation of collagen I into fibrils, the amount of collagen I incorporated, and the diameter of the fibrils formed. *J Biol Chem* 1991 July 5;266(19):12703-9.

(106) Kocher O, Skalli O, Bloom WS, Gabbiani G. Cytoskeleton of rat aortic smooth muscle cells. Normal conditions and experimental intimal thickening. *Lab Invest* 1984 June;50(6):645-52.

(107) Carlson MA, Longaker MT, Thompson JS. Wound splinting regulates granulation tissue survival. *J Surg Res* 2003 March;110(1):304-9.

(108) Thannickal VJ. Mechanisms of pulmonary fibrosis: role of activated myofibroblasts and NADPH oxidase. *Fibrogenesis Tissue Repair* 2012 June 6;5 Suppl 1:S23.

(109) Grinnell F. Fibroblast biology in three-dimensional collagen matrices. *Trends Cell Biol* 2003 May;13(5):264-9.

(110) Desmouliere A, Chaponnier C, Gabbiani G. Tissue repair, contraction, and the myofibroblast. *Wound Repair Regen* 2005 January;13(1):7-12.

(111) Aarabi S, Bhatt KA, Shi Y, Paterno J, Chang EI, Loh SA, Holmes JW, Longaker MT, Yee H, Gurtner GC. Mechanical load initiates hypertrophic scar formation through decreased cellular apoptosis. *FASEB J* 2007 October;21(12):3250-61.

(112) Larson AM, Yeh AT. Ex vivo characterization of sub-10-fs pulses. *Opt Lett* 2006 June 1;31(11):1681-3.

(113) Hu JJ, Humphrey JD, Yeh AT. Characterization of engineered tissue development under biaxial stretch using nonlinear optical microscopy. *Tissue Eng Part A* 2009 July;15(7):1553-64.

(114) Mohler W, Millard AC, Campagnola PJ. Second harmonic generation imaging of endogenous structural proteins. *Methods* 2003 January;29(1):97-109.

(115) Soo C, Beanes SR, Hu FY, Zhang X, Dang C, Chang G, Wang Y, Nishimura I, Freymiller E, Longaker MT, Lorenz HP, Ting K. Ontogenetic transition in fetal wound transforming growth factor-beta regulation correlates with collagen organization. *Am J Pathol* 2003 December;163(6):2459-76.

(116) Tuan TL, Song A, Chang S, Younai S, Nimni ME. In vitro fibroplasia: matrix contraction, cell growth, and collagen production of fibroblasts cultured in fibrin gels. *Exp Cell Res* 1996 February 25;223(1):127-34.

(117) Grouf JL, Throm AM, Balestrini JL, Bush KA, Billiar KL. Differential effects of EGF and TGF-beta1 on fibroblast activity in fibrin-based tissue equivalents. *Tissue Eng* 2007 April;13(4):799-807.

(118) Yeh AT, Gibbs H, Hu JJ, Larson AM. Advances in nonlinear optical microscopy for visualizing dynamic tissue properties in culture. *Tissue Eng Part B Rev* 2008 March;14(1):119-31.

(119) Kim JK, Xu Y, Xu X, Keene DR, Gurusiddappa S, Liang X, Wary KK, Hook M. A novel binding site in collagen type III for integrins alpha1beta1 and alpha2beta1. *J Biol Chem* 2005 September 16;280(37):32512-20.

(120) Duffield JS, Lupher M, Thannickal VJ, Wynn TA. Host responses in tissue repair and fibrosis. *Annu Rev Pathol* 2013 January 24;8:241-76.

(121) Braun-Dullaeus RC, Mann MJ, Dzau VJ. Cell cycle progression: new therapeutic target for vascular proliferative disease. *Circulation* 1998 July 7;98(1):82-9.

(122) Mehran R, Dangas G, Abizaid AS, Mintz GS, Lansky AJ, Satler LF, Pichard AD, Kent KM, Stone GW, Leon MB. Angiographic patterns of in-stent restenosis: classification and implications for long-term outcome. *Circulation* 1999 November 2;100(18):1872-8.

(123) Gallo R, Padurean A, Jayaraman T, Marx S, Roque M, Adelman S, Chesebro J, Fallon J, Fuster V, Marks A, Badimon JJ. Inhibition of intimal thickening after balloon angioplasty in porcine coronary arteries by targeting regulators of the cell cycle. *Circulation* 1999 April 27;99(16):2164-70.

(124) Marx SO, Jayaraman T, Go LO, Marks AR. Rapamycin-FKBP inhibits cell cycle regulators of proliferation in vascular smooth muscle cells. *Circ Res* 1995 March;76(3):412-7.

(125) Marx SO, Marks AR. Bench to bedside: the development of rapamycin and its application to stent restenosis. *Circulation* 2001 August 21;104(8):852-5.

(126) Liu J, Farmer JD, Jr., Lane WS, Friedman J, Weissman I, Schreiber SL. Calcineurin is a common target of cyclophilin-cyclosporin A and FKBP-FK506 complexes. *Cell* 1991 August 23;66(4):807-15.

(127) Sigal NH, Dumont FJ. Cyclosporin A, FK-506, and rapamycin: pharmacologic probes of lymphocyte signal transduction. *Annu Rev Immunol* 1992;10:519-60.

(128) Nourse J, Firpo E, Flanagan WM, Coats S, Polyak K, Lee MH, Massague J, Crabtree GR, Roberts JM. Interleukin-2-mediated elimination of the p27Kip1 cyclin-dependent kinase inhibitor prevented by rapamycin. *Nature* 1994 December 8;372(6506):570-3.

(129) Manning BD, Cantley LC. AKT/PKB signaling: navigating downstream. *Cell* 2007 June 29;129(7):1261-74.

(130) Hemmings BA, Restuccia DF. PI3K-PKB/Akt pathway. *Cold Spring Harb Perspect Biol* 2012 September;4(9):a011189.

(131) Fayard E, Tintignac LA, Baudry A, Hemmings BA. Protein kinase B/Akt at a glance. *J Cell Sci* 2005 December 15;118(Pt 24):5675-8.

(132) Altomare DA, Testa JR. Perturbations of the AKT signaling pathway in human cancer. *Oncogene* 2005 November 14;24(50):7455-64.

(133) Poston RS, Billingham M, Hoyt EG, Pollard J, Shorthouse R, Morris RE, Robbins RC. Rapamycin reverses chronic graft vascular disease in a novel cardiac allograft model. *Circulation* 1999 July 6;100(1):67-74.

(134) Mancini D, Pinney S, Burkhoff D, LaManca J, Itescu S, Burke E, Edwards N, Oz M, Marks AR. Use of rapamycin slows progression of cardiac transplantation vasculopathy. *Circulation* 2003 July 8;108(1):48-53.

(135) Vogelbacher R, Meister S, Guckel E, Starke C, Wittmann S, Stief A, Voll R, Daniel C, Hugo C. Bortezomib and sirolimus inhibit the chronic active antibody-mediated rejection in experimental renal transplantation in the rat. *Nephrol Dial Transplant* 2010 November;25(11):3764-73.

(136) Russell ME, Adams DH, Wyner LR, Yamashita Y, Halnon NJ, Karnovsky MJ. Early and persistent induction of monocyte chemoattractant protein 1 in rat cardiac allografts. *Proc Natl Acad Sci U S A* 1993 July 1;90(13):6086-90.

(137) Wynn TA. Common and unique mechanisms regulate fibrosis in various fibroproliferative diseases. *J Clin Invest* 2007 March;117(3):524-9.

(138) Shi C, Lee WS, He Q, Zhang D, Fletcher DL, Jr., Newell JB, Haber E. Immunologic basis of transplant-associated arteriosclerosis. *Proc Natl Acad Sci U S A* 1996 April 30;93(9):4051-6.

(139) Servant G, Weiner OD, Herzmark P, Balla T, Sedat JW, Bourne HR. Polarization of chemoattractant receptor signaling during neutrophil chemotaxis. *Science* 2000 February 11;287(5455):1037-40.

(140) Sasaki T, Irie-Sasaki J, Jones RG, Oliveira-dos-Santos AJ, Stanford WL, Bolon B, Wakeham A, Itie A, Bouchard D, Kozieradzki I, Joza N, Mak TW, Ohashi PS, Suzuki A, Penninger JM. Function of PI3Kgamma in thymocyte development, T cell activation, and neutrophil migration. *Science* 2000 February 11;287(5455):1040-6.

(141) Gomez-Cambronero J. Rapamycin inhibits GM-CSF-induced neutrophil migration. *FEBS Lett* 2003 August 28;550(1-3):94-100.

(142) Baetta R, Granata A, Canavesi M, Ferri N, Arnaboldi L, Bellosta S, Pfister P, Corsini A. Everolimus inhibits monocyte/macrophage migration in vitro and their accumulation in carotid lesions of cholesterol-fed rabbits. *J Pharmacol Exp Ther* 2009 February;328(2):419-25.

(143) Danner S, Sigrist S, Moreau F, Mandes K, Vodouhe C, Langlois A, Soskin S, Fichbach M, Pinget M, Kessler L. Influence of rapamycin on rat macrophage viability and chemotaxis toward allogenic pancreatic islet supernates. *Transplant Proc* 2008 March;40(2):470-2.

(144) Ganesan LP, Wei G, Pengal RA, Moldovan L, Moldovan N, Ostrowski MC, Tridandapani S. The serine/threonine kinase Akt Promotes Fc gamma receptor-

mediated phagocytosis in murine macrophages through the activation of p70S6 kinase. *J Biol Chem* 2004 December 24;279(52):54416-25.

(145) Boehm M, Olive M, True AL, Crook MF, San H, Qu X, Nabel EG. Bone marrow-derived immune cells regulate vascular disease through a p27(Kip1)-dependent mechanism. *J Clin Invest* 2004 August;114(3):419-26.

(146) Gillen JR, Zhao Y, Harris DA, Lapar DJ, Stone ML, Fernandez LG, Kron IL, Lau CL. Rapamycin blocks fibrocyte migration and attenuates bronchiolitis obliterans in a murine model. *Ann Thorac Surg* 2013 May;95(5):1768-75.

(147) Zuckermann A, Barten MJ. Surgical wound complications after heart transplantation. *Transpl Int* 2011 July;24(7):627-36.

(148) Smith AD, Bai D, Marroquin CE, Tuttle-Newhall JE, Desai DM, Collins BH, Muir A, Kuo PC, McHutchison J, Rockey DC. Gastrointestinal hemorrhage due to complicated gastroduodenal ulcer disease in liver transplant patients taking sirolimus. *Clin Transplant* 2005 April;19(2):250-4.

(149) Moses JW, Leon MB, Popma JJ, Fitzgerald PJ, Holmes DR, O'Shaughnessy C, Caputo RP, Kereiakes DJ, Williams DO, Teirstein PS, Jaeger JL, Kuntz RE. Sirolimus-eluting stents versus standard stents in patients with stenosis in a native coronary artery. *N Engl J Med* 2003 October 2;349(14):1315-23.

(150) Joner M, Finn AV, Farb A, Mont EK, Kolodgie FD, Ladich E, Kutys R, Skorija K, Gold HK, Virmani R. Pathology of drug-eluting stents in humans: delayed healing and late thrombotic risk. *J Am Coll Cardiol* 2006 July 4;48(1):193-202.

(151) Daemen J, Wenaweser P, Tsuchida K, Abrecht L, Vaina S, Morger C, Kukreja N, Juni P, Sianos G, Hellige G, van Domburg RT, Hess OM, Boersma E, Meier B, Windecker S, Serruys PW. Early and late coronary stent thrombosis of sirolimus-eluting and paclitaxel-eluting stents in routine clinical practice: data from a large two-institutional cohort study. *Lancet* 2007 February 24;369(9562):667-78.

(152) Lagerqvist B, James SK, Stenestrand U, Lindback J, Nilsson T, Wallentin L. Long-term outcomes with drug-eluting stents versus bare-metal stents in Sweden. *N Engl J Med* 2007 March 8;356(10):1009-19.

(153) Carter AJ, Aggarwal M, Kopia GA, Tio F, Tsao PS, Kolata R, Yeung AC, Llanos G, Dooley J, Falotico R. Long-term effects of polymer-based, slow-release, sirolimus-eluting stents in a porcine coronary model. *Cardiovasc Res* 2004 September 1;63(4):617-24.

(154) Lafont A. The Cypher stent: no longer efficacious at three months in the porcine model? *Cardiovasc Res* 2004 September 1;63(4):575-6.

(155) Dordoni PL, Della VM, Stefanelli A, Iannace E, Paparella P, Rocca B, Accorra F. Effect of ketorolac, ketoprofen and nefopam on platelet function. *Anaesthesia* 1994 December;49(12):1046-9.

(156) Rothschild BM. Comparative antiplatelet activity of COX1 NSAIDS versus aspirin, encompassing regimen simplification and gastroprotection: a call for a controlled study. *Reumatismo* 2004 April;56(2):89-93.

(157) Van Solingen RM, Rosenstein ED, Mihailescu G, Drejka ML, Kalia A, Cohen AJ, Kramer N. Comparison of the effects of ketoprofen on platelet function in the presence and absence of aspirin. *Am J Med* 2001 September;111(4):285-9.

(158) Nakazawa G, Finn AV, Joner M, Ladich E, Kutys R, Mont EK, Gold HK, Burke AP, Kolodgie FD, Virmani R. Delayed arterial healing and increased late stent thrombosis at culprit sites after drug-eluting stent placement for acute myocardial infarction patients: an autopsy study. *Circulation* 2008 September 9;118(11):1138-45.

(159) Pepin M, Schwarze U, Superti-Furga A, Byers PH. Clinical and genetic features of Ehlers-Danlos syndrome type IV, the vascular type. *N Engl J Med* 2000 March 9;342(10):673-80.

(160) Beighton P, De Paepe A, Danks D, Finidori G, Gedde-Dahl T, Goodman R, Hall JG, Hollister DW, Horton W, McKusick VA, . International Nosology of Heritable Disorders of Connective Tissue, Berlin, 1986. *Am J Med Genet* 1988 March;29(3):581-94.

(161) Uhlig P, Bruckner P, Dittrich R, Ringelstein EB, Kuhlenbaumer G, Hansen U. Aberrations of dermal connective tissue in patients with cervical artery dissection (sCAD). *J Neurol* 2008 March;255(3):340-6.

(162) Volker W, Besselmann M, Dittrich R, Nabavi D, Konrad C, Dziewas R, Evers S, Grewe S, Kramer SC, Bachmann R, Stogbauer F, Ringelstein EB, Kuhlenbaumer

G. Generalized arteriopathy in patients with cervical artery dissection. *Neurology* 2005 May 10;64(9):1508-13.

(163) Volker W, Dittrich R, Grewe S, Nassenstein I, Csiba L, Herczeg L, Borsay BA, Robenek H, Kuhlenbaumer G, Ringelstein EB. The outer arterial wall layers are primarily affected in spontaneous cervical artery dissection. *Neurology* 2011 April 26;76(17):1463-71.

(164) Schievink WI, Debette S. Etiology of cervical artery dissections: the writing is in the wall. *Neurology* 2011 April 26;76(17):1452-3.

(165) Niklason LE, Yeh AT, Calle EA, Bai Y, Valentin A, Humphrey JD. Enabling tools for engineering collagenous tissues integrating bioreactors, intravital imaging, and biomechanical modeling. *Proc Natl Acad Sci U S A* 2010 February 23;107(8):3335-9.

(166) Niklason LE, Yeh AT, Calle EA, Bai Y, Valentin A, Humphrey JD. Enabling tools for engineering collagenous tissues integrating bioreactors, intravital imaging, and biomechanical modeling. *Proc Natl Acad Sci U S A* 2010 February 23;107(8):3335-9.

(167) Marti HH, Risau W. Angiogenesis in ischemic disease. *Thromb Haemost* 1999 September;82 Suppl 1:44-52.

(168) Reilkoff RA, Bucala R, Herzog EL. Fibrocytes: emerging effector cells in chronic inflammation. *Nat Rev Immunol* 2011 June;11(6):427-35.

(169) Tanaka K, Sata M, Hirata Y, Nagai R. Diverse contribution of bone marrow cells to neointimal hyperplasia after mechanical vascular injuries. *Circ Res* 2003 October 17;93(8):783-90.

(170) Hoglund VJ, Dong XR, Majesky MW. Neointima formation: a local affair. *Arterioscler Thromb Vasc Biol* 2010 October;30(10):1877-9.

Vita

Amy Jean Reid was born in Lubbock, Texas on August 1, 1980 to Deborah Jane Reid and Randal Lynis Reid. After graduating from James W. Martin High School in Arlington, Texas in 1998, she attended Stanford University in Stanford, California and earned her A.B with Honors in 2002 from the Program in Human Biology. She subsequently attended the University of Texas in Austin for post-baccalaureate premedical coursework through the spring semester of 2003. Afterward, she worked for two years as a research assistant in the laboratory of Paul K.-Y. Wong in the Department of Carcinogenesis at the Science Park campus of M.D. Anderson Cancer Center in Smithville, Texas. She then matriculated into the M.D./Ph.D. Program at the University of Texas Medical School at Houston and the University of Texas Health Science Center at Houston Graduate School of Biomedical Sciences. Following the conferral of her M.D. and Ph.D. degrees, she will enter into medical residency in Internal Medicine and the Physician Scientist Development Program at the University of Chicago in Chicago, Illinois.

Permanent Address:

3702 Wentworth Dr.

Arlington, Texas 76001